NTNU

Norwegian University of
Science and Technology

Sandstone Provenance of the De Geerdalen Formation, Svalbard

Emphasis on Petrography and Chromium Spinel Compositions

Trond Svånå Harstad

Geology
Submission date: May 2016

Supervisor: Mai Britt E. Mørk, IGB
Co-supervisor: Atle Mørk, IGB
Snorre Olaussen, Universitetssenteret i Svalbard

Norwegian University of Science and Technology
Department of Geology and Mineral Resources Engineering

Abstract

Detrital chromium spinel mineral-chemical analyses, in combination with sandstone petrography, were conducted on samples from the Upper Triassic De Geerdalen Formation from several locations on Svalbard, in order to interpret sandstone provenance. Petrographic identification of detrital minerals and lithic fragments was used to identify source rock lithology. The accessory mineral chromium spinel was used as a petrogenetic marker to distinguish tectonic setting of mafic and ultra- mafic source rocks to the De Geerdalen Formation.

All detrital chromium spinels have a Fe^{3+} content above 25% and an Al content below 30%, when comparing the trivalent cations Cr, Fe^{3+} and Al. Comparing the divalent cations Mg and Fe^{2+}, the Mg content is between 38 and 94%. Apatite, chromium spinel, garnet, rutile, tourmaline and zircon heavy minerals are observed in sandstones along with various lithic fragments of volcanic and metapelitic origin. A considerable polycrystalline quartz content represents deformed quartzite grains, chert and spiculites.

Comparing the observed chromium spinel compositional range to that in the literature indicates a compositional match with mafic to ultra- mafic continental intrusions, covering flood basalts, sub- volcanic intrusions and layered intrusions. The observed volcanic lithic fragments in the De Geerdalen Formation may have a similar origin as the detrital chromium spinels. On the other hand, the lithic clasts and heavy minerals indicate varying source rock lithologies of metasedimentary, sedimentary, volcanic and felsitic intrusive origin.

The closest known possible source to chromium spinel of continental intrusion composition, and likely source to De Geerdalen Formation chromium spinel, is located on the Taimyr peninsula, representing the northernmost part of the Siberian Traps Large Igneous Province. This provenance interpretation is supported by the existence of Siberian Traps related zircon age peaks in detrital zircons of the De Geerdalen Formation. No observations suggesting varying provenance between the different Svalbard locations and samples are made.

Sammendrag

Analyser av grunnstoff-fordelingen i detritale kormspinell samt petrografske analyser er utført på sandsteinsprøver fra Øvre Trias De Geerdalenformasjonen på ulike steder på Svalbard, for å finne sandsteinsprovenance. Petrografisk identifikasjon av mineraler og bergartsfragmenter brukes til å identifisere kildebergart-litologi. Det aksessoriske mineralet kromspinell benyttes som petrogenetisk markør for å skille mafiske og ultramafiske kildebergarter dannet i ulike tektoniske miljø.

Alle detritale kromspinell i studien har et Fe^{3+} innhold over 25% og et Al innhold under 30%, når man sammenligner de treverdige kationene: Cr, Fe^{3+} og Al. Sammenlignes de toverdige kationene Mg og Fe^{2+} er Mg- innholdet mellom 38 og 94%. Apatitt, kromspinell, granat, rutil, turmalin og zirkon er tungmineralene observert i sandsteinen, sammen med bergartsfragmenter av vulkansk og metapelittisk opprinnelse. Polykrystallin kvarts består av deformerte kvartskorn, flint og spikulitter.

Ved å sammenligne kjemisk sammensetning av ulike kromspinell med publiserte kjemiske sammensetninger, sannsynliggjøres en mafisk eller ultramafisk kontinental intrusjon som opprinnelse. Kontinentale intrusjoner dekker bergarter som flombasalter, grunne vulkanske intrusjoner og lagdelte intrusjoner. De observerte vulkanske bergartsfragmentene i De Geerdalenformasjonen og kromspinellene kan ha lignende opprinnelse. Ellers indikerer bergartsfragmenter og tungminerealer varierende kildebergartlitologi av metasedimentær, sedimentær, vulkansk og felsisk opprinnelse.

Den nærmeste kjente mulige kilde til kromspinell med kontinental intusjonsammensetning, og den sannsynlige kilden til De Geerdalenformasjonens kromspinell, ligger på Taimyrhalvøya, som representerer den nordligste delen av de Sibirske Trappene Store Magmatiske Provins. Denne provenancetolkningen støttes av zirkonaldre i De Geerdalenformasjonen relatert til de Sibirske Trappene. Ingen observasjoner tyder på varierende provenance mellom ulike steder eller prøver på Svalbard.

Acknowledgments

I would like to thank Professor Mai Britt Engerness Mørk, my supervisor, for good feed- back and guidance through this process. I would also thank Atle Mørk and Sintef for initiating this project as well as organizing the fieldwork in collaboration with the Norwegian Petroleum Directorate and the University Centre in Svalbard. Thank you Gareth Lord, Turid Haugen and Jonas Enga for your help logging and sampling in the field. Finally, I would like to thank my wife Alan, my daughter Sunniva and all of my family for your support and patience.

Table of content

List of figures

List of tables

1 Introduction

This study aims to investigate the sandstone provenance of the De Geerdalen Formation, Svalbard, by petrographic analysis and chemical variations in the accessory mineral chromium spinel. Earlier works on the De Geerdalen Formation provenance describe mineralogical immature sandstones with a high lithic clasts proportion, as well as a diverse heavy mineral composition (Mørk, 1999, Riis et al., 2008, Mørk, 2013). Petrographic analysis provides a tool in this thesis to identify provenance relevant De Geerdalen Formation sandstone characteristics. When accessory heavy minerals such as zircon and chromium spinel are investigated in detail, they may provide information about mineral age or petrogenesis. A focus in this thesis is on the chemical composition of the mineral chromium spinel. When comparing chromium spinel compositions to empirical data, a tectonic setting of the mafic to ultra-mafic source rock could be revealed.

2 Geological background

To evaluate possible provenance to the De Geerdalen Formation sandstones an understanding of Svalbard's geology and surrounding areas geology is necessary. The geology of Svalbard is closely tied to the Barents Sea (Worsley, 2008), shown in Figure 2.1, an area of continental crust buried under sedimentary rocks and ocean. The Barents Shelf is bordered by the Arctic Ocean, North Russia with Novaya Zemlya to the east, Norway and the Kola peninsula to the south while the North Atlantic Ocean and Greenland lays to the west. Possible sources to Barents shelf sediments can be expected to be found in the areas surrounding the Barents Sea, paleo heights within it, or Greenland.

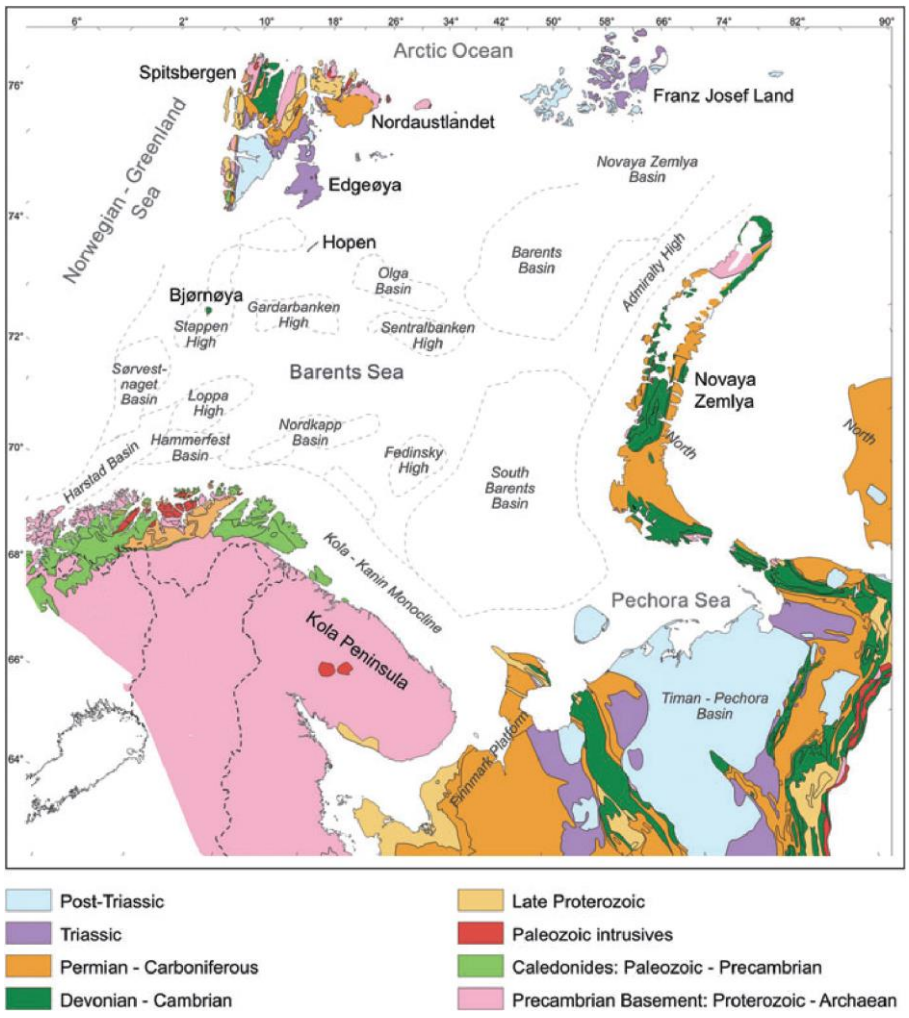

Figure 2.1 *present day Barents Sea with surrounding geology (Mørk 1999, in Worsley et al. 2008)*

2.1 Post Caledonian geologic history of Svalbard

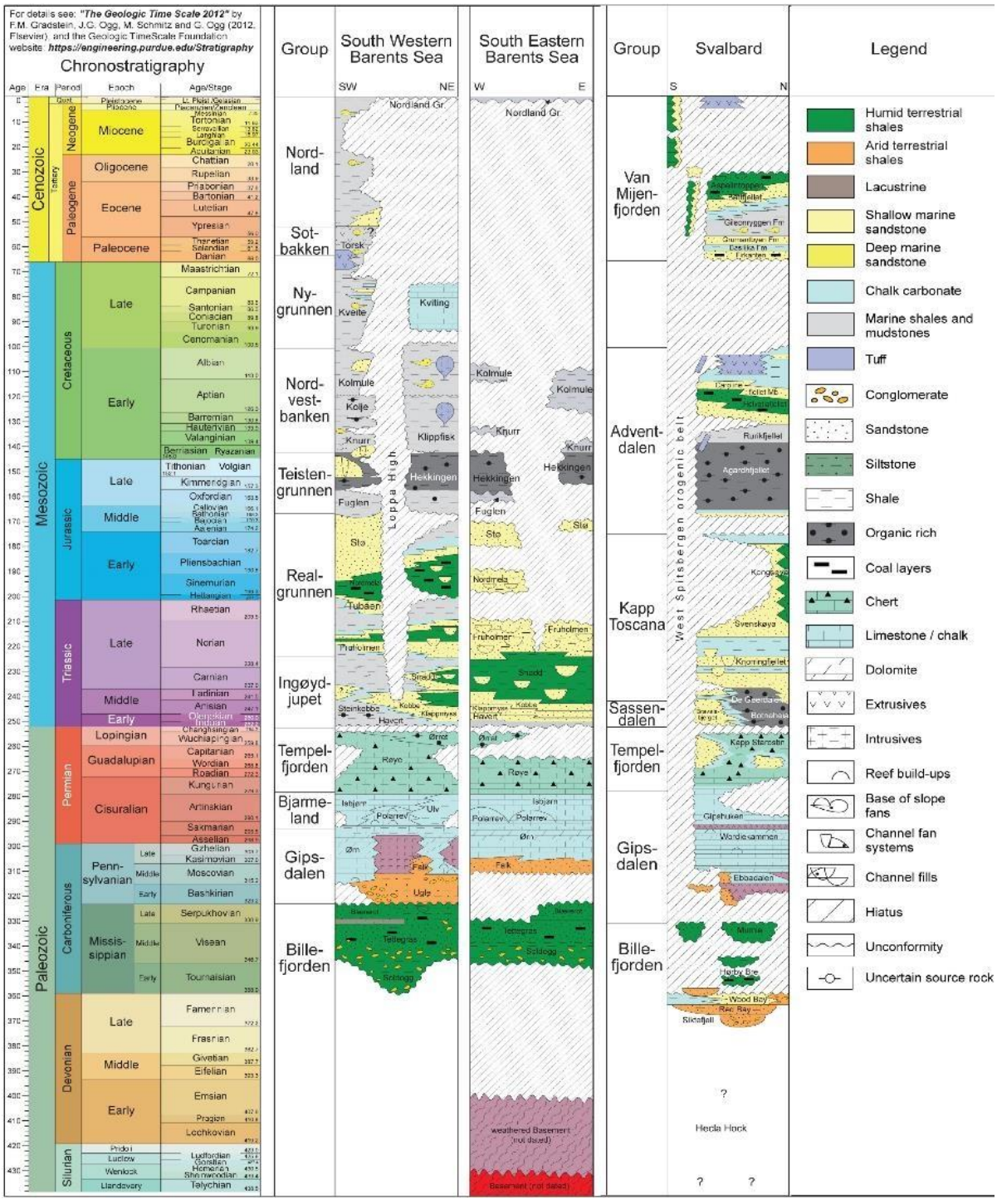

Figure 2.2 *Combined lithostratigraphic and chronostratigraphic column of the post Caledonian Svalbard and Barents Sea. The Stratigraphy is based on Worsley (2008), Worsley et al. (1988), Dallmann (1999) and Larssen et al. (2005).*

Svalbard displays an almost continuous sedimentary succession on which paleolatitude and tectonic regimes in areas surrounding the Barents Sea have had a major impact. A continuous northward drift since the Devonian have brought Svalbard through different environments, to

its present high arctic position (Worsley, 2008). The northward drift was at its fastest in the Paleozoic and early Mesozoic, with a relative slower drift in the Jurassic and Cretaceous. A rock record of different environments from tropical wet, to, arid, temperate and cold are represented in the different formations (Dallmann, 1999, Worsley, 2008). In the archipelago, strong NNW-SSE lineaments represent Caledonian faults that subsequently have been reactivated in later tectonic events (Fossen et al., 2006). Important tectonic events occurred in Late Devonian- Early Carboniferous and Middle Jurassic - Early Cretaceous. The final opening of the North Atlantic on the Paleocene- Eocene border leads to a transpressure event creating the West Spitsbergen Fold- and Thrust Belt on Svalbard (Dallmann, 1999). This resulted in extensive folding and abducting of the earlier strata, including the De Geerdalen Formation.

The first post Caledonian sedimentary deposits are the Devonian "Old Red Sandstones". They are deposited in extensional rift basins mainly on land (Fossen et al., 2006). Later Carboniferous and Permian deposits change from a fluvial terrestrial setting in the Early Carboniferous into evaporites and a stable carbonate platform in Early Permian (Worsley, 2008). The Early Cretaceous Gipsdalen Group fluvial sandstones, shales and coal reflect a humid climate compared to the arid Billefjorden Group carbonates, evaporites and red sandstones (Worsley, 2008, Dallmann, 1999). By the late Permian, a change in climate caused by shifting seaways and higher latitudes resulted in predominantly clastic sediment deposition (Worsley, 2008). The late Permian sediments also have a high biogenic silica content (Worsley, 2008).

Early and Middle Triassic is characterized by deposition of mainly mudstones, with some sand beds in more proximal areas in west Spitsbergen (Worsley, 2008, Riis et al., 2008). The Middle Triassic Botneheia and Bravaisberget formations are organic rich, and deposited in a stable anoxic environment (Riis et al., 2008). In the Late Triassic, the shallow marine to delta top De Geerdalen Formation is deposited. As the De Geerdalen Formation is the topic of this study, it is presented in more detail in a following sub-chapter. The uppermost Triassic and Lower Jurassic sediments are coarser, and more mineralogical mature compared to older Triassic strata (Riis et al., 2008, Worsley, 2008). Less sediment input at this time combined with slower subsidence favour local reworking and coarser sediments (Worsley, 2008).

A general transgression in the Jurassic leads to the formation of Middle and Upper Jurassic black shales deposited in relative deep water and under anoxic conditions (Worsley, 2008). In the Early Cretaceous deposition of fine-grained muds prevail until an uplift in the northern Barents Sea leads to deposition of southward wedges with coarser material (Worsley, 2008,

Dallmann, 1999). At the same time, a volcanic region cantered east of present day Svalbard was active, resulting in several magmatic intrusions found in the sedimentary formations (Grogan et al., 2000). The Upper Cretaceous strata are eroded on Svalbard, but a thick Paleogene sequence is present, deposited to the east of the tertiary fold-and-thrust belt on west Spitsbergen. In Neogene, glaciations combined with general uplift caused extensive erosion and deposition of glacial related sediments (Worsley, 2008). Some volcanic activity to the northwest of Svalbard is also present in the early Quaternary (Worsley, 2008).

2.1.1 The De Geerdalen Formation

The highly heterogeneous clay, silt, coal and sand containing De Geerdalen Formation outcrop in several localities in the Svalbard Archipelago. The formation is deposited in the Carnian to Early Norian in the Late Triassic (Riis et al., 2008, Vigran et al., 2014), the offshore equivalent, the Snadd Formation, are of a similar age (Figure 2.3) (Lundschien et al., 2014). On Svalbard the thickness of the formation varies from over 600 meters in the east on Hopen, to below 200 meters in the west (Lord et al., 2014). The dominant lithology is mudstones constituting of clay and silt. Sandstone bodies of varying geometries are common in the formation, deposited in what is interpreted to be a delta top depositional environment (Riis et al., 2008). Several paleosols, typically associated with thin coal seams are common in the formation (Rød et al., 2014, Klausen et al., 2015, Riis et al., 2008).

The De Geerdalen Formation can be described as delta top sediments representing the top of prograding clinoforms (Lundschien et al., 2014, Klausen et al., 2015). The regressive nature of the formation favour different local depositional environments. Floodplain facies with well-developed channel sandstones are present as well as tidal and wave dominated depositional environments (Rød et al., 2014). High sediment supply and a broad sallow shelf created low laying deltas with non-marine deposition (Klausen et al., 2015). In transgressions significant landward coastline shifts covered and partially reworked the sediments (Klausen et al., 2015).

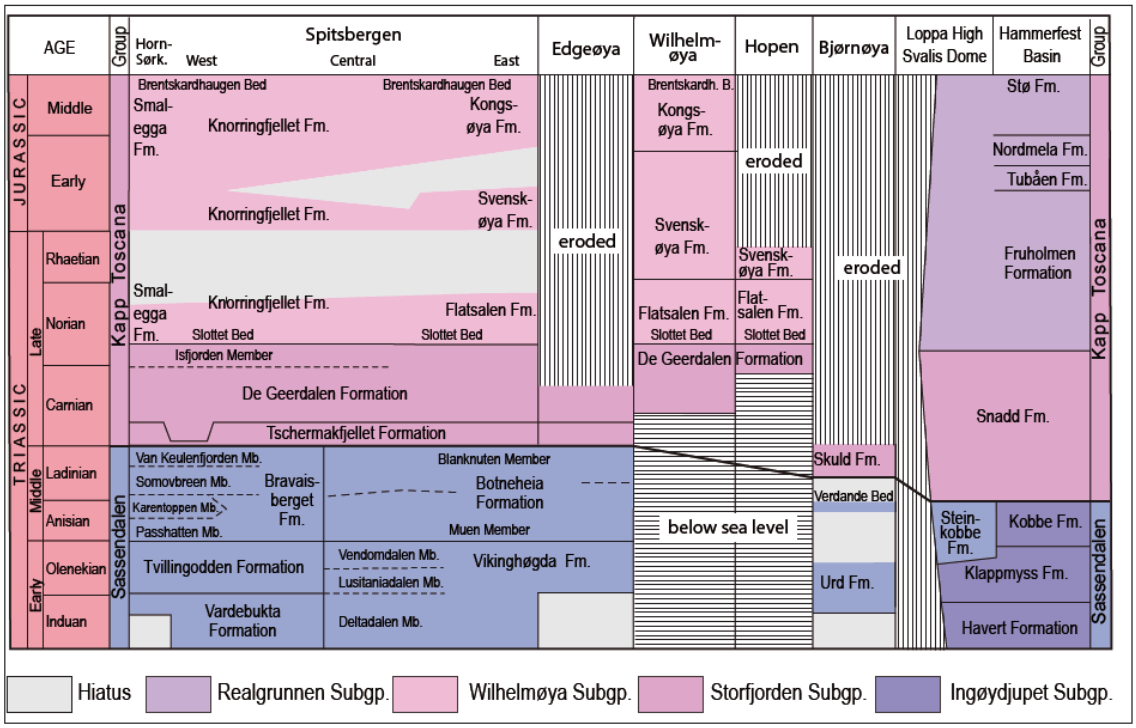

Figure 2.3 *a lithostratigraphical scheme of the Sassendalen and Kapp Toscana Groups. The Barents Sea Snadd Formation are interpreted to be the offshore equivalent of the onshore De Geerdalen and Tschermakfjellet Formations. From Lundschien et al. (2014) based on Dallmann (1999).*

The De Geerdalen Formation sandstones are described by Mørk (1999) and (Mørk, 2013) as shown in Figure 2.4 to be arkosic arenites to lithic arenites. The sand is very fine to medium grained and very well sorted (Mørk, 2013), and with clasts that are described as angular to sub-angular (Mørk, 1999). Channels with medium grained sand represent the coarsest fraction of the siliciclastic sediments.

A high proportion of lithic fragments are present in the formation. Some mica and mica schist are present, but volcanic and polycrystalline quartz are more abundant (Mørk, 1999, Riis et al., 2008, Mørk, 2013). The volcanic clasts are often fine-grained crystals or altered glass, and typically associated with fine grained mafic diagenetic minerals such as chlorite (Mørk, 2013). Polycrystalline quartz constitute the most significant part of the lithic fragments (Riis et al., 2008), and can have several origins. Soloviev et al. (2015) working on the De Geerdalen Formation equivalent on Franz Josef Land, describe felsitic volcanic clasts.

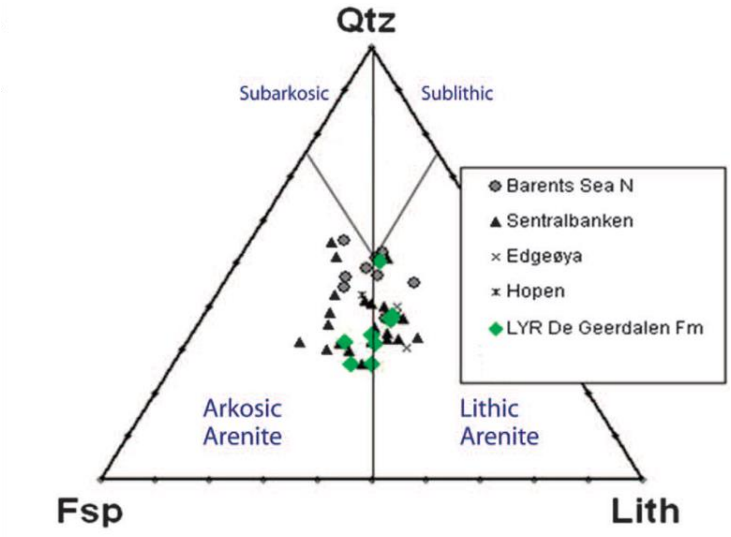

Figure 2.4 *Bulk modal analysis of the De Geerdalen Formation from Svalbard and shallow drill cores offshore in the Northern Barents Sea. Mica, accessory heavy minerals and ploygranular rock fragments, including quartz, are plotted as lithic fragments (Lith). The formation is immature, and no clear regional variations can be observed from this plot. LYR = Longyearbyen, modified after Mørk (2013).*

The accessory heavy mineral composition of the formation is described as generally similar, but with some differences between Svalbard and other localities in the Northern Barents Sea (Riis et al., 2008). Chromium spinel, zircon, tourmaline, rutile and garnet are described from Svalbard and the Northern Barents Sea in Riis et al. (2008), while observations of the Snadd Formation on Kong Karls Land describe less rutile but a presence of undifferentiated opaque minerals. On Franz Josef Land the heavy mineral distribution is similar to Svalbard's but with abundant garnet and less chromium spinel (Riis et al., 2008). In Soloviev et al. (2015) this difference is however not remarked and spinel is described in similar abundance as garnet. Additional accessory minerals described from heavy minerals fractions in Soloviev et al. (2015) are apatite and leucoxene.

2.2 Crystalline geology of the surrounding area

In Figure 2.5 the Barents Sea with its surrounding cratons together with three important orogenic events are mapped by Gee et al. (2006). As much of the area is covered by water, sea, ice or Mesozoic and younger sediments (Gee et al., 2006) some interpretation have been inferred regarding the extent of the different tectonic events that mark the area. Svalbard's own crystalline rocks are said to be a continuation of the Laurentian continent.

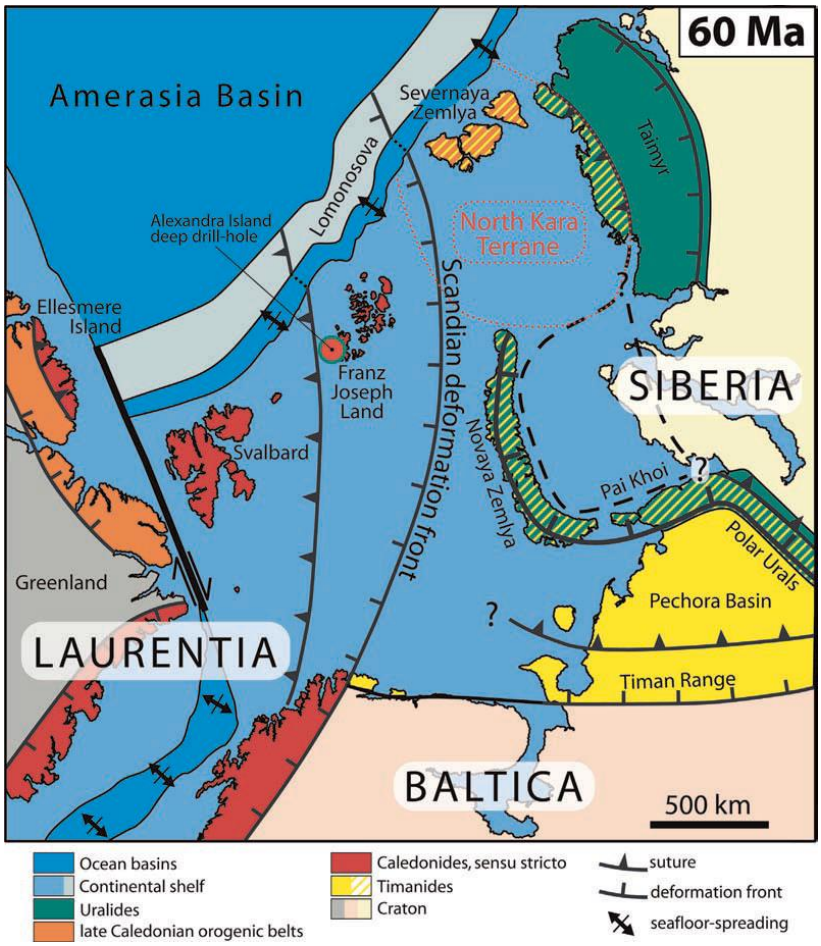

Figure 2.5 *Map of the Barents Sea and surrounding areas showing relative positions by 60 Ma from Gee et al. (2006).*

2.2.1 Baltica, Siberia and Laurentia

The geology of the continental cratons surrounding the Barents Sea are complex, with diverse rocks of Archean to Neoproterozoic ages (Gee et al., 2006, Bue and Andresen, 2013). Different intrusive and metamorphic rocks of Neoarchean and Paleoproterozoic age are known both from Laurentia and Baltica (Bue and Andresen (2013) and references therein), while the oldest rock recorded on Svalbard have an age of ca. 2710 Ma. The rocks in the northern part of Baltica have a typical Paleo- to Mesoproterozoic age, rocks of the same ages are reported from Greenland (Bue and Andresen (2013) and references therein). In the northern and western part of Siberia Grenvillian age granites, as well as other Neoproterozoic granites are present in some abundance (Bue and Andresen 2013 and references therein). The North Kara terrene as shown in Figure 2.5 is interpreted to be a distal part of Baltica showing Timanide affinities (Gee et al., 2006).

2.2.2 Timanides

The Timanid orogeny is a Neoproterozoic to Cambrian orogeny located in the north and east of the Baltic Craton, and are thought to be caused by a collision between Baltica and Arctida (Gee et al., 2006, Kuznetsov et al., 2007). The orogenic zone can at present be traced on land from north Russia until the Varanger Peninsula, where it is truncated by the Caledonian orogenic front (Gee et al., 2006). A continuation of the Timanides together with reworked underlying Grenvillian basement into the Barents Sea shelf edge is interpreted (Puchkov, 2013, Gee et al., 2006). This includes the polar Urals, including Southern Novaya Zemlya, where several Timanid complexes are present. The rocks constitute of volcanic- sedimentary series, granitoids and a few ophiolites, the intrusive rocks are mainly andesitic, granites and rhyolites with some mafic melts present (Gee et al., 2006, Kuznetsov et al., 2007). Intrusive rocks aged between 700 to 515 Ma are associated with subduction/collisional magmatism, while extensional magmatism are observed from 565 Ma until 500 Ma (Kuznetsov et al., 2007).

2.2.3 Caledonides

Convergence between the Laurentian, Avalonia and Baltican shields ultimately led to collision and formation of the Caledonides in the Late Silurian – Early Devonian (Roberts, 2003). The Caledonian orogenic belt covered a large area, from today's Svalbard and North East Greenland, to Ireland and Nova Scotia in Canada (Roberts, 2003). This collision extended into what is now the Barents Sea, with an expected Caledonian suture between present day Svalbard and the Franz Josef Land Islands, see Figure 2.5 (Gee et al., 2006). Caledonian rocks are typically found to be between 500 and 390 Ma (Bue and Andresen, 2013) representing diverse rocks of ophiolites to gneisses, eclogites and granites.

Svalbard itself represent the Laurentian crust and display progressively higher metamorphic grade in the east, this is similar to North and East Greenland (Gee et al., 2006). Caledonian rock ages are also described from granitoids in Severnaya Zemlya.

2.2.4 Uralides

The Middle Devonian to Late Permian Uralid orogeny were caused by the convergence, subduction and eventual collision of Baltica, Kazakhstania and Siberia (Puchkov, 2009). In the Polar Urals, Baltica and Siberia collided in an almost N – S strike direction with the emplacement of an orogenic front further west by Novaya Zemlya and again turning east and

culminating in the Taimyr region (Puchkov, 2009, Gee et al., 2006). The area somewhat resembles the smaller Miocene to Quaternary Ural orogeny which is easily seen today as moderately high mountains (Puchkov, 2009).

The rocks that constitute the Uralides can be grouped a series of N – S striking zones (Puchkov, 2013, Puchkov, 2009), starting to the west and progressing east;

- Foreland Permian age sedimentary rocks.
- Paleozoic sedimentary succession.
- Meso- and Neoproterozoic crystalline basement rocks of Baltican origin, including Timanide remnants.
- Ordovician to Early Carboniferous oceanic crust and island arcs including a set of mafic- ultramafic layered intrusions.
- Zone of gneisses and sediments with large volumes of granite intrusions.
- Zone of diverse pre Carboniferous rocks (Puchkov, 2009) including weakly metamorphosed sediments and intrusive rocks.

Today only the three westernmost of these zones are outcropping in the polar Urals, but they are presumed to be present underneath the cover of sea, sedimentary rocks and the volcanic rocks of the Siberian Traps Large Igneous Province (LIP) (Puchkov, 2009).

2.2.5 Siberian Traps Large Igneous Province

The main collisional phase of the Uralid orogeny was in decline with onset of the Siberian Traps Large Igneous Province magmatism beginning at the Permian-Triassic boundary (Puchkov, 2009 and references therein). The enormous volumes of basalt erupted in a period 22- 26 Ma beginning 249,5 Ma ± 0,7 with surges of intense basalt formation separated by calmer periods (Puchkov, 2009). The Large Igneous Province flood basalts covers a large area of the Siberia shield from the Urals and eastwards (Gee et al., 2006), ending in the north with its youngest components in Taimyr around 230 Ma. Mainly mafic magmatism is associated with the Large Igneous Province, but basic magmatism is also present (Puchkov, 2012). With the upwelling of the Siberian mantle plume in the Triassic plume-swelling would have let to uplift affecting a large area, probably also Taimyr (Zhang et al., 2016).

3 Approaches to provenance

In order to find sediment provenance, several different approaches can be applied. This study applies two approaches, one based on the chemical composition of the accessory heavy minerals chromium spinel. Chromium spinel is a common accessory heavy mineral in the De Geerdalen Formation sandstones, and is investigated in detail to plot chemical composition and derive tectonic setting of the source. The other approach uses petrographic observations of sandstone clasts, texture and mineralogy to derive source rock characteristics. In literature other methods like have been applied, and given important information about the De Geerdalen Formation source rock.

3.1 Sandstone composition

Sandstones are typically enriched in clasts and minerals that are stable under surface and diagenetic conditions. The mineral distribution and proportions of sedimentary rocks are influenced by processes as weathering, transportation, deposition and diagenesis as shown in Figure 3.1 (Morton and Hallsworth, 1999). Conditions such as climate and time until removal by sediment transport influence the impact of weathering on the sediment mineral composition (Morton and Hallsworth, 1999). If detritus is positioned in soil for a long of time, chemical reactions will have time to impact the detritus more, this is especially true for some of the heavy minerals such as apatite (Morton and Hallsworth, 1999). Transportation in rivers or by wind will influence the minerals by rounding and a reduction of size and weight, but it will not reduce the mineral diversity (Morton and Hallsworth, 1999). Hydrodynamic processes at deposition will sort the sediments according to parameters such as density, size and shape (Morton and Hallsworth, 1999). The heavy mineral clasts will typically be smaller than their surrounding quartz and feldspar clasts in a sandstone according to the hydraulic equivalence principle accounting for higher specific gravity (Morton and Hallsworth, 1999).

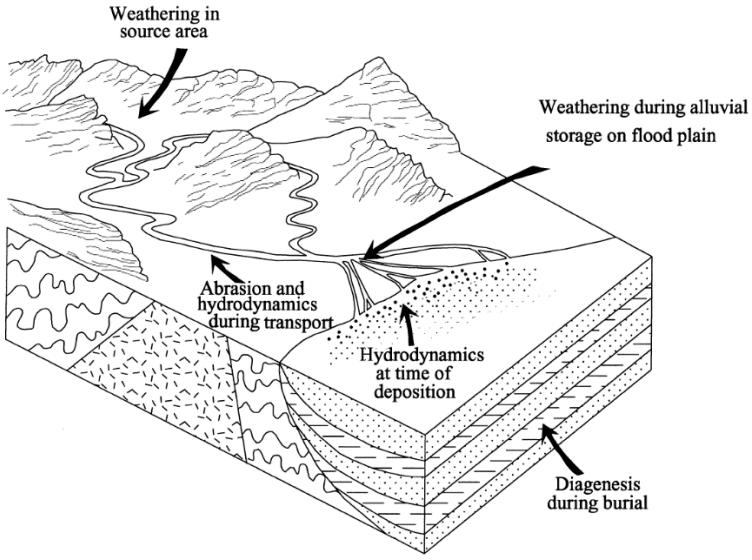

Figure 3.1 *Processes controlling the sediment assemblage in sandstones. From (Morton and Hallsworth, 1999)*

After deposition sediments will, over geologic time and continuous burial, be progressively affected by diagenesis. The most stable rock common mineral during sandstone diagenesis is quartz, followed by a general trend from felsic to mafic-ultramafic minerals being continuously more unstable (Worden and Burley, 2003). The heavy minerals also experience various grades of instability, in Table 3.1 an overview of heavy mineral stability in different basins can be used to both evaluate burial depth and evaluate diagenetic imprint on minerals when using them for provenance. Several of the heavy minerals described in the De Geerdalen Formation on Svalbard are found to be very stable according to the table.

Table 3.1 *Stability of accessory heavy minerals in sandstones from four different basins. The most stable minerals are at the top. (Morton and Hallsworth, 1999, and references therein)*

North Sea	US Gulf Coast	New Zealand	Yugoslavia
Apatite, Monazite, Spinel, TiO_2 minerals, Tourmaline, Zircon	Apatite, Chloritoid, Monazite, Spinel, TiO_2 minerals, Tourmaline, Zircon	Apatite, Chloritoid, Spinel, TiO_2 minerals, Tourmaline, Zircon	Apatite, Chloritoid, Garnet, Spinel, TiO_2 minerals, Tourmaline, Zircon
Chloritoid			
Garnet	Garnet	Garnet	
Staurolite		Staurolite	
Kyanite			
Titanite	Titanite		Titanite
Epidote	Epidote		Epidote
	Kyanite		Kyanite
Calcic amphibole	Calcic amphibole		
Andalusite, Sillimanite			
Pyroxene	Pyroxene		
Olivine			

3.2 Heavy mineral chemical composition

Investigating chemical compositions of selected heavy minerals can help provenance studies by giving more information about the source rocks igneous, metamorphic or tectonic setting (Morton, 1991). Staruolite is an example of minerals where mineral chemistry is sensitive to metamorphic grade of the source rock (Morton, 1991). The mineral chemistry of garnet is also sensitive to paragenesis, and can therefore provide source rock characteristics. A challenge with unstable minerals is different solubility depending on mineral chemistry. In the case of garnet this can result in relative enrichment of Ca-poor garnets at depth, as Ca-rich garnets would dissolve at shallower depths (Morton, 1991). The mafic to ultra-mafic mineral chromium spinel have different chemistry dependent on the tectonic setting at formation. This can subsequently be useful in identifying tectonic setting of a mafic to ultra-mafic source rock (Cookenboo et al., 1997, Barnes and Roeder, 2001).

3.2.1 Chromium spinel in provenance

Unlike other mafic to ultra-mafic minerals, chromium spinel is stable under surface and diagenetic conditions (Morton and Hallsworth, 1999). Much investigated stable minerals such as zircon or garnet gives information about the felsic or metamorphic history of a source rock, chromium spinel compositions on the other hand can give information about the mafic to ultra-mafic history (Barnes and Roeder, 2001). When chemical composition of several mineral grains are plotted and compared Cookenboo et al. (1997), Arai (1992), Barnes and Roeder (2001) and Kamenetsky et al. (2001) have been able to describe the tectonic setting in which a mafic – ultramafic source rock have been formed, based on detrital chromium spinel. The different igneous and metamorphic processes controlling chromium spinel chemical compositions in different tectonic environments are discussed at length in work such as Kamenetsky et al. (2001), Barnes and Roeder (2001) and will not be discussed further in this study.

The name “chromium spinel” are in this thesis used to describe the minerals in the spinel group that contain the element chromium. A generalized formula of the spinel group minerals; XY_2O_4 covers a range of different minerals in solid- solution (Barnes and Roeder, 2001). Divalent cations such as Mg, Fe^{+2}, Ni, Mn, Co and Zn constitute the X position, while the trivalent cations Cr, $Fe^{+3}$and Al are constitutes the Y position in the mineral formula (Barnes and Roeder, 2001 with corrections after personal communication, January 2016). Ti and V are also associated with spinel group minerals, Ti in lamellae of Ti^{+4} $Fe^{+2}{}_2$ O_4, ulvöspinel (Biagioni and

Pasero, 2014, Barnes and Roeder, 2001). V has variable valence and are in this study treated as in Barnes and Roeder (2001) and taken in as a theoretical $Fe_7V_2O_{12}$ component, there are however spinels such as culsonite where V is the trivalent cation (Biagioni and Pasero, 2014). A (Mg, Fe) (Cr, Al, Fe)$_2$ O_4 formula include the major elements inspected, while the other substitutions are not uncommon.

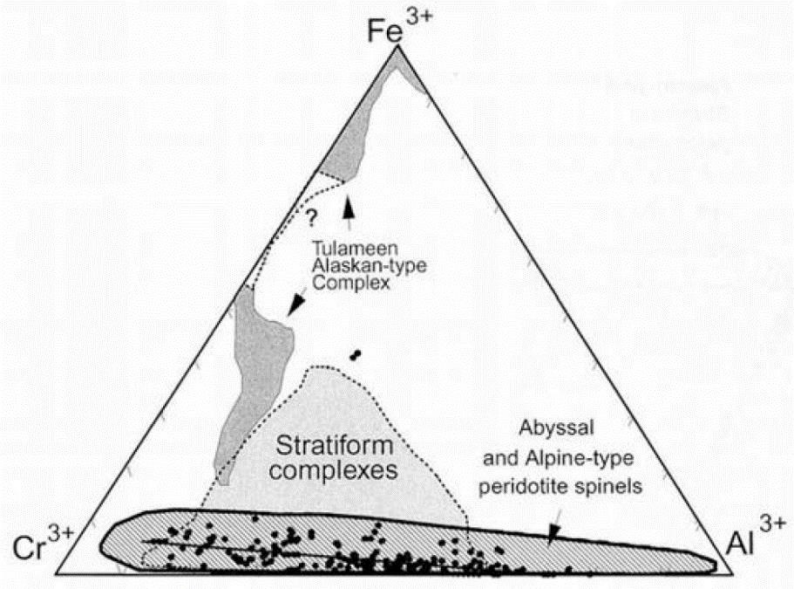

Figure 3.2 *Triplot of the major trivalent chromium spinel cations with contours showing magmatic environments associated with some compositions. After Cookenboo et al. (1997)*

After plotting chromium spinel compositions in discrimination diagrams, tectonic environment is determined when comparing values to empirical data such as in Barnes and Roeder (2001). Figure 3.2 show the different types of magmatic melts plotted within defined areas, allowing petrogenic discrimination. Discriminating the Ti content in chromium spinels can also indicate type of magma as shown by (Arai, 1992, Kamenetsky et al., 2001). Barnes and Roeder (2001) have developed several discrimination diagrams from a range of magmatic environments applicable for comparing this kind of detrital chromium spinel data.

3.3 Previous work on the De Geerdalen Formation provenance

Several works using different approaches both in data type and interpretation, contribute to the present day understanding of the De Geerdalen Formation provenance. The different

approaches to provenance relevant information can be grouped as based on sedimentology, seismic interpretation, petrography/petrology and geochronology.

3.3.1 Sedimentological evidence and depositional geometries

Crossbedding in fluvial channels in the upper De Geerdalen Formation of eastern Spitsbergen are reported by Knarud (1980) as referenced in Riis et al. (2008) to give a west northwest trending sedimentation direction. This observation is supported in later work such as Klausen and Mørk (2014). In Rød et al. (2014) a more proximal depositional environment was observed in east southeast indicating a northwestward sediment deposition.

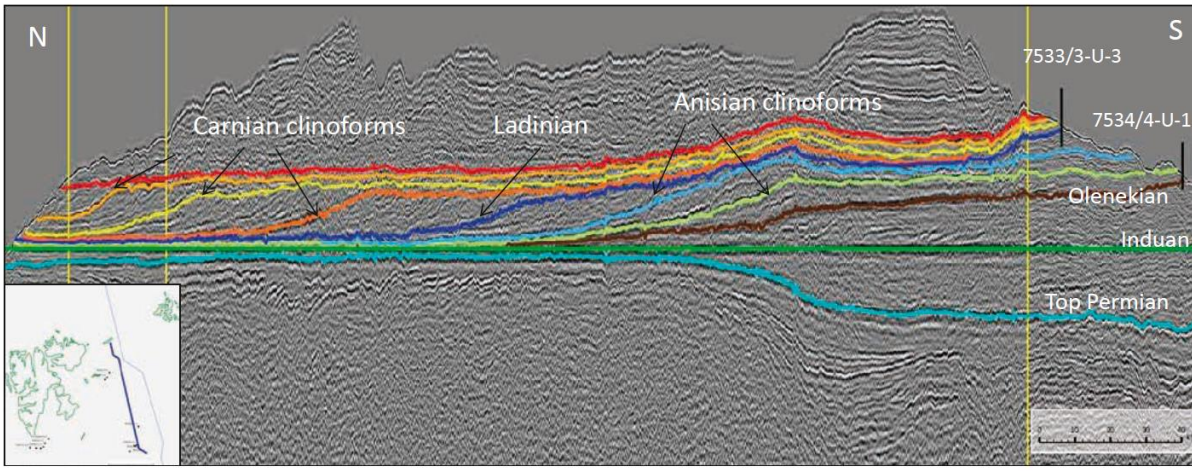

Figure 3.3 *showing prograding clinoforms north of the Olga basin, offshore east Svalbard. The seismic section is flattened on top Induan. Figure from Lundschien et al. (2014)*

Several studies based on seismic interpretation of the Norwegian Barents Sea have described northwestward prograding clinoforms of the Middle to Late Triassic Snadd Formation (Riis et al., 2008, Høy and Lundschien, 2011, Klausen et al., 2015). In Figure 3.3 a flattened seismic cross section of the Triassic is presented along with interpreted horizons. In Figure 3.4 the clinoforms breaks are mapped out and a west, northwestwardly progradation of the clinoforms fronts becomes visible (Lundschien et al., 2014). The prograding clinoforms and their direction are suggested to show a southeast source area for the Snadd and De Geerdalen Formations (Riis et al., 2008, Lundschien et al., 2014, Klausen et al., 2015).

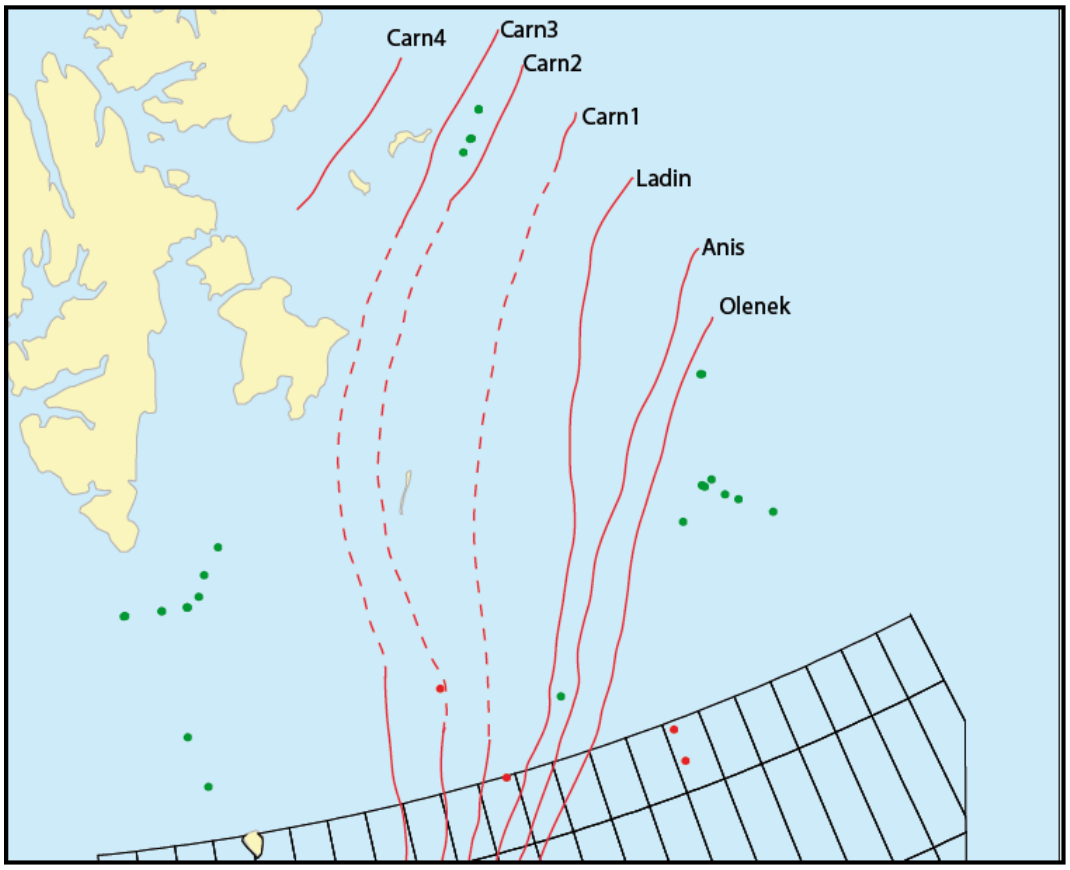

Figure 3.4 *showing outlines of the Middle to Late Triassic prograding clinoforms of the Northern Barents Sea. Red labelled lines are seismically detectable breaks in the clinoforms. Green marks are Norwegian Petroleum Directorate stratigraphic boreholes. Red marks are IKU-SINTEF stratigraphic boreholes. Black grid represents Norwegian Petroleum Directorate quadrants for petroleum exploration. Figure modified after Lundschien et al. (2014).*

3.3.2 Petrographic and petrologic evidence

Quantitative modal analysis of the formation, as show in Figure 2.4, shows a mineralogical immature sandstone with a similar appearance at different locations on Svalbard (Mørk, 2013). The immature sandstones may reflect both the depositional environment of the De Geerdalen Formation and the tectonic setting of the sediment source, as discussed in e.g. Mørk (1999).

By detailed trace element and cathodoluminescence of different detrital quartz Muller and Knies (2013) describe characteristics of the De Geerdalen Formation quartz population based on samples from a location on Blanknuten, Edgeøya. Cathodoluminescence properties of quartz according can help classify quartz origin. Muller and Knies (2013) classify the investigated De Geerdalen Formation sandstones in four distinct categories. Two of the quartz types correspond to between 48 - 63% of the total quartz population, originate as low- grade metamorphic quartzite and/or low- temperature hydrothermal alteration (Muller and Knies, 2013).

Polycrystalline and polyphase quartz grains constitute 10 – 18% of the bulk proportion, and originate as low grade metamorphic quartzite (Muller and Knies, 2013). The last type of grains, constituting 27 – 34% of the quartz, originate in plutonic or high grade metamorphic rocks (Muller and Knies, 2013).

The lithic clasts, that is mica, mica schist, volcanic fragments and polycrystalline quartz (Mørk, 1999) reveal provenance sensitive information. The mica schist present in the sediments indicate important contributions from the metamorphic source rock. A source to the commonly observed volcanic fragments are not suggested in literature on Svalbard (Riis et al., 2008), on Franz Josef Land the detrital magmatic rock input is suggested to come from the Siberian Plume system (Soloviev et al., 2015). The Upper Permian biogenic silica enriched deposits in the Kapp Starostin Formation of Svalbard are suggested by Riis et al. (2008) as a possible source to De Geerdalen polycrystalline quartz.

The accessory heavy minerals described from De Geerdalen thin sections are zircon, chromium spinel, tourmaline, rutile and garnet (Mørk, 1999, Mørk, 2013). As the chemical stability of different minerals varies during burial diagenesis, the presence of some minerals is dependent on diagenetic evolution (Morton and Hallsworth, 1999). The heavy minerals on Svalbard are however mostly stable, with garnet being the least stable (Morton and Hallsworth, 1999). The very presence of chromium spinel indicates a mafic or ultra-mafic source contribution, while the presence of zircons indicates felsic sources (Soloviev et al., 2015). The zircons on Franz Josef Land are from morphological studies described as sourced from peraluminous granites in association with calcalkaline, subalkalie and alkaline granitoids (Soloviev et al., 2015). Garnets indicate mainly metamorphic origin. For the most stable heavy minerals such as zircon, recycling of older sediments is a distinct possibility, as these minerals are so stable that they can remain over several cycles of redeposition (Morton and Hallsworth, 1999).

3.3.3 Geochronological evidence

Provenance relevant evidence from detrital uranium – lead zircon geochronological ages on sedimentary rocks on Svalbard and other areas around the Barents Sea displays a distinct zircon age distribution for the De Geerdalen and equivalent formations (Bue and Andresen, 2013, Soloviev et al., 2015). Bue and Andresen (2013) generated zircon age distributions for the Mesozoic sedimentary layers on Svalbard, and in that way being able to compare the imprint of different provenance areas. The De Geerdalen Formation was sampled at three different

locations on Svalbard, as described in Figure 3.5, showing a similar zircon age distribution distinct from the underlying Middle and Lower Triassic sediment distribution (Bue and Andresen, 2013). The uppermost Triassic and Lower Jurassic display a mixed signature, and probable recycling of earlier deposited zircons (Bue and Andresen, 2013). Comparable results are reported in Soloviev et al. (2015) focusing on Franz Josef Land Triassic sediments. This article also displayed a distinct detrital zircon age distribution for an equivalent formation to the De Geerdalen Formation (Soloviev et al., 2015).

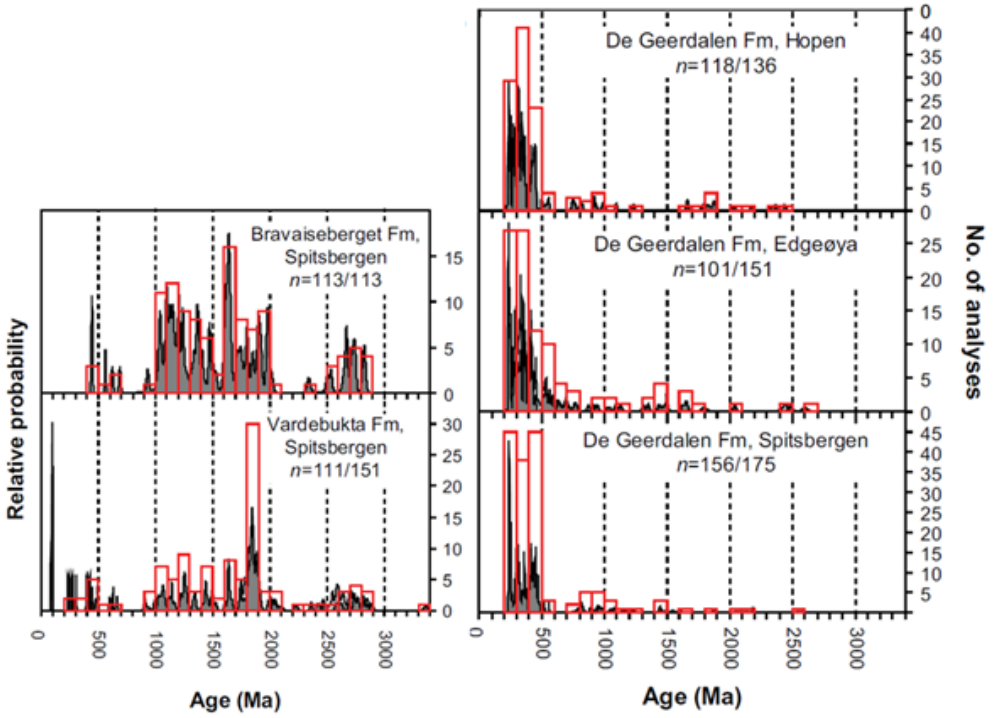

Figure 3.5 *showing the U/Pb zircon age distribution of Bravaisberget, Vardebukta and De Geerdalen formations sampled at different localities on Svalbard. The De Geerdalen Formation signature is recognized with Palaeozoic and Mesozoic age peaks, and few older zircons represented. The underlying formations are distinct different with Proterozoic and Archean zircon peaks dominating the sediments. Bue and Andresen (2013).*

As seen in Figure 3.5 the distinct signature of the De Geerdalen Formation zircons are younger with only minor contributions giving Proterozoic and Archean ages, this is distinctly different from the underlying formations. Both Bue and Andresen (2013) and Soloviev et al. (2015) attributed the different zircon age signature to a change in provenance, and that the zircon ages correlates well with Uralide ages (Soloviev et al., 2015, Bue and Andresen, 2013). An increase in Caledonian zircons are also present, inferring a source of this age, either from the Caledonian orogeny, or from the east as this age is observed on Severnaya Zemlya (Bue and Andresen,

2013). The youngest ages are suggested to be related to Large Igneous Province magmatism of the Siberian Traps, ending around 230 Ma (Bue and Andresen, 2013, Soloviev et al., 2015).

4 Sampling strategy

Samples were collected in two different expeditions to Svalbard in August 2014. The first expedition, organized by the Norwegian Petroleum Directorate, went to Edgeøya and Hopen. A second expedition, organized by Sintef, the Norwegian University of Science and Technology and the University Centre in Svalbard, went to Kapp Toscana in west Spitsbergen. With samples from different locations in Svalbard, a more regional approach to the De Geerdalen Formation could be achieved. Samples were for each location collected in regular intervals in sandstones and siltstones. Possible variations in petrography and chromium spinel composition, based on differences in depositional environment or sedimentary facies of the sample, have not been investigated further. Stratigraphic logging and sampling were done in collaboration with individuals such as Jonas Enga, Turid Haugen and Gareth Lord, all connected to NTNU.

Table 4.1 *Sampling locations with UTM coordinates and number of samples taken during fieldwork on Svalbard August 2014.*

Location name	Location description	Position	UTM	Stratigraphic column	Number of Samples	Approx. sampling distance
Iversenfjellet	Hopen	X0446533 N8487870	35	Appendix 2	30	3-4 m
Negerfjellet	Edgeøya	X0392064 Y8585416	35	Appendix 3	36	3-4 m
Tjuvfjordhorga	Edgeøya	X0395946 Y8592314	35	Appendix 4	22	10 m
Blanknuten	Edgeøya	X0366863 Y8661964	35	Samples only	3	n/a
Kapp Toscana	Spitsbergen	X0501340 Y8608640	33	Sampled sandstones	24	4-5 m
Bravaisodden	Spitsbergen	X0500390 Y8614306	33	Sampled sandstones	16	4-5 m
Festningen	Spitsbergen	- -	33	Festningen Kapp Toscana Gp stratigraphic column from Vigran et al. (2014)	28	4-5 m

Sandstone and siltstone samples were collected at regular intervals while logging. Interval distance varied between locations because of allocated time, weather and wildlife conditions. Regular sampling distance was emphasised with grain size, sedimentary structures or other observations not influencing the sampling. In Table 4.1 approximate sampling distances in vertical meters are listed, the table also describes sampling locations and numbers of samples taken at the different locations. Field observations of lithologies, grain size, sorting and

structures are combined into stratigraphic columns, later digitalized using a legend of Vigran et al. (2014). Three stratigraphic columns showing sampling points were produced (Appendix 3-5).

5 Method

5.1 Optical microscopy

Thin sections were used for a petrographic analysis of De Geerdalen Formation sediments. Polarized thin sections were prepared with blue epoxy at the thin section laboratory at the Department of Geology and Mineral Recourses Engineering, Norwegian University of Science and Technology (NTNU). A standard petrographic microscope under plain- and cross-polarized light were used to describe textures and mineralogy. The grain clasts were described for identification of possible source area characteristics. Investigation of accessory heavy minerals, with emphasis on chromium spinel was performed by optical microscopy for planning of electron microprobe analyses of selected minerals.

In all 31 thin sections are studied, 23 from fieldwork in Svalbard 2014 and supplemented with existing thin sections from a former expedition (see sample location subchapter). Descriptive data such as sorting, roundness and grain size were gathered by visually comparison to available standards.

5.2 Concentrating chromium spinel

As the bulk rock composition of chromium spinel in the De Geerdalen Formation sandstones is accessory, an attempt to concentrate the mineral was made. The processes included several steps where at first 10 samples were crushed in a small size jaw crusher until the maximum clast size were 5 cm. The samples were then crushed several times in a smaller Retsch jaw crusher until the maximum grainsize were within the sand fraction (less than 2mm diameter). Sieving of the samples distributed the clasts in 4 different clast sizes; below 0,064 mm, between 0,064 mm and 0,125 mm, between 0,125 mm and 0,256 mm and above 0,256 mm.

As chromium spinel is a low magnetic mineral with a magnetic susceptibility of 0,2-0,3 Ampere for chromium spinel $(Fe,Mg)(Cr,Al)_2O_4$, magnetic separation of the mineral using a Franz model LFC-2 were conducted. The most magnetic minerals were removed using a single magnet before Franz separation, thus producing an own magnetic fraction for later investigation. The steps each of the samples went through are described in **Table 2**. The Franz were set up with a 15^{o} tilt of magnet, 14^{o} tilt of sideway slope and 20^{o} tilt of forward slope.

Table 5.1 *showing the different steps each sample went through in order to concentrate chromium spinel, and prepare the sample for investigation.*

Name	Chrusing and Sieving	Fractions	Magnetic fraction	Fraction undergone magnetic separation			Perepared for SEM	Thick section
				Below 0,064mm	0,064 - 0,124 mm	0,124 - 0,256 mm		
EØ 10	Yes	4	Yes	Yes	Yes	Yes	No	No
EØ 25	Yes	4	Yes	Yes	Yes	Yes	All 4 fractions	Below 0,064 fraction and 0,064 - 0,124 fraction
FES 5	Yes	4	Yes	No	Yes	No	0,064 - 0,124 fraction	No
FES 24	Yes	4	Yes	Yes	Yes	Yes	No	Below 0,064 fraction
H 18	Yes	4	Yes	Yes	Yes	Yes	No	
H 30	Yes	4	Yes	Yes	Yes	Yes	No	No
KTO 14	Yes	4	Yes	Yes	Yes	Yes	Below 0,064 fraction and 0,124 - 0,256 mm fraction	No
KTO 24	Yes	3	Yes	No	No	Yes	No	No
TJU 3	Yes	4	Yes	Yes	No	Yes	No	No
TJU 15	Yes	4	Yes	Yes	Yes	Yes	No	No

5.3 SEM analysis

5.3.1 Scanning electron microscope (SEM)

A Hitachi SU6600 Field Emission Scanning Electron Microscope were used to evaluate the concentration process described in section 3.4. Several carbon coated glass sections with mineral concentrate attached to tape were examined for chromium spinel grains in order to understand which samples and clast size were the most concentrated in the mineral.

5.3.2 Electron probe micro analyser

A JOEL JXA- 8500F Electron Probe Micro Analyser (EPMA) was used to identify heavy mineral composition and with focus on quantitative mineral analysis chemical composition of different chromium spinel mineral grains. SEM electron backscatter images were used to navigate the investigated surfaces as wells as providing a textural framework of the investigated minerals.

EPMA analyses were performed on two types of sample preparates. Four carbon coted polished thin sections were examined for chromium spinel and other heavy minerals by quantitative spectrometer analyses using mineral standards (Table 8.2)

Table 5.2 *list of standardization*

Oxide	Standardization used
Al_2O_3	Albite
Cr_2O_3	Chromite
CuO	Diopside
FeO	Hematite
K_2O	Sanidine
MgO	Diopside
MnO	Bustamite
Na_2O	Albite
P_2O_5	Apatite
SiO_2	Albite
TiO_2	Rutile
Y_2O_3	Y-ganet
ZnO	Wellimnite

The second approach used three polished thick sections of fine-grained mineral concentrates based on magnetic separation. In a third approach chromium spinel grains were studied with 4 carbon coated glass sections with mineral concentrate attached to tape. The mineral concentrates were of different grain sizes and shapes. Chromium spinel element distribution and element oxide distribution was acquired as well as calibration standards.

5.4 Sources of error

Observation during fieldwork and logging are open to human errors and misinterpretations. When doing optical microscopy, it is necessary to distinguish different minerals by its properties. Classifying partially dissolved grains, volcanic clasts of different mineral composition and different types of chert/quartz have been challenging, and human error may have occurred.

In EPMA analysis errors related to the validity of results from sample points with uneven surfaces can be discussed. Several data points were gathered from mineral grains attached to tape, and were therefore expressing uneven surfaces on the individual grains. This may cause a different scattering of electrons than what the EPMA would be expecting in order to make correct calculations. Grain topography may also cause overshadowing of the lower laying grains by higher, this would also potentially lead to distorted scattering of elections within the EPMA, and erroneous analytical results. There may also be errors related to the standardizations of the mineral chemical analyses.

Pollution of the samples by metal or dirt while crushing and sieving could be a source of error, and could potentially have happened at several steps during the processing of samples. The jaw crushers did use metal parts, and pieces of metal could easily be chipped of into a sample.

A possible cause of errors is related to the magnetic separation process, as the predicted magnetic susceptibility is 0,2 to 0,3 Ampere. This is based on empirical data that do not include Iron in the trivalent position of the spinel formula. Since iron in this position greatly influence the minerals magnetic susceptibility, and approaches magnetite in pure form, it is reasonable to assume a wider spectra of magnetic susceptibility. Errors of either overrepresentation or underrepresentation of the iron rich chromium spinels are therefore present.

6 Results

Results from the petrographic investigations as well as chromium spinel chemical compositions are presented. Thin section and SEM petrographic observations providing information about a source constituting of metamorphic and volcanic rocks as well as cherty sediments. Chromium spinel compositions have been plotted and compared to each other to assess quality of data, and used to find petrogenesis.

6.1 Field observations and sampling

Systematic sampling and stratigraphic logging during the two expeditions in Svalbard provided an extensive set of samples. In Figure 6.1 sampling locations are displayed on a geological map of Svalbard. Two thin sections sets were prepared from the Blanknuten second location (SV-4-7) and Adventdalen (DH4-875-36) locations in addition to samples taken as a part of the study.

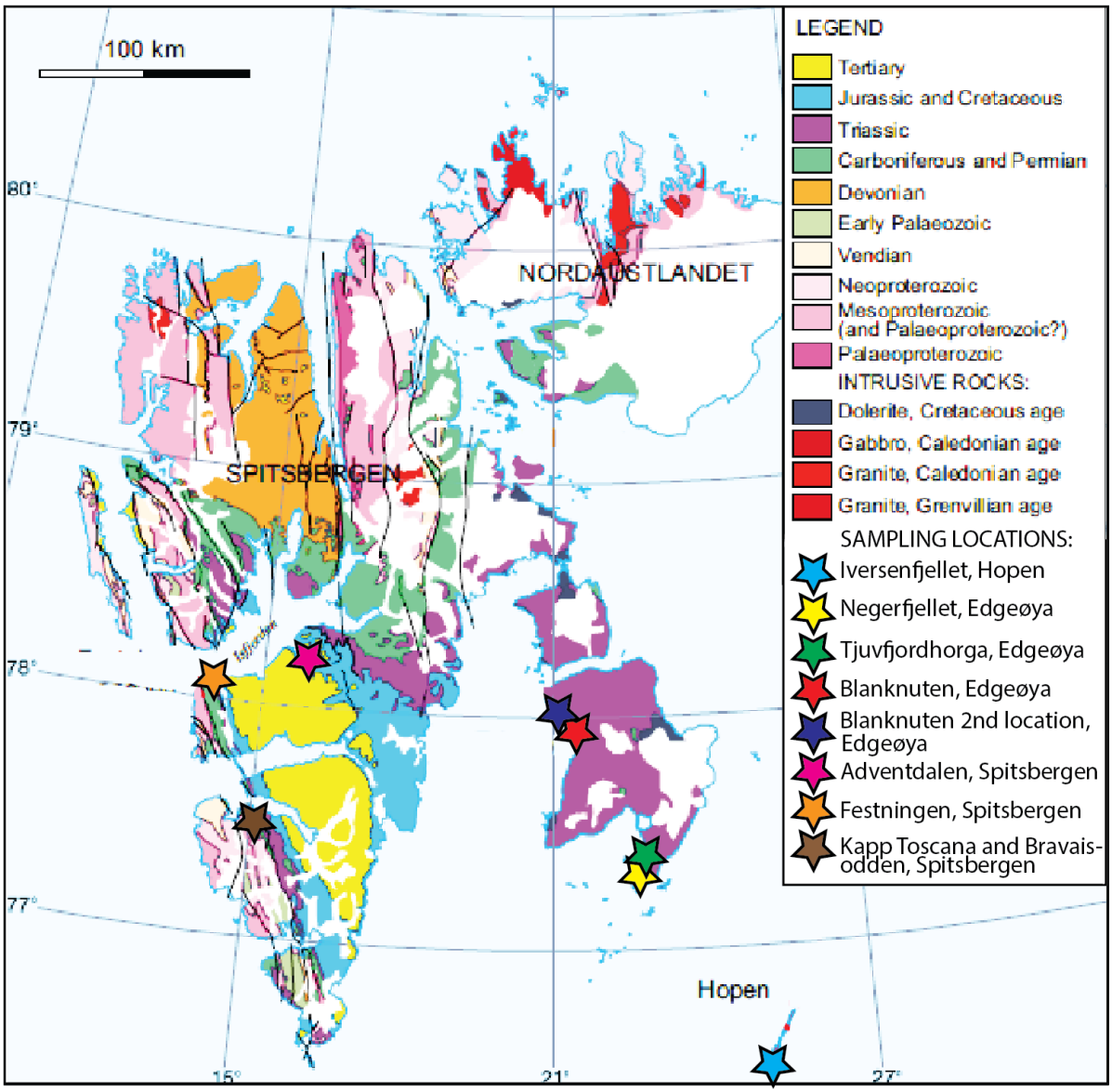

Figure 6.1 *Geological map of Svalbard with sample locations. Adventdalen and Blanknuten 2nd location is provided by NTNU, other samples by the author. Map modified after Dallman et al. (2002).*

Altogether 159 rock samples were collected as a part of the fieldwork as seen in Figure 6.1. Twenty-three thin sections were made as described in Table 6.1, the eleven thin sections in the first batch were randomly picked from each location. The second batch of thin sections had an emphasis on more course grained rocks. At three of the locations: Iversenfjellet - Hopen, Negerfjellet – Edgeøya and Tjuvfjordhorga – Edgeøya, stratigraphic columns containing sampling points, were created (Appendix 3-5).

Table 6.1 *List of thin sections and their corresponding sample*

Thin section	Batch	Location	Lithology
BLA1	1	Blanknuten, Edgøya	Sandstone, fine
BLA3	1	Blanknuten, Edgøya	Sandstone, fine
BRO10	1	Bravaisodden, Spitsbergen	Siltstone
BRO14	1	Bravaisodden, Spitsbergen	Sandstone, fine
BRO15	1	Bravaisodden, Spitsbergen	Siltstone
EØ1	2	Negerfjellet, Edgeøya	Sandstone, very fine
EØ12	2	Negerfjellet, Edgeøya	Sandstone, fine - medium
EØ20	2	Negerfjellet, Edgeøya	Sandstone, fine
FES12	1	Festningen, Spitsbergen	Sandstone, fine
FES21	1	Festningen, Spitsbergen	Sandstone, fine
H11	2	Iversenfjellet, Hopen	Sandstone, fine - medium
H12	1	Iversenfjellet, Hopen	Sandstone, fine
H13	2	Iversenfjellet, Hopen	Sandstone, very fine - medium
H28	2	Iversenfjellet, Hopen	Sandstone, fine
H6	2	Iversenfjellet, Hopen	Sandstone, very fine
KTO13	1	Kapp Toscana, Spitsbergen	Siltstone
KTO18	2	Kapp Toscana, Spitsbergen	Sandstone, fine
KTO19	1	Kapp Toscana, Spitsbergen	Sandstone, fine - medium
KTO22	2	Kapp Toscana, Spitsbergen	Sandstone, fine
KTO24	2	Kapp Toscana, Spitsbergen	Sandstone, fine
TJU10	2	Tjuvfjordhorga, Edgeøya	Sandstone, very fine
TJU11	2	Tjuvfjordhorga, Edgeøya	Sandstone, fine
TJU20	1	Tjuvfjordhorga, Edgeøya	Sandstone, very fine

As the western samples have been buried deeper and abducted by tectonic forces, differences between eastern and western De Geerdalen Formation samples can be expected. During fieldwork the differences are observed as a higher degree of diagenetic alteration and compaction in sandstones in the western locations Festningen, Kapp Toscana and Bravaisodden.

6.2 Petrographic observations

Optical and SEM backscatter observations from thin- sections in the De Geerdalen Formation are presented. All pictures have a scale bar and identified clasts are labelled according to **Feil! Fant ikke referansekilden.**6.2 Presented observations in each picture have a larger label size than other labels. Results from the thin section observations are organized in the following sub-chapters starting with the most common mineral clasts found in the De Geerdalen Formation sandstones. Other sub- chapters present the heavy minerals, the lithic fraction other than the

polycrystalline quartz, and polycrystalline quartz. In the end some observations concerning diagenetic alteration and autigenic minerals are included as well as observations of sandstone textures.

Table 6.2 *Labels used in the microphotographs to identify different clasts and a short description of the clast type.*

Label	Clast	Type of Clast
AlFd	Alkali feldspar	Detrital single mineral grain. (Minor)
Alt	Altered clast	Clast altered during diagenesis of unknown original composition.
Ap	Apatite	Detrital single mineral grain. (accessory)
Bar	Barite	Autigenic mineral.
BQtz	Biogenic quartz	Clast of several quartz crystals of biogenic origin.
CalC	Calcite cement	Autigenic calcite.
CarC	Carbonate cement	Autigenic carbonate cement undifferentiated.
Clay	Clay minerals	Autigenic clay minerals undifferentiated.
Clr	Chlorite clay	Autigenic clay mineral.
CrSp	Chromium spinel	Detrital single mineral grain. (accessory)
Kao	Kaolinite clay	Autigenic clay mineral.
Lith	Lithic fragment	Lithic fragment undifferentiated.
MiSc	Mica schist	Detrital metamorphic lithic fragment
Ms	Muscovite	Detrital single mineral grain. (Minor)
Opq	Opaque clast	Opaque mineral(s) undifferentiated.
ParD	Partially dissolved clast	Partially dissolved clast of unknown original composition.
Pl	Plagioclase	Detrital single mineral grain. (major)
PQtz	Polycrystalline quartz	Undifferentiated clast of many quartz crystals, lithic fragment
Py	Pyrite	Autigenic mineral
Qtz	Quartz	Detrital single mineral grain. (major)
QtzC	Quartz cement	Autigenic quartz.
Rt	Rutile	Detrital single mineral grain. (accessory)
Sd	Siderite	Autigenic carbonate mineral.
Tur	Tourmaline	Detrital single mineral grain. (accessory)
Vol	Volcanic fragment	Detrital volcanic lithic fragment.
Zir	Zircon	Detrital single mineral grain. (accessory)

6.2.1 Major and minor single mineral grains

Quartz, plagioclase, alkali feldspar and muscovite are the dominating detrital single mineral clasts found in the De Geerdalen Formation. In Figure 2.4 these elements would be classified as quartz, feldspar and lithics, respectively.

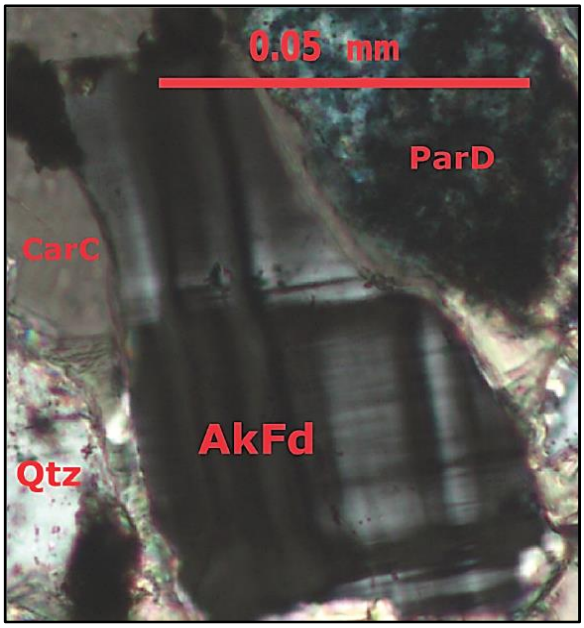

Figure 6.2 *Alkali feldspar in cross polarized light. BLA1, Blanknuten, Edgeøya.*

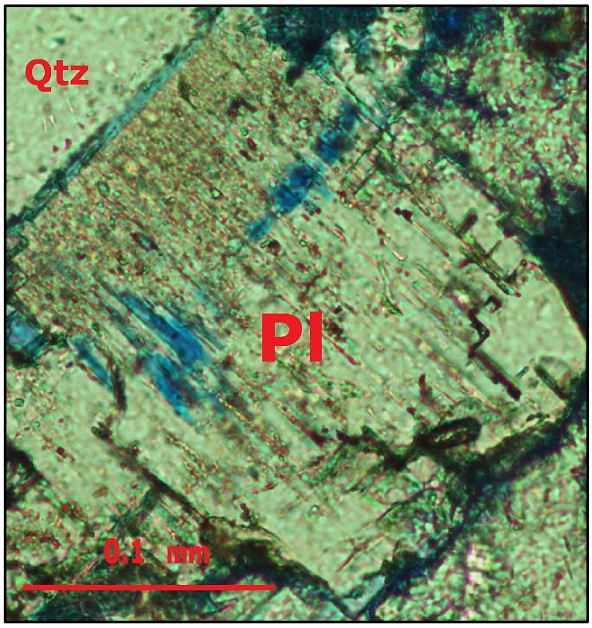

Figure 6.3 *Plagioclase in plane polarized light. H11, Iversenfjellet, Hopen.*

Few optically identifiable alkali feldspar grains, as e.g. Figure 6.2, are observed in the investigated thin sections. SEM backscatter observations reveal that there are more alkali feldspars than observed optically. Plagioclase feldspar (Figure 6.3) occurs as a major mineral in the thin sections. Plagioclase grains display a rectangular shape and sometimes visible mineral cleavage. Partial dissolution and alteration of plagioclase grains are observed in most thin sections that have not been carbonate cemented in eogenesis. Dissolution and alteration are typically observed along the cleavage of the mineral.

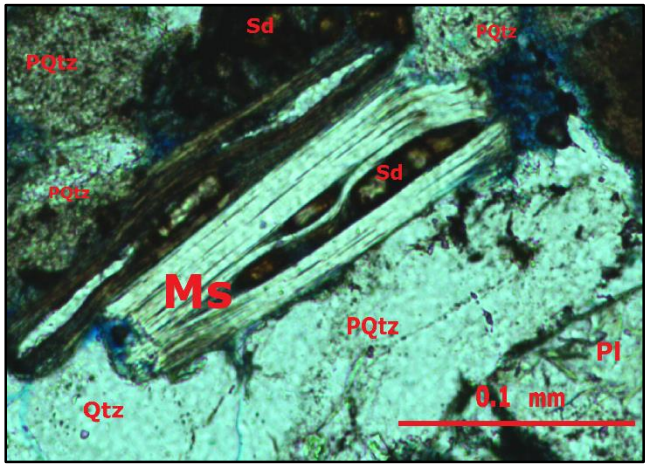

Figure 6.4 *Muscovite in plane polarized light. H12, Iversenfjellet, Hopen.*

Single mineral mica is only observed in the form of muscovite as in Figure 6.4. It is found in most thin sections in low quantitates, making it a minor mineral in the formation. In addition to the single mineral clasts, mica minerals are observed as the dominant part of metapelitic lithic fragments. Diagenetic impact on muscovite grains include bending by compaction and some dissolution as in the figure.

Monocrystalline quartz as shown in Figure 6.5 typically constitutes the highest proportion of the mineral clasts. The grains vary in degree of rounding from angular to round, possibly with quartz cementation.

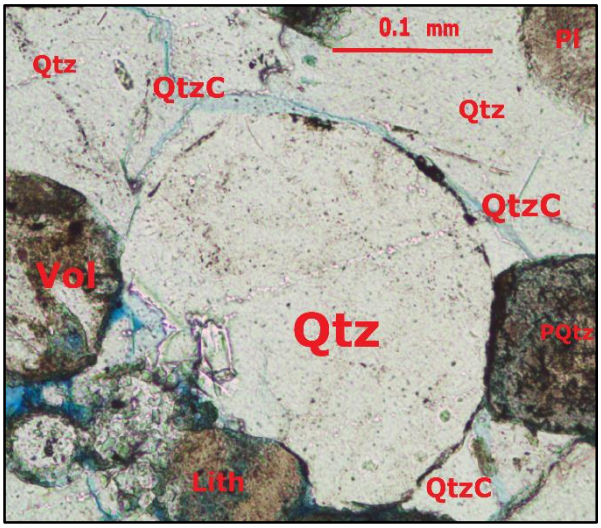

Figure 6.5 *Quartz with quartz cement in plane polarized light. H12, Iversenfjellet Hopen*

6.2.2 Accessory heavy minerals

The accessory minerals observed are presented in an alphabetical order starting with apatite. An additional heavy mineral to the ones being presented is garnet, that has been identified in thin sections from Adventdalen and Hopen.

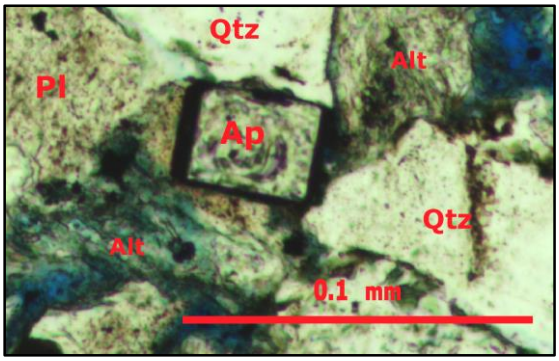

Figure 6.6 *Apatite in plane polarized light. H11, Iversenfjellet, Hopen.*

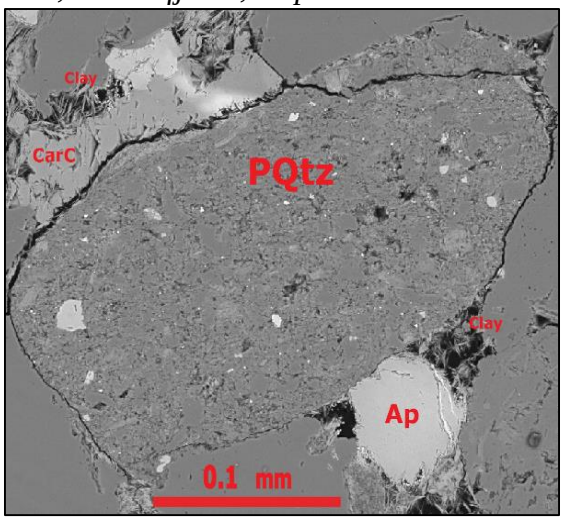

Figure 6.7a *SEM backscatter image of detrital apatite and polycrystalline quartz with inclusions. H11, Iversenfjellet, Hopen*

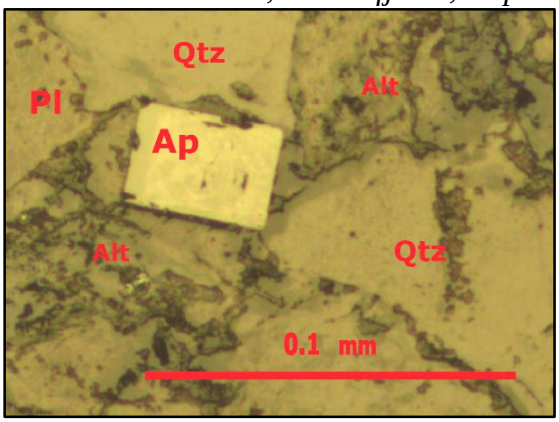

Figure 6.7b *Apatite in reflective light microscopy. H11, Iversenfjellet, Hopen.*

Apatite is present as an accessory mineral in several thin sections. An euhedral apatite crystal is observed in Figure 6.6 and Figure 6.7b. Observed apatites are both euhedral and of a more rounded shape, as seen in the SEM backscatter image in Figure 6.7b. Apatite is observed as mineral inclusions in quartz in several thin sections, and as a part of a volcanic lithic fragment

as in Figure 6.19. Apatite grains are generally smaller in size than the surrounding sand grains showing typical hydrodynamic sorting of denser material. Dissolution textures are not observed on apatites in the De Geerdalen Formation. Apatite occurs throughout the geographical area covered by this study and can be described as a common accessory mineral in the De Geerdalen Formation sandstones.

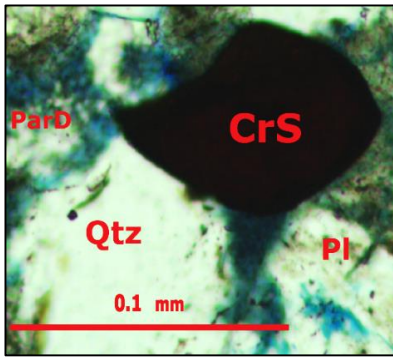

Figure 6.8 *Chromium spinel in plane polarized light. SV7-4, Adventdalen, Spizbergen.*

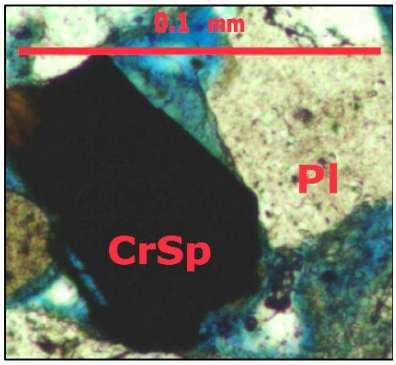

Figure 6.9 *Chromium spinel in plane polarized light. H11, Iversenfjellet, Hopen..*

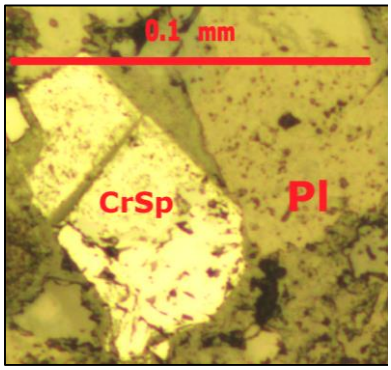

Figure 6.10 *Chromium spinel in reflective light microscopy. H11, Iversenfjellet, Hopen.*

In Figure 6.8 to Figure 6.10 two chromium spinel grains are identified. When the mineral is present, typically one to four chromium spinel grains per thin section can be identified, although most chromium spinel grains were identified using SEM. By optical microscopy chromium spinel was only found in fine- and medium grained sandstones still retaining some permeability or having undergone early carbonate cementation, sampled in central and eastern Svalbard (Adventdalen, Edgeøya, Hopen). After chromium spinel mineral separation and concentration, abundant chromium spinel was found in samples from west Svalbard (Kapp Toscana, Festningen) as well, they were however of a smaller silt size.

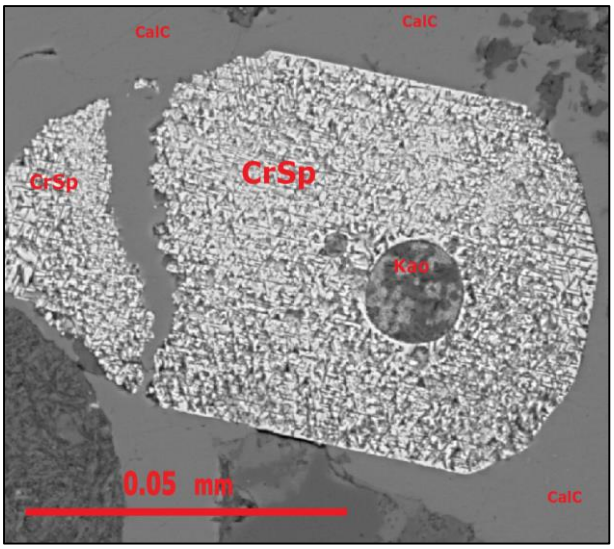

Figure 6.11 *SEM backscatter image of partially dissolved chromium spinel mineral grain. BLA3, Blanknuten, Edgeøya*

All chromium spinel observed with one exception, both in thin section and in SEM backscatter images, did not show signs of diagenetic alteration or dissolution. The exception can be seen in Figure 6.11 where the grain has partially dissolved in a patchy pattern throughout the observed mineral grain. Dissolution is post- depositional as the original grain outline is visible. The grain is surrounded by carbonate cement and the content of the circular feature, originally a melt or liquid inclusion, has been altered to kaolinite. Element chemistry of the mineral grain shows higher, but not extraordinary, ZnO (5,9%) and MnO (1,5%) content than in other chromium spinel samples in this study.

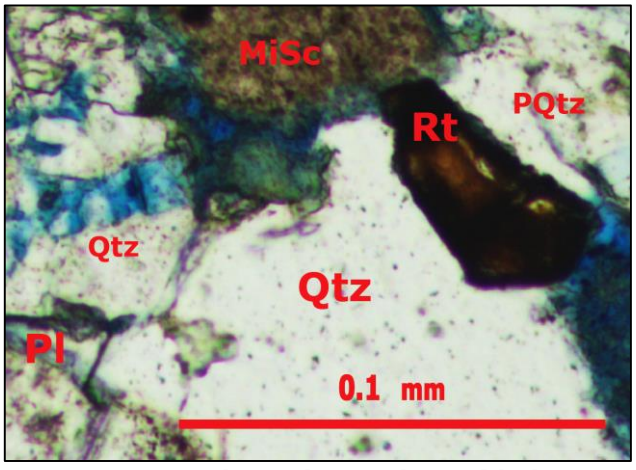

Figure 6.12 *Rutile in plane polarized light. H11, Iversenfjellet, Hopen..*

Detrital rutile is observed both in thin- section (Figure 6.12) and in SEM backscatter images (Figure 6.13). Rutile typically retains an angular shape and no dissolution textures are observed. The mineral is a common accessory mineral in the De Geerdalen Formation, observed in thin sections from both east (Hopen and Edgeøya), central (Adventdalen) and west (Kapp Toscana, Festningen) Svalbard.

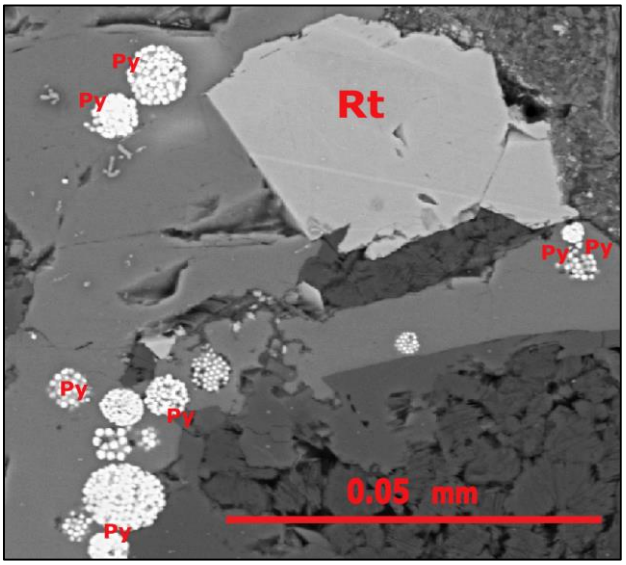

*Figure 6.**13** SEM backscatter image of detrital rutile grain and biogenic pyrite. BLA3, Blanknuten, Edgeøya.*

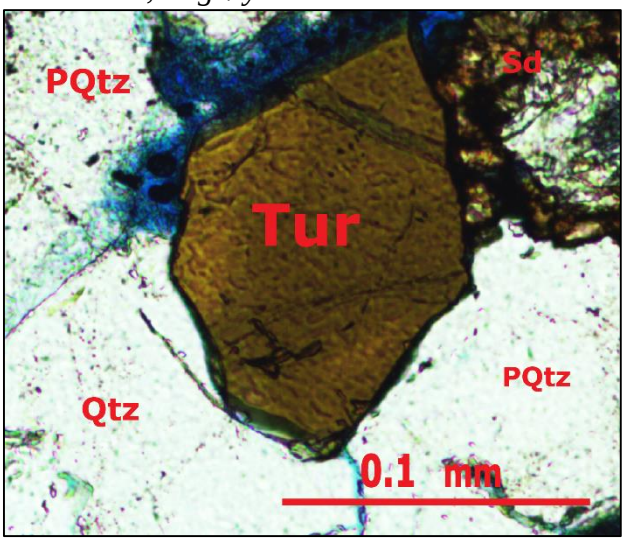

***Figure 6.14** Tourmaline in plane polarized light. H11, Iversenfjellet, Hopen*

Tourmaline, as observed in Figure 6.14, is observed in thin-sections on Hopen and Edgeøya. The mineral was not found by SEM backscatter imaging, as it has similar density and grain size as the surrounding sandstone grains. In all thin- sections with tourmaline present, more than one grain is observed, suggesting a common mineral in the sandstones.

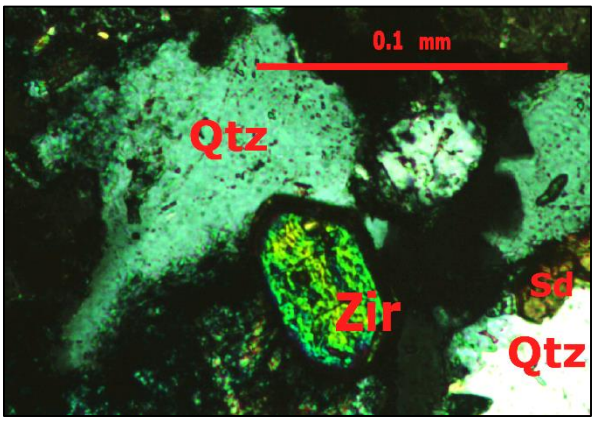

Figure 6.15 *Zircon in cross polarized light. H11, Iversenfjellet, Hopen.*

Zircon, with an example in Figure 6.15, is found optically and in SEM backscatter images throughout the De Geerdalen Formation sandstones. Zircon grains commonly retain the euhedral shape as seen in the images, and occur as independent clasts or as mineral inclusions in quartz. No changes in appearance or abundance can be observed stratigraphically or between locations.

6.2.3 Lithic fragments

The lithic fragments found in the De Geerdalen Formation sandstones can be grouped in three categories. In this sub- chapter volcanic as well as mica schist lithic fragments are presented, while different types of polycrystalline quartz grains are presented in a following sub-chapter. The term mica schist is in this study applied to all clasts identifiable as metapelitic lithic fragments, a precise description of metamorphic facies would be uncertain for many of the small clasts.

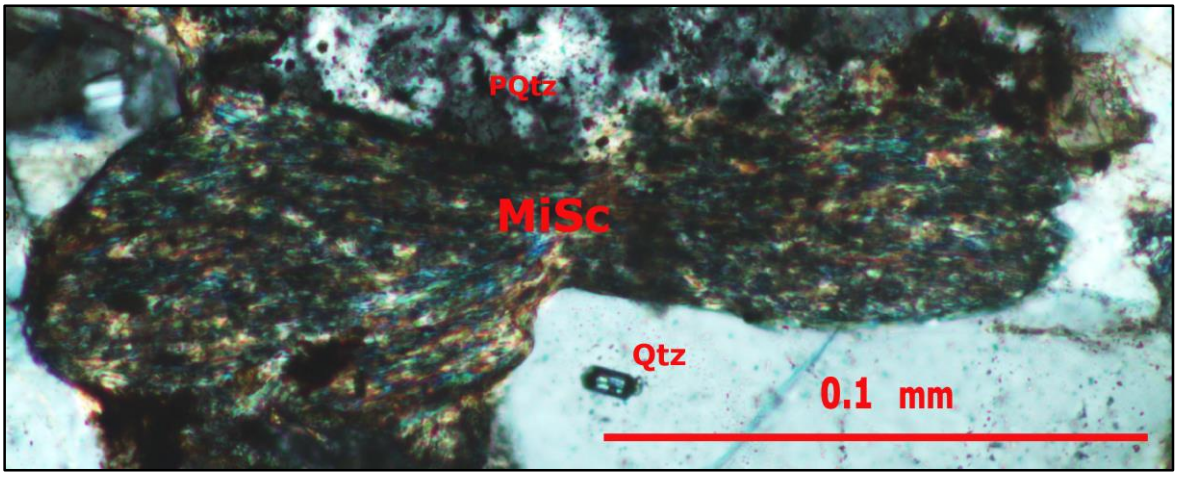

Figure 6.16 *Mica schist lithic fragment in cross polarized light. KTO19, Kapp Torscana, Spizbergen.*

The metapelitic higher greenschist to lower amphibolite facies metamorphic rock, mica schist (Figure 6.16 and Figure 6.17), is a major clast component of the sandstones. Mica schist lithic fragments are identified by polycrystalline mica and visible foliation. In Figure 6.17 for instance, both foliation and foliation direction are visible. Alteration and dissolution of mica schist fragments as in Figure 6.33 is observed in most thin sections. Dissolved and dissolving lithic clasts are a common observation in the formation, and much of the secondary porosity may be dissolution of mica schist lithic fragments, although volcanic fragments are observed to dissolve earlier. The alteration products of different clay minerals often retain the foliation of the original mica schist fragment.

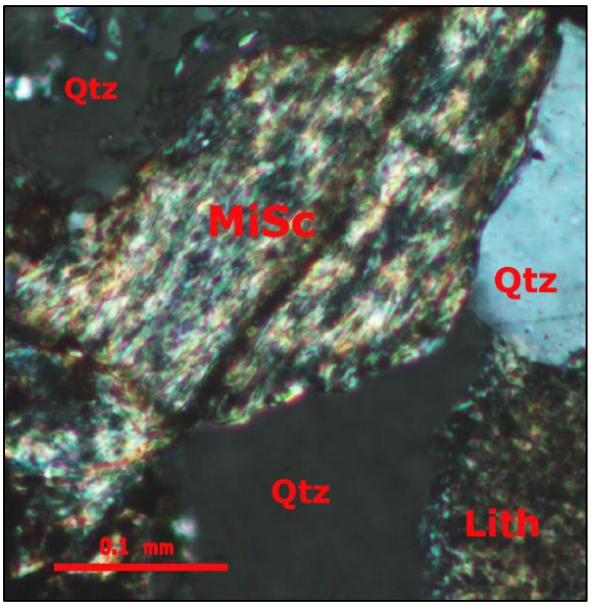

Figure 6.*17 Mica schist lithic fragment in cross polarized light. KTO19, Kapp Torscana, Spizbergen.*

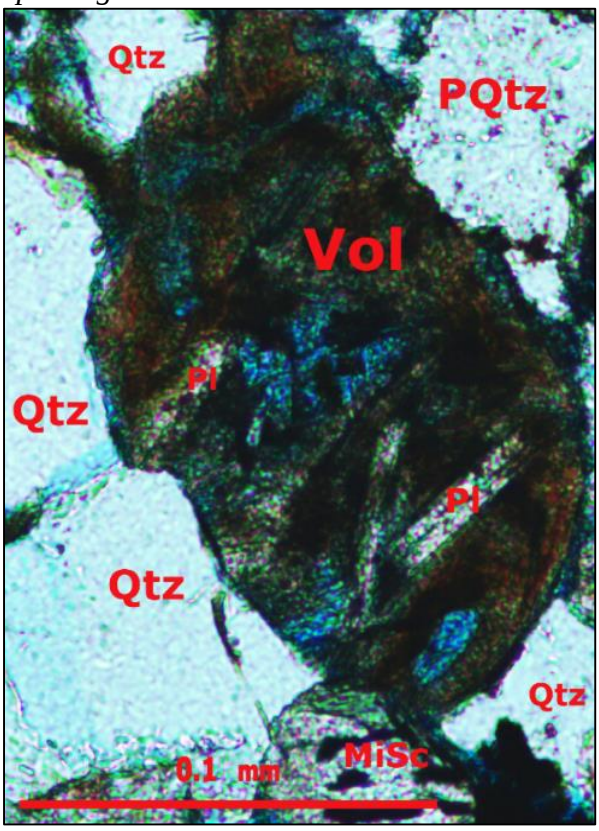

Figure 6.18 *Volcanic lithic fragment in plane polarized light. H12, Iversenfjellet, Hopen..*

Mafic volcanic clasts in the De Geerdalen Formation are recognizable as elongated plagioclase crystals of varying size and a random orientation, laying in a darker matrix. A volcanic lithic fragment is observed in Figure 6.18 where partial dissolution of matrix have generated some

secondary porosity. In Figure 6.19 a SEM backscatter image of a volcanic clast showing textures in higher detail, the volcanic lithic clast includes an apatite crystal. Dissolution and alteration of volcanic fragments are normal, generating secondary porosity, (see Figure 6.35). The mafic matrix is generally dissolved or altered to green clay minerals in the observed thin sections.

More felsic or intermediary volcanic clasts are possibly observed in the formation, an example are suggested to be Figure 6.20. As these are more similar to the polycrystalline quartz aggregates common in the formation, clear identifying criteria were not obtained.

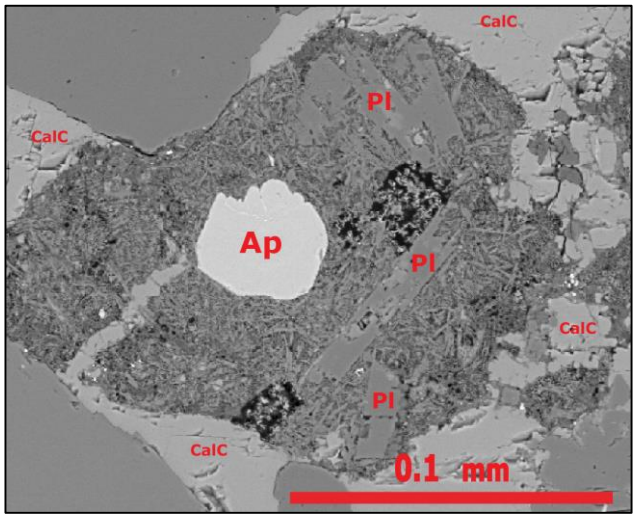

Figure 6.19 *SEM backscatter image of volcanic lithic clast constituting of plagioclase, apatite and matrix, surrounded by calcite cement. BLA3, Blanknuten, Edgeøya.*

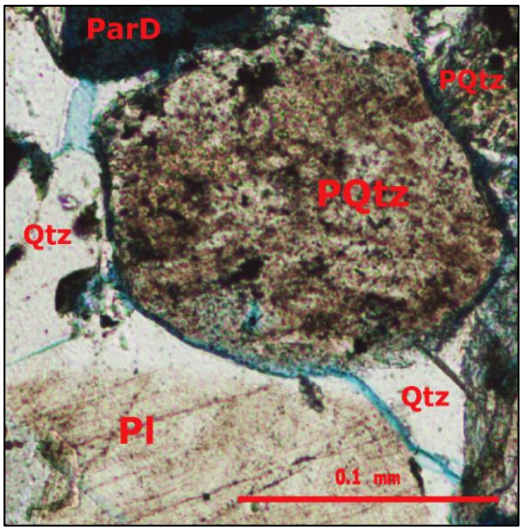

Figure 6.20 *Possible felsic volcanic fragment that optically share characteristic with polycrystalline quartz. Plane polarized light. H11, Iversenfjellet, Hopen*

6.2.4 Polycrystalline quartz lithic fragments

As observed in Figure 6.21 and Figure 6.22 the polycrystalline quartz lithic clasts of the De Geerdalen Formation display different characteristics in crystal size, shape, inclusions and colour. The clasts display varying degree of alteration, with some clasts easily seen in plane polarized light due to chemical alteration. Other clasts appear unaltered and not identifiable as lithic clasts in plane polarized light. Polycrystalline quartz lithic clasts can in many instances be sorted according to origin. In this study, biogenic and metamorphic quartz are described with an additional possible explanation of felsic volcanic fragments.

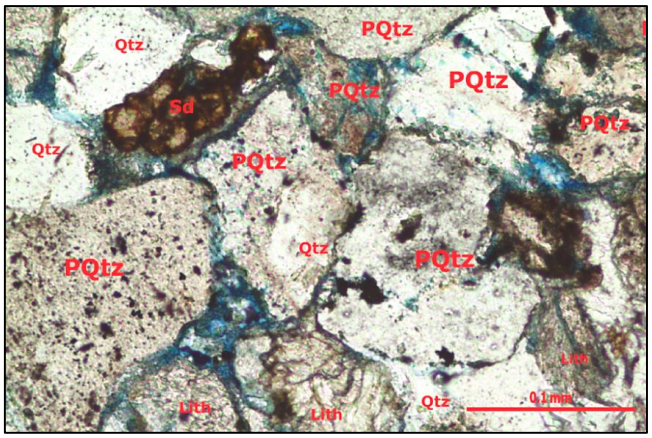

Figure 6.21 *Several different types of polycrystalline quartz clasts in plane polarized light. H11, Iversenfjellet, Hopen..*

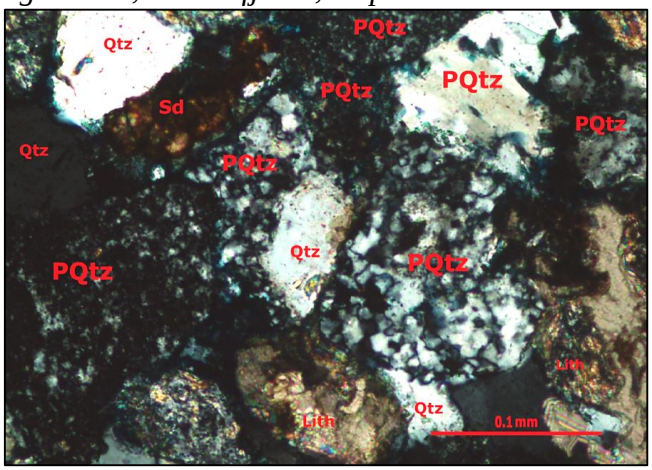

Figure 6.22 *Several differnent types of polycrystalline quartz clasts in cross polarized light. H11, Iversenfjellet, Hopen..*

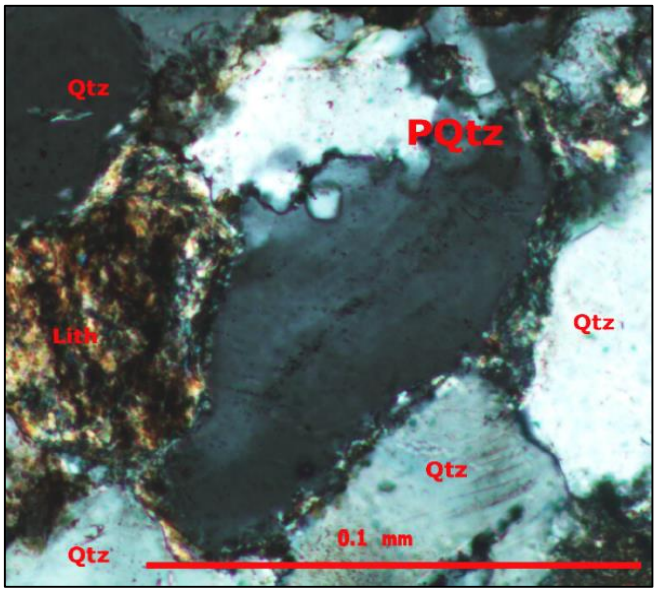

Figure 6.23 *Polygranular quartz grain showing quartz deformation textures in cross polarized light. KTO19, Kapp Toscana, Spitsbergen.*

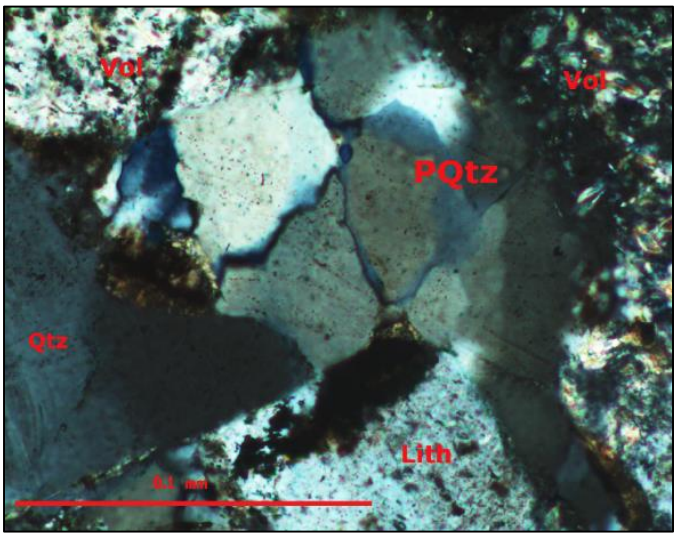

Figure 6.24 *Polygranular quartz in cross polarized light. Metamorphic deformation fabrics are observed. KTO19, Kapp Toscana, Spitsbergen.*

A group of polycrystalline quartz show ductile deformation textures and fabrics comparable to metamorphic greenschist facies quartzites (Hirth and Tullis, 1992). Quartz showing deformation bands are observed in Figure 6.24 and slow grain boundary migration fabrics be observed in Figure 6.23 (Hirth and Tullis, 1992). These deformation fabrics are created within Hirth and Tullis (1992) regime 1, in temperatures above 280^{O} C. In addition to the exemplified deformation fabrics are chessboard pattern and bulging recrystallization fabrics observed, as well as undulating extinction in quartz. Most polycrystalline quartz in the formation are fine-grained throughout, possibly corresponding to deformation in regime 2 of Hirth and Tullis (1992). This is however hard to distinguish from biogenic polycrystalline quartz.

Figure 6.25 *Biogenic spiculite quartz in cross polarized light. KTO19, Kapp Toscana, Spitsbergen.*

Two locations with of biogenic silica are found in the samples. One in Kapp Toscana in west Spitsbergen (Figure 6.25). The other fromin Negerfjellet, Edgeøya seen in Figure 6.26. The observed spiculites show the same characteristics as spiculites of late Permian formations of Svalbard and the Barents Sea. In addition to this, chert or biogenic polycrystalline aggregates are present in the formation. They are however difficult to distinguish from other types of polycrystalline quartz.

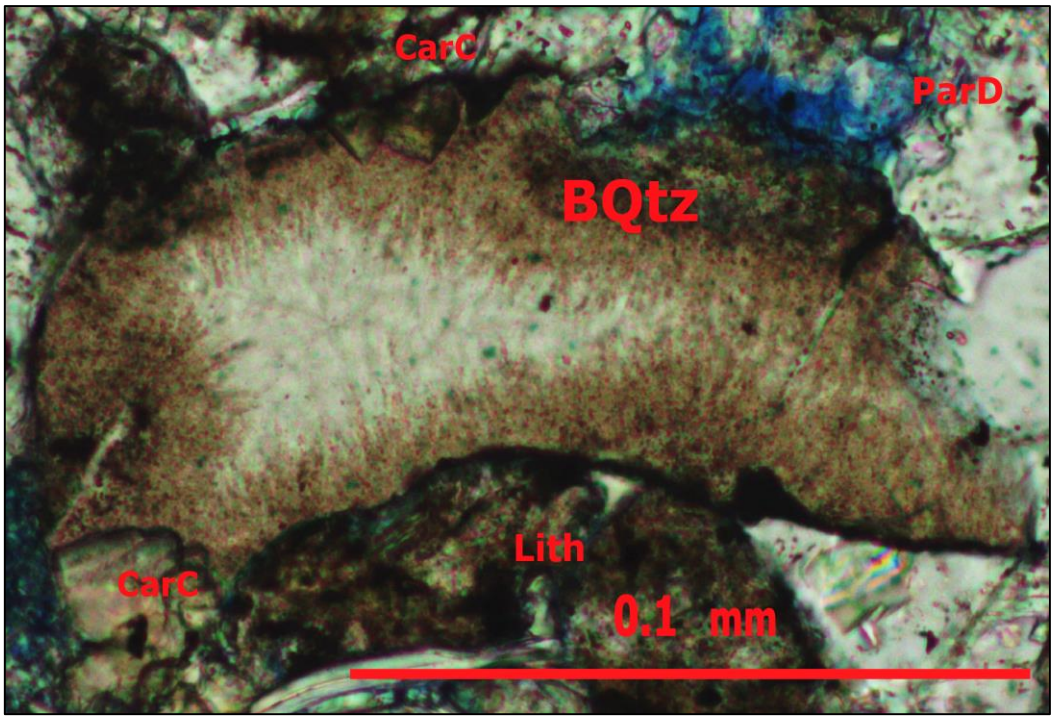

Figure 6.26 *Biogenic spiculite quartz in plane polarized light. EO1, Negerfjellet, Edgeøya.*

6.2.5 Autigenic minerals and alteration

Autigenic minerals present in the formation have not been a focus of this study. Some mineral observations are included as following. The described autigenic minerals do not cover clay minerals. Some observation concerning alteration of the sediments are presented.

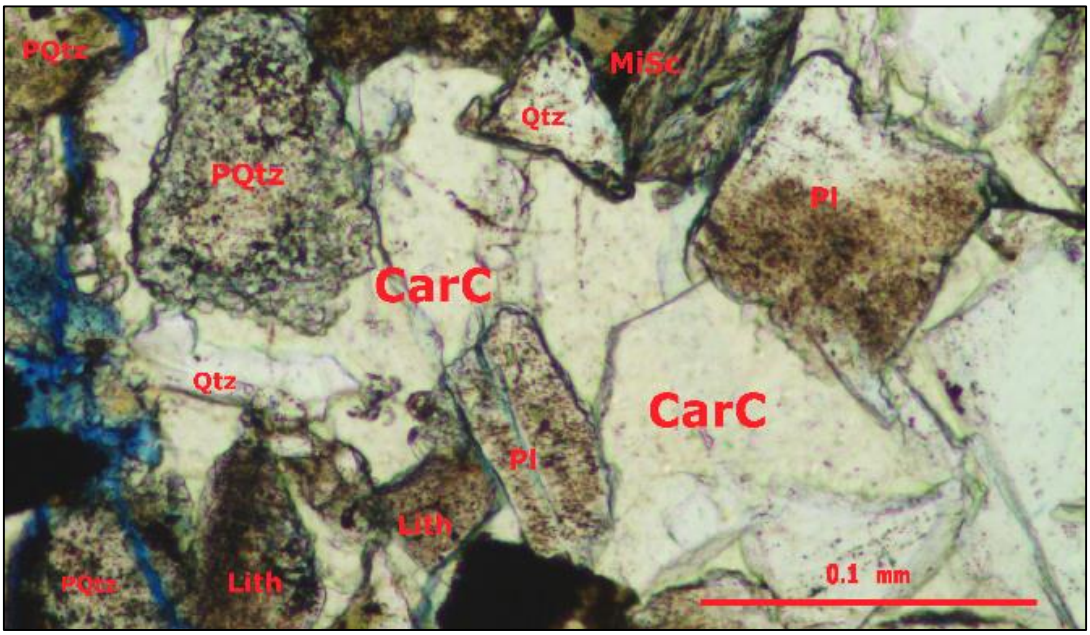

Figure 6.27 *Eogenetic cabonate cemented rock sample. BLA3 Blanknuten, Edgeøya*

Different carbonate cements are observed in samples including siderite and calcite. Eogenetic cementation, as observed in Figure 6.27 are often observed to be calcite. Siderite crystals such as the one in Figure 6.22 have grown alone, or more commonly as in Figure 6.21 in aggregates in the formation. Siderite aggregates are often associated with unstable grains, this is seen in Figure 6.28, showing siderite autigenic growth around lithic fragments. In Figure 6.4 siderite growth in the mineral cleavage of a muscovite grain has contributed to bending of the grain. The siderite in Figure 6.30 displays internal zoning, reflecting changing microconditions when growing.

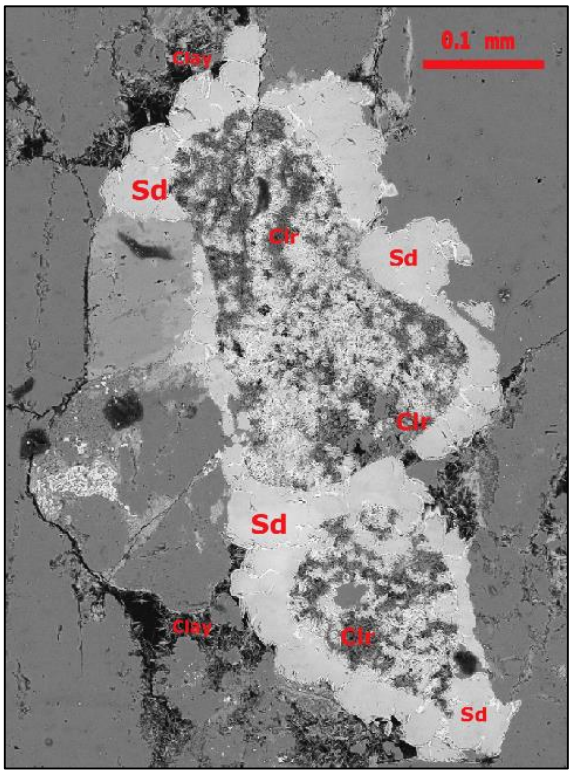

Figure 6.28 *SEM backscatter image of a lithic fragment surrounded by autigenic siderite. H11, Iversenfjellet, Hopen.*

Quartz cementation, with an example in Figure 6.5 is common in samples without extensive carbonate cementation. The degree of quartz cementation varies, but compaction by quartz cementation are stronger in fine-grained rocks, and in west Spitsbergen where the rocks have undergone deeper burial.

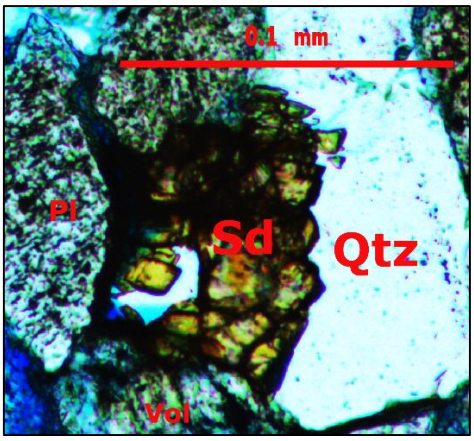

Figure 6.29 *Autigenic Siderite in plane polarized light. H12, Iversenfjellet, Hopen.*

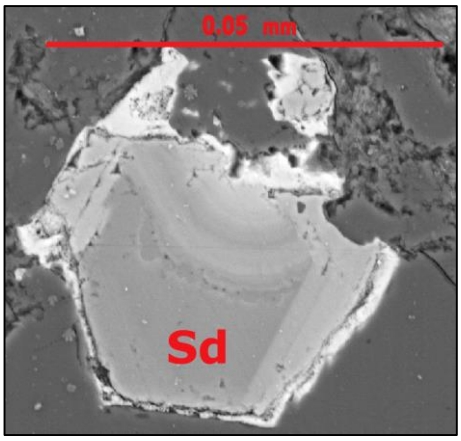

Figure 6.30 *SEM bacscatter image of zoned autigenic siderite. BRO14, Bravaisodeen, Spitsbergen.*

Autigenic barite and anatase are observed in the formation. Barite, as observed in Figure 6.31 grow during diagenesis in available pore space. The mineral is observed both in Kapp Toscana, Hopen and Edgøya in thin sections, indicating favourable conditions for formation in the De Geerdalen Formation in Svalbard. Autigenic titanium oxides like that observed in Figure 6.32, probably anatase, is observed at two locations, Hopen and Adventdalen.

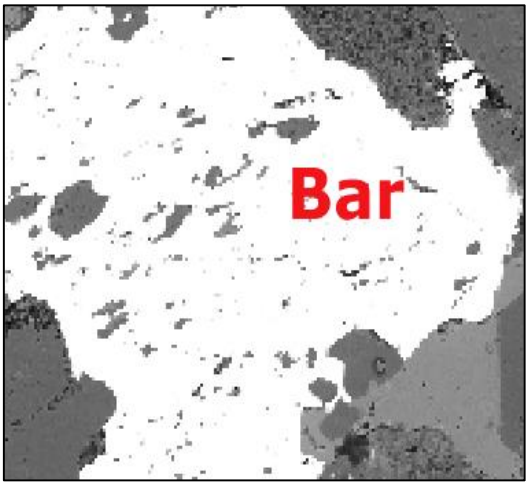

Figure 6.31 *SEM backscatter image showing autigenic barite. H11, Iversenfjellet, Hopen.*

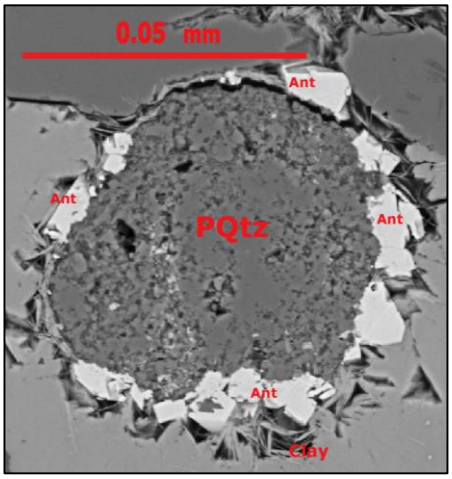

Figure 6.32 *SEM backscatter image of the autigenic anatase, growing as a rim around a polygranular quartz grain. H11, Iversenfjellet, Hopen.*

In Figure 6.33 alteration and partial dissolution of some lithic clasts can be observed. In sub chapter 9.2.3 typical alteration of the lithic clasts was mentioned, Figure 6.33 shows alteration processes representative of many of the investigated samples. While the mica schist fragment

dissolve differently following foliation, another lithic fragment is almost completely dissolved, with green clay and secondary porosity left. Other volcanic lithic clasts and plagioclase grains show signs of alteration. The diagenetic products are dark green clays, opaques and microcrystalline minerals.

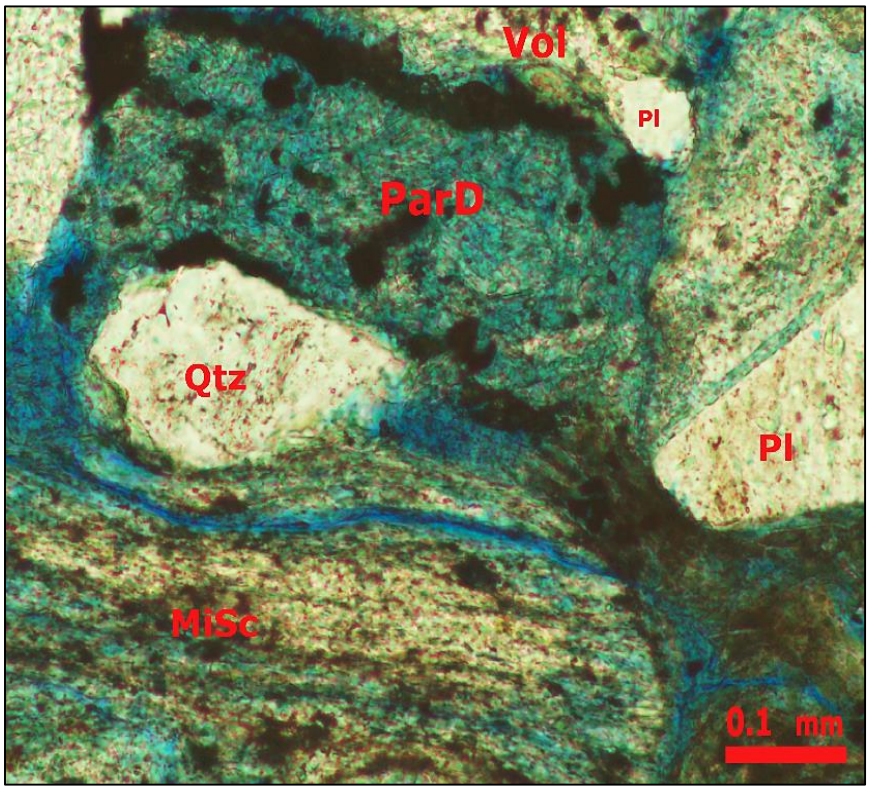

Figure 6.33 *Alteration and dissolution process of unstable detrital minerals to green clay minerals. Plane polarized light. H11, Iversenfjellet, Hopen.*

6.2.6 Sandstone textures

The sandstones of the De Geerdalen Formation can be described as mineralogically immature, generally well sorted with angular to rounded clasts. Textures at deposition are best preserved in samples that have been carbonate cemented during eogenesis, as the examples in Figure 6.34 and Figure 6.35**.**

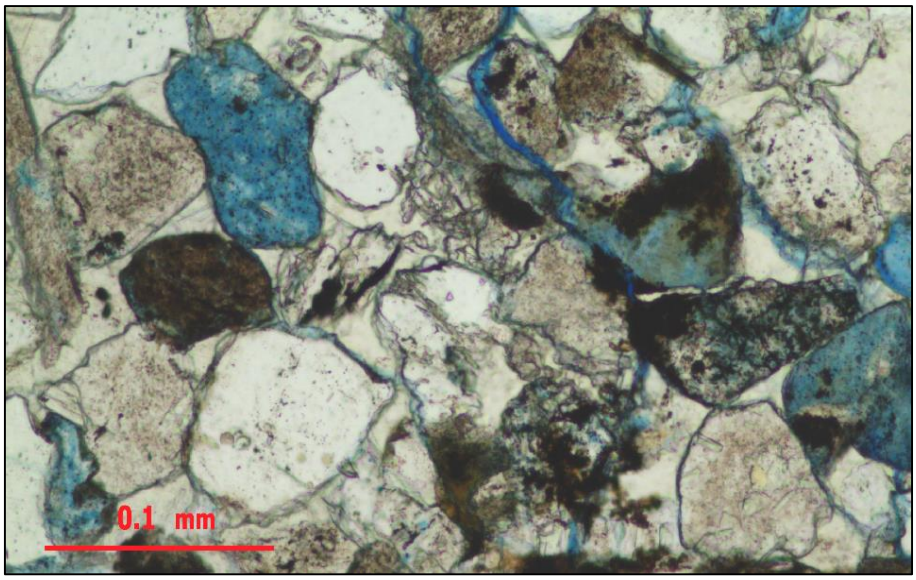

Figure 6.34 *Clast rounding. Image in plane polarized light. BLA1, Blanknuten, Edgeøya.*

Variations in clast rounding seem bimodal with one set of rounded to sub- rounded clasts, and another set of sub- angular to angular clasts. Clast type may be different for the two sets of rounding; especially volcanic lithic fragments are generally rounded. Mica schist lithic fragments are also typically sub- rounded or rounded. Feldspars are found to be mostly sub-angular to angular, while polycrystalline quartz and quartz clasts are observed both as rounded and angular.

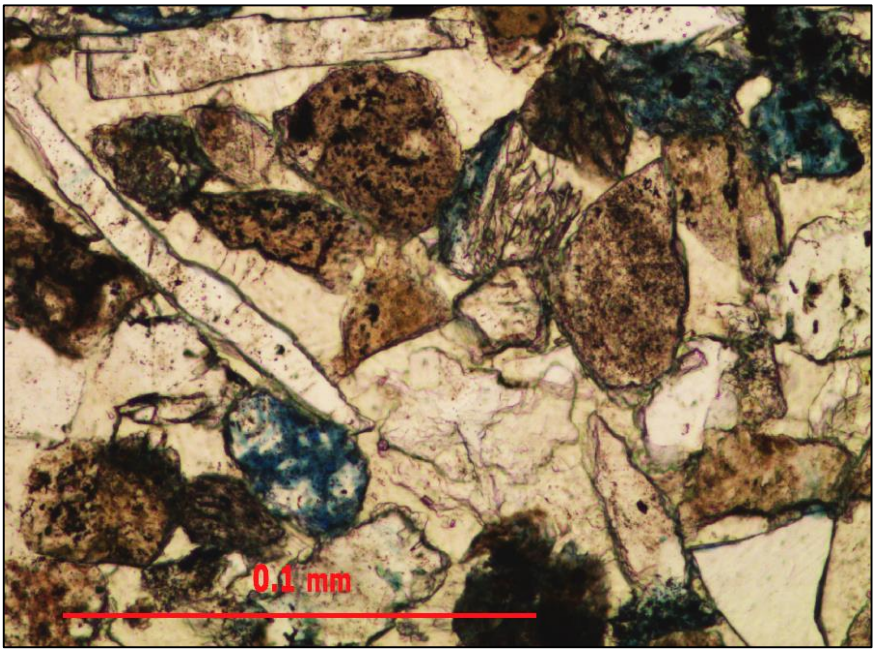

Figure 6.35 *Clast rounding. Image in plane polarized light. BLA1, Blanknuten, Edgeøya.*

In Figure 6.34 predominantly round and sub- round clasts can be observed, the dissolved grains most probably represent volcanic fragments. Figure 6.35 better show the angular clasts, the elongated grains being plagioclase. Angular quartz can be seen in the lower right corner.

6.3 Mineral concentrate generation

After spending time inspecting thin sections by microprobe for chromium spinels, but finding few, the mineral was tried concentrated by magnetic separation. Before making polished thick sections of the separate, samples were sieved, magnetically separated and mounted on tape. In Figure 6.36 a flow chart describing steps taken to acquire chromium spinel compositional data is included. Samples on tape were investigated using SEM, revealing a higher concentration of chromium spinel grains in several of the investigated tape samples. The degree of chromium spinel in the samples varied from up to 5% to very few or absent in other samples.

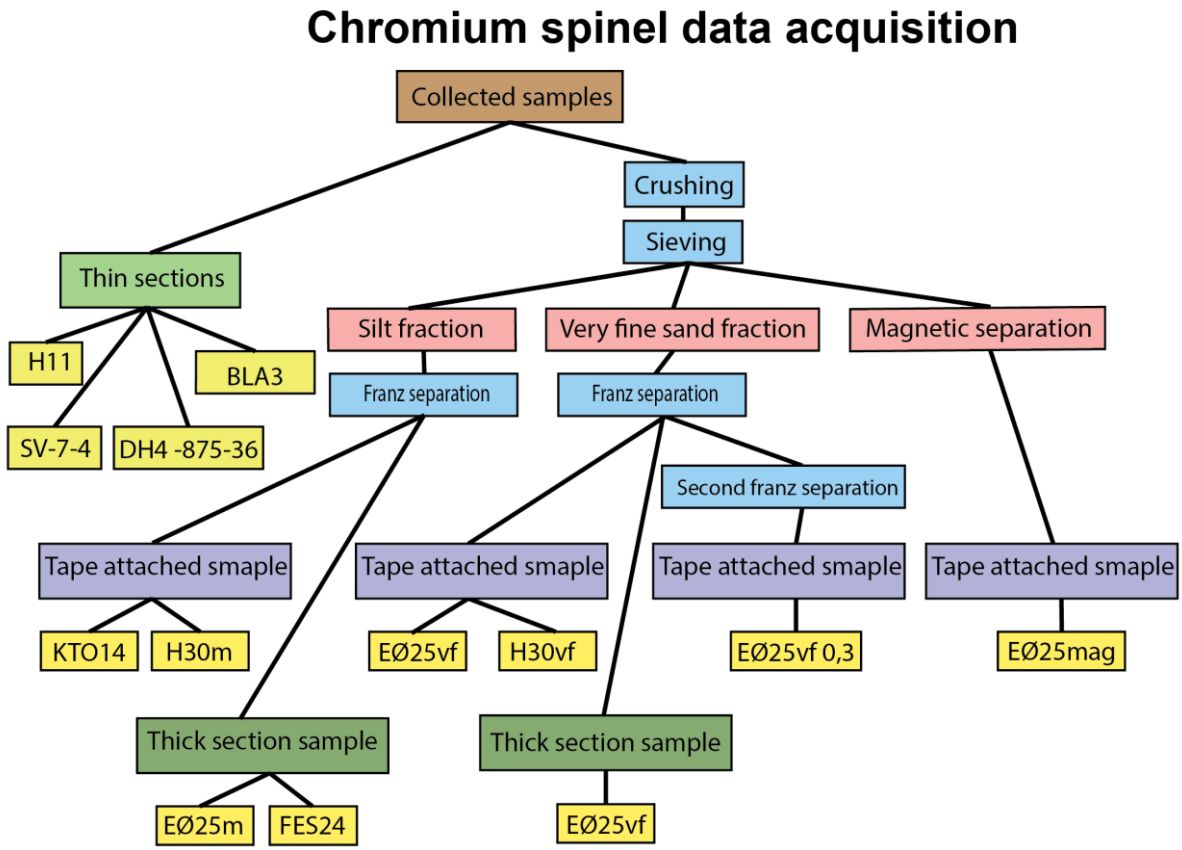

Figure 6.36 *Flow chart describing the preparation of samples before microprobe mineral composition data were acquired. More samples were processed, but only listed samples were applied.*

In Figure 6.37 an example of the concentrates is shown. A majority of the Spitsbergen chromium spinel grains were found in the silt size fraction, and in Edgeøya and Hopen samples in the very fine sand fraction. A contamination of chromium containing stainless steel were observed in the separates, probably originating from initial sample crushing. They could however be identified and excluded from the dataset as the stainless steel filings did not contain O, and generally had a flaky form.

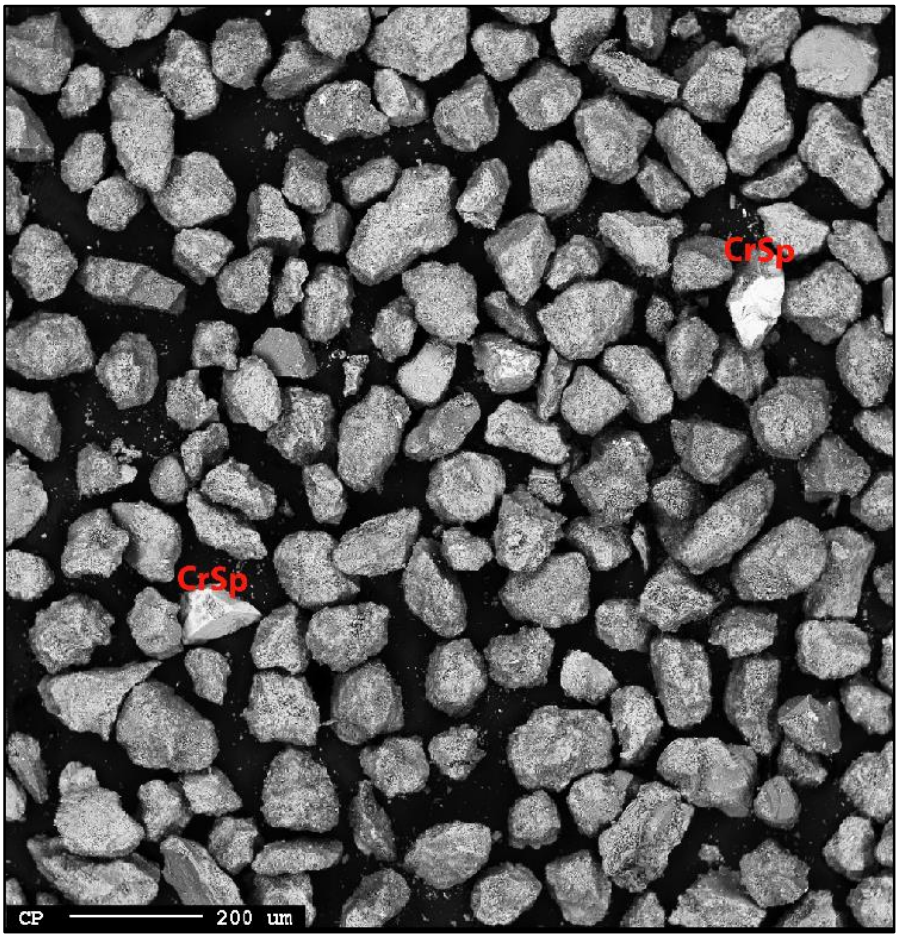

Figure 6.37 *SEM image of separate on tape, showing two chromium spinel grains. From the H30 very fine sand fraction separate. Iversenfjellet, Hopen.*

Polished thick sections were prepared of selected separates identified by use of SEM as containing chromium spinels. When investigating the polished thick sections for EPMA analysis, no chromium spinel grains were identified with the exception of one, found by mapping for selected elements (see Figure 6.38). The reason for not finding chromium spinel in the epoxy casted thick sections is probably that the concentration was too low. Gravitational

stratification in the samples and polishing to another depth may be an explanation. After investigating the thick sections, separates prepared on tape were examined for compositional data. These data are from grains laying scattered producing an uneven surface, sometimes shadowing from each other.

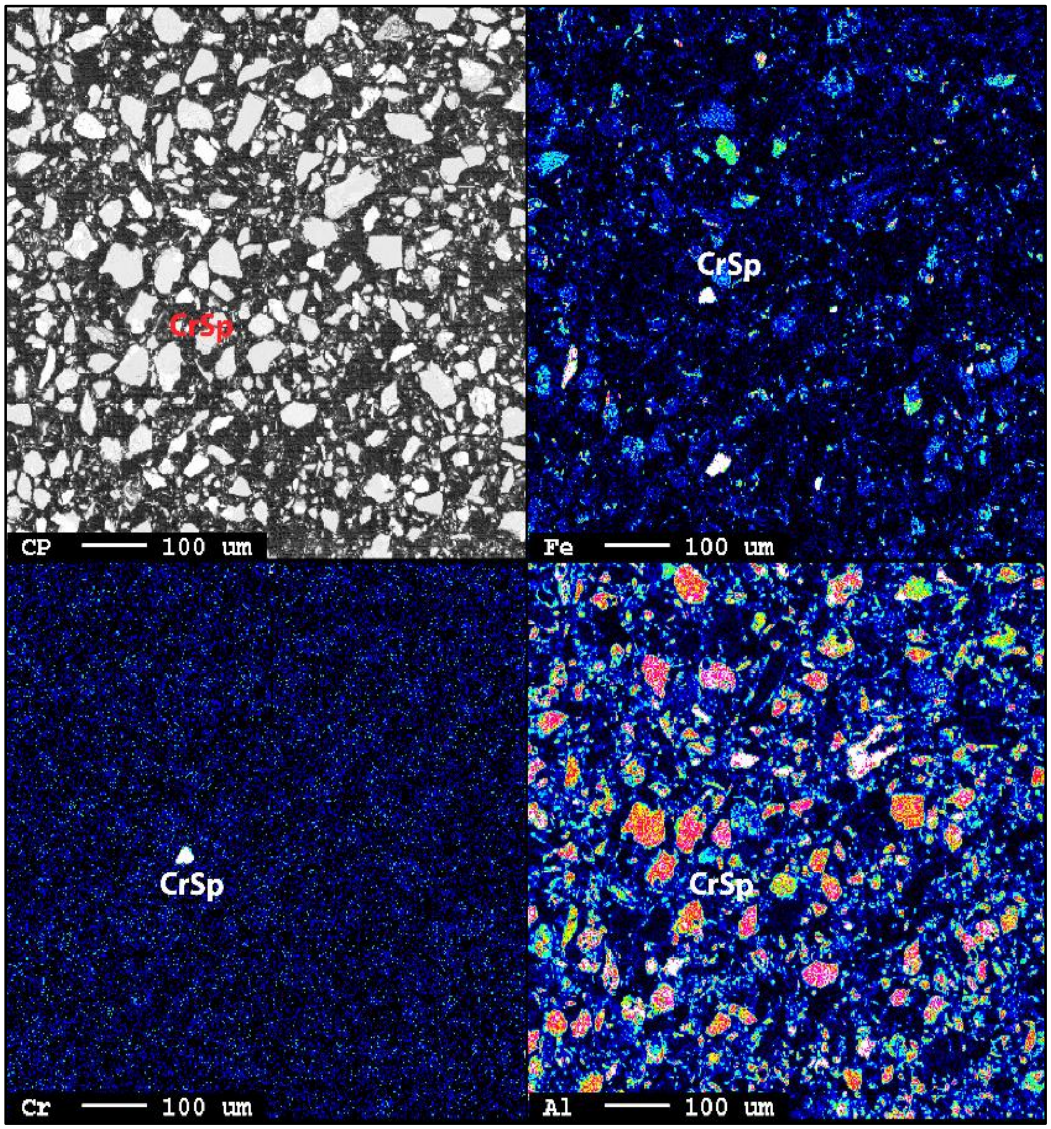

Figure 6.38 *EPMA element map for Fe, Cr and Al and backscatter image of the FES24m thick section. Indicated are the only chromium spinel observed in the thick sections. Clay and silt fraction separate from Festningen, Spitsbergen.*

6.4 Chemical compositions of detrital chromium spinel

As the chemical composition of chromium spinels is used as a petrogenic indicator (Cookenboo et al., 1997, Arai, 1992, Barnes and Roeder, 2001, and Kamenetsky et al., 2001), examining detrital spinels can be an efficient provenance tool, describing the tectonic setting of a mafic or ultra- mafic source rock. In order to discriminate between various possible tectonic settings at

creation, comparative chemical elements have been plotted and compared to the density distribution plots of Barnes and Roeder (2001). The chromium spinel composition data plots in a loose cluster, indicating similar tectonic setting as source to the majority of the detrital chromium spinel grains.

Different ways of sample preparation were applied in order to find chromium spinel grains. This process is described in Figure 6.37. Direct observations on selected thin sections and minerals concentrated using magnetic Franz separation, either casted in epoxy and polished, or attached to tape were applied.

6.4.1 Chromium spinel data set

The acquired chromium spinel compositional data are presented in the following **Feil! Fant ikke referansekilden.**6.3 including sampling point and the method of sample preparation. A similar oxide chart is included (Appendix 1). Calculations to get comparative compositional data are implemented in the same way as in, Barnes and Roeder (2001), deriving the Fe^{2+}/Fe^{3+} ratio stoichiometricly. This is done by first removing V and Ti bound Fe, assuming iron in an ulvöspinel, and theoretical $Fe_7V_2O_{12}$ component. Assuming a perfect spinel formula, the Fe^{3+}content can then be calculated assuming 2/3 of cations are trivalent and 1/3 divalent. Errors in all major elements influence a stoichiometry based calculation of iron, inferring an uncertainty with the method that must be recognized. Important chromium spinel components like Mn and Zn are not included in Barnes and Roeder (2001) and cannot be compared to empirical data, they will therefore not be applied in this study.

The compositional data and data quality vary between the thin section data and data from concentrated samples. There is a difference in elements investigated in the two sets. Since the stoichiometric calculation of Fe are corrected for vanadium, this may have a minor influence on the comparability of the sample sets. Co, Cu, Ni and Zn, elements not included in the thin section data, can sometimes constitute a considerable part of the chromium spinels, and be important for source interpretation. The total oxide values (Appendix 1) include chromium spinels with total sums at the cut- off of 65%. This introduce a considerable uncertainty in the processed and concentrated chromium spinel data. Steps are taken to evaluate the reliability of these data in a later sub- chapter.

Table 6.3 *The complete chrome spinel chemical composition data set in mol% based on EPMA data.*

Sample	Separate Type	Location	Preparate	Al	Na	K	Cr	Si	Mg	Ca	Mn	Y	Ti	Fe	V	Co	Ni	Cu	Zn	O	Total
BLA-3, 1	Thin section	Blanknuten, Edgeøya	Thin section	6,122	0,233	0,138	16,196	5,397	1,246	1,208	2,458	0,000	0,807	58,249	n/a	n/a	n/a	n/a	7,946	n/a	100,000
BLA-3, 3	Thin section	Blanknuten, Edgeøya	Thin section	7,855	0,026	0,000	27,716	0,058	2,001	0,260	0,394	0,000	0,149	60,732	n/a	n/a	n/a	n/a	0,802	n/a	99,993
DH4-875-36, 1	Thin section	Adventdalen, Spitsbergen	Thin section	13,830	0,020	0,022	30,259	0,163	15,095	0,031	0,486	0,000	0,354	39,330	n/a	n/a	n/a	n/a	0,410	n/a	100,000
DH4-875-36, 2	Thin section	Adventdalen, Spitsbergen	Thin section	8,189	0,039	0,032	40,204	0,293	13,939	0,039	0,606	0,000	0,161	36,281	n/a	n/a	n/a	n/a	0,193	n/a	99,978
DH4-875-36, 3	Thin section	Adventdalen, Spitsbergen	Thin section	8,217	0,028	0,018	28,018	0,254	14,643	0,026	0,651	0,021	0,872	47,127	n/a	n/a	n/a	n/a	0,115	n/a	99,991
DH4-875-36, 5	Thin section	Adventdalen, Spitsbergen	Thin section	10,861	0,058	0,003	27,980	0,501	13,614	0,000	0,546	0,000	0,709	45,547	n/a	n/a	n/a	n/a	0,169	n/a	99,988
DH4-875-36, 6	Thin section	Adventdalen, Spitsbergen	Thin section	7,304	0,026	0,004	38,517	0,441	13,930	0,003	0,603	0,003	0,209	38,851	n/a	n/a	n/a	n/a	0,108	n/a	99,998
EO25mag, 1	Intial Magnetic	Nergerfjellet, Egeøya	Tape	4,558	0,102	0,126	14,311	1,127	3,128	0,135	0,564	0,000	0,118	19,340	0,086	0,101	0,082	0,019	0,541	55,662	100,000
EO25mag, 2	Intial Magnetic	Nergerfjellet, Egeøya	Tape	5,606	0,000	0,015	8,035	0,498	3,450	0,041	0,151	0,004	0,730	20,017	0,321	0,037	0,080	0,017	0,134	60,865	100,000
EO25mag, 3	Intial Magnetic	Nergerfjellet, Egeøya	Tape	3,359	0,094	0,120	16,017	2,230	1,871	0,153	0,706	0,000	0,082	20,316	0,075	0,101	0,043	0,027	0,457	54,348	100,000
EO25mag, 4	Intial Magnetic	Nergerfjellet, Egeøya	Tape	0,739	0,573	0,000	13,670	0,333	0,464	0,039	0,316	0,012	0,008	13,615	0,069	0,071	0,032	0,019	0,910	69,131	100,000
EO25mag, 5	Intial Magnetic	Nergerfjellet, Egeøya	Tape	0,781	0,210	0,020	21,476	0,000	0,627	0,016	0,253	0,000	0,056	18,661	0,027	0,076	0,106	0,000	0,062	57,630	100,000
EO25mag, 6	Intial Magnetic	Nergerfjellet, Egeøya	Tape	0,732	0,065	0,013	9,492	0,120	0,802	0,001	0,224	0,000	0,000	13,354	0,024	0,078	0,011	0,012	0,080	74,993	100,000
EO25mag, 7	Intial Magnetic	Nergerfjellet, Egeøya	Tape	0,159	0,239	0,063	0,993	0,558	0,602	0,226	0,793	0,000	0,077	29,330	0,024	0,066	0,305	0,203	0,000	66,363	100,000
EO25mag, 8	Intial Magnetic	Nergerfjellet, Egeøya	Tape	3,129	0,174	0,171	21,100	2,882	1,118	0,091	0,759	0,006	0,306	29,946	0,119	0,025	0,000	0,001	0,676	39,496	100,000
EO25mag, 9	Intial Magnetic	Nergerfjellet, Egeøya	Tape	0,426	0,764	0,601	0,059	0,922	0,094	0,007	0,137	0,000	0,000	31,046	0,013	0,106	0,000	0,012	0,000	65,814	100,000
EO25mag, 10	Intial Magnetic	Nergerfjellet, Egeøya	Tape	1,184	0,602	0,223	11,954	1,093	1,389	0,039	0,542	0,000	0,141	24,523	0,082	0,049	0,094	0,024	0,049	58,012	100,000
EO25mag, 11	Intial Magnetic	Nergerfjellet, Egeøya	Tape	0,327	0,137	0,053	17,265	0,348	0,689	0,059	0,688	0,000	0,275	23,762	0,087	0,027	0,006	0,045	0,551	55,682	100,000
EO25mag, 12	Intial Magnetic	Nergerfjellet, Egeøya	Tape	1,018	0,028	0,048	0,123	1,271	0,232	0,250	0,366	0,000	0,023	37,187	0,009	0,059	0,018	0,000	0,000	59,368	100,000
EO25mag, 13	Intial Magnetic	Nergerfjellet, Egeøya	Tape	6,584	0,121	1,190	11,874	4,869	2,087	0,055	0,261	0,000	0,315	18,915	0,062	0,034	0,029	0,000	0,133	53,472	100,000
EO25mag, 14	Intial Magnetic	Nergerfjellet, Egeøya	Tape	2,217	0,152	0,100	4,070	8,211	0,639	9,092	0,497	0,000	0,785	20,068	0,109	0,066	1,335	0,052	0,000	52,609	100,000

Sample	Separate Type	Location	Preparate	Al	Na	K	Cr	Si	Mg	Ca	Mn	Y	Ti	Fe	V	Co	Ni	Cu	Zn	O	Total
EO25mag, 15	Intial Magnetic	Nergerfjellet, Egeøya	Tape	1,295	0,000	0,077	13,145	0,172	1,073	0,045	0,969	0,000	0,586	29,668	0,631	0,079	0,136	0,029	0,017	52,082	100,000
EO25mag, 16	Intial Magnetic	Nergerfjellet, Egeøya	Tape	2,062	0,188	0,093	21,848	1,152	2,190	0,075	0,174	0,020	0,051	27,983	0,094	0,092	0,063	0,087	0,200	43,629	100,000
EO25mag, 17	Intial Magnetic	Nergerfjellet, Egeøya	Tape	1,492	0,179	0,133	21,308	1,054	1,852	0,054	0,124	0,002	0,077	16,984	0,060	0,134	0,033	0,012	0,346	56,157	100,000
EO25mag, 18	Intial Magnetic	Nergerfjellet, Egeøya	Tape	0,379	0,061	0,165	18,016	0,340	1,600	0,136	0,826	0,011	0,120	19,916	0,057	0,070	0,029	0,048	0,616	57,612	100,000
EO25mag, 19	Intial Magnetic	Nergerfjellet, Egeøya	Tape	2,334	0,227	0,178	10,433	1,852	2,792	0,379	0,420	0,009	0,249	28,181	0,080	0,099	0,028	0,037	0,681	52,020	100,000
EO25mag, 20	Intial Magnetic	Nergerfjellet, Egeøya	Tape	2,150	0,279	0,078	18,729	1,253	1,266	0,059	1,080	0,032	0,274	27,541	0,130	0,090	0,014	0,028	0,294	46,703	100,000
EO25vf, 1	Franz 1 time	Nergerfjellet, Egeøya	Tape	2,255	0,072	0,032	18,899	0,595	1,878	0,070	0,316	0,000	0,050	22,824	0,077	0,069	0,084	0,000	0,305	52,474	100,000
EO25vf, 2	Franz 1 time	Nergerfjellet, Egeøya	Tape	1,883	0,120	0,139	16,044	1,058	1,997	0,091	0,325	0,022	0,097	12,635	0,061	0,056	0,016	0,000	0,679	64,776	100,000
EO25vf, 3	Franz 1 time	Nergerfjellet, Egeøya	Tape	1,281	0,065	0,046	20,073	0,507	7,069	0,016	0,177	0,000	0,017	7,740	0,036	0,037	0,014	0,006	0,017	62,899	100,000
EO25vf, 4	Franz 1 time	Nergerfjellet, Egeøya	Tape	0,071	0,086	0,054	32,025	0,133	4,255	0,000	0,350	0,009	0,071	21,967	0,085	0,091	0,071	0,004	0,175	40,555	100,000
EO25vf, 5	Franz 1 time	Nergerfjellet, Egeøya	Tape	1,472	0,054	0,086	21,293	0,433	7,642	0,021	0,984	0,004	0,028	15,925	0,013	0,100	0,109	0,001	0,204	51,632	100,000
EO25vf, 6	Franz 1 time	Nergerfjellet, Egeøya	Tape	1,096	0,023	0,114	18,435	5,821	0,037	1,367	0,999	0,012	0,066	64,154	0,065	0,169	6,216	0,214	0,000	1,211	100,000
EO25vf, 7	Franz 1 time	Nergerfjellet, Egeøya	Tape	3,124	1,165	0,080	13,163	2,842	1,379	0,132	0,887	0,000	0,746	16,814	0,118	0,055	0,000	0,005	0,995	58,495	100,000
EO25vf, 8	Franz 1 time	Nergerfjellet, Egeøya	Tape	8,828	0,135	0,203	11,513	4,051	7,359	0,023	0,157	0,000	0,047	9,510	0,068	0,018	0,049	0,010	0,110	57,921	100,000
EO25vf, 9	Franz 1 time	Nergerfjellet, Egeøya	Tape	8,752	0,066	0,088	11,932	3,383	7,718	0,016	0,177	0,018	0,051	10,000	0,060	0,059	0,035	0,010	0,139	57,497	100,000
EO25vf, 10	Franz 1 time	Nergerfjellet, Egeøya	Tape	4,485	0,074	0,184	15,348	2,159	1,356	0,068	0,544	0,004	0,039	27,798	0,098	0,049	0,061	0,009	0,158	47,567	100,000
EO25vf, 11	Franz 1 time	Nergerfjellet, Egeøya	Tape	2,755	0,025	0,197	19,749	0,417	5,492	0,041	0,147	0,000	0,645	10,172	0,119	0,037	0,056	0,002	0,226	59,922	100,000
EO25vf, 12	Franz 1 time	Nergerfjellet, Egeøya	Tape	3,933	0,043	0,041	9,401	0,333	4,680	0,117	0,508	0,011	0,022	23,802	0,016	0,049	0,047	0,029	0,101	56,866	100,000
EO25vf, 14	Franz 1 time	Nergerfjellet, Egeøya	Tape	1,021	0,227	0,046	17,075	0,771	3,044	0,049	0,960	0,011	0,095	16,243	0,000	0,049	0,045	0,000	0,351	60,015	100,000
EO25vf, 16	Franz 1 time	Nergerfjellet, Egeøya	Tape	2,144	0,523	0,061	16,615	1,878	6,215	0,072	2,006	0,000	0,029	19,916	0,008	0,139	0,243	0,006	0,431	49,715	100,000
EO25vf, 18	Franz 1 time	Nergerfjellet, Egeøya	Tape	11,280	0,186	0,110	21,130	2,197	5,447	0,025	0,281	0,014	0,226	11,491	0,078	0,063	0,019	0,020	0,113	47,319	100,000

Sample	Separate Type	Location	Preparate	Al	Na	K	Cr	Si	Mg	Ca	Mn	Y	Ti	Fe	V	Co	Ni	Cu	Zn	O	Total
EO25vf, 20	Franz 1 time	Nergerfjellet, Egeøya	Tape	13,519	0,046	0,022	10,674	0,364	5,825	0,024	0,198	0,000	0,128	10,342	0,027	0,057	0,026	0,003	0,125	58,620	100,000
EO25vf, 21	Franz 1 time	Nergerfjellet, Egeøya	Tape	9,690	0,314	0,035	27,228	1,601	1,248	0,240	0,486	0,048	0,398	38,812	0,207	0,103	0,236	0,000	0,755	18,597	100,000
EO25vf, 22	Franz 1 time	Nergerfjellet, Egeøya	Tape	5,509	0,069	0,028	11,351	0,529	3,712	0,029	0,196	0,015	1,986	21,559	0,486	0,069	0,099	0,002	0,130	54,231	100,000
EO25vf, 23	Franz 1 time	Nergerfjellet, Egeøya	Tape	1,324	0,378	0,033	17,773	1,567	1,583	0,321	0,982	0,000	0,305	17,840	0,220	0,081	0,032	0,046	1,016	56,500	100,000
EO25vf, 24	Franz 1 time	Nergerfjellet, Egeøya	Tape	3,621	0,102	0,078	11,652	1,774	3,233	0,038	0,215	0,000	0,185	18,439	0,087	0,068	0,030	0,006	0,105	60,369	100,000
EO25vf, 25	Franz 1 time	Nergerfjellet, Egeøya	Tape	0,395	0,373	0,003	16,963	9,210	0,147	0,069	0,821	0,057	0,034	59,161	0,072	0,132	6,029	0,202	0,000	6,332	100,000
EO25vf, 26	Franz 1 time	Nergerfjellet, Egeøya	Tape	1,256	0,129	0,036	21,658	0,637	0,537	0,021	0,283	0,000	0,097	23,153	0,099	0,084	0,162	0,000	0,221	51,628	100,000
EO25vf, 27	Franz 1 time	Nergerfjellet, Egeøya	Tape	1,152	0,096	0,166	22,213	0,578	0,524	0,010	0,307	0,000	0,059	23,218	0,079	0,110	0,169	0,000	0,265	51,056	100,000
EO25vf, 28	Franz 1 time	Nergerfjellet, Egeøya	Tape	12,242	0,378	0,451	4,933	7,854	4,368	0,106	0,075	0,022	0,060	7,587	0,024	0,030	0,010	0,000	0,052	61,809	100,000
EO25vf, 29	Franz 1 time	Nergerfjellet, Egeøya	Tape	3,536	0,000	0,209	17,304	1,047	8,897	0,014	0,124	0,000	0,154	8,772	0,046	0,035	0,035	0,000	0,012	59,817	100,000
EO25vf, 30	Franz 1 time	Nergerfjellet, Egeøya	Tape	6,186	0,133	0,077	10,726	6,421	4,085	0,033	0,189	0,000	0,307	12,735	0,049	0,024	0,049	0,000	0,034	58,953	100,000
EO25vf, 31	Franz 1 time	Nergerfjellet, Egeøya	Tape	5,027	0,100	0,075	15,203	2,282	4,598	0,058	0,165	0,003	0,024	10,161	0,069	0,033	0,003	0,000	0,082	62,118	100,000
EO25vf, 33	Franz 1 time	Nergerfjellet, Egeøya	Tape	3,322	0,594	0,226	12,832	3,912	5,208	0,124	0,171	0,011	0,067	16,991	0,055	0,069	0,039	0,021	0,074	56,285	100,000
EO25vf, 34	Franz 1 time	Nergerfjellet, Egeøya	Tape	0,228	0,038	0,032	0,003	0,919	0,103	0,056	0,639	0,015	0,005	35,717	0,004	0,067	0,071	0,060	0,000	62,044	100,000
EO25vf, 37	Franz 1 time	Nergerfjellet, Egeøya	Tape	2,280	0,062	0,032	21,023	0,639	1,955	0,025	0,944	0,000	0,334	24,153	0,070	0,071	0,009	0,056	0,179	48,169	100,000
EO25vf, 38	Franz 1 time	Nergerfjellet, Egeøya	Tape	5,420	0,473	0,205	13,051	3,255	1,438	0,148	0,472	0,011	0,282	17,449	0,162	0,045	0,032	0,035	0,907	56,615	100,000
EO25vf, 39	Franz 1 time	Nergerfjellet, Egeøya	Tape	5,173	0,387	0,120	22,379	2,046	1,805	0,101	0,301	0,000	0,212	14,920	0,009	0,017	0,045	0,000	2,144	50,341	100,000
EO25vf 0,3, 1	Franz 2 times	Nergerfjellet, Egeøya	Tape	2,167	0,049	0,051	26,461	0,240	5,582	0,067	1,019	0,006	0,046	8,137	0,045	0,039	0,007	0,000	0,201	55,884	100,000
EO25vf 0,3, 3	Franz 2 times	Nergerfjellet, Egeøya	Tape	6,715	0,100	0,102	21,792	0,866	6,918	0,019	0,382	0,000	0,025	12,377	0,091	0,068	0,075	0,000	0,123	50,345	100,000
EO25vf 0,3, 4	Franz 2 times	Nergerfjellet, Egeøya	Tape	3,018	0,180	0,036	37,183	1,377	0,336	0,255	0,858	0,016	0,033	46,959	0,195	0,122	0,126	0,038	0,365	8,903	100,000
EO25vf 0,3, 5	Franz 2 times	Nergerfjellet, Egeøya	Tape	2,348	0,256	0,062	21,410	0,768	2,450	0,030	0,207	0,000	0,109	12,761	0,031	0,050	0,031	0,008	0,142	59,338	100,000

Sample	Separate Type	Location	Preparate	Al	Na	K	Cr	Si	Mg	Ca	Mn	Y	Ti	Fe	V	Co	Ni	Cu	Zn	O	Total
EO25vf 0,3, 6	Franz 2 times	Nergerfjellet, Egeøya	Tape	2,922	0,028	0,298	12,605	1,885	6,926	0,021	0,146	0,000	0,009	6,358	0,045	0,046	0,016	0,000	0,053	68,643	100,000
EO25vf 0,3, 7	Franz 2 times	Nergerfjellet, Egeøya	Tape	5,842	0,005	0,183	19,934	0,435	5,889	0,023	0,222	0,000	0,072	14,365	0,079	0,075	0,017	0,017	0,182	52,660	100,000
EO25vf 0,3, 9	Franz 2 times	Nergerfjellet, Egeøya	Tape	4,650	0,014	0,018	21,157	0,181	6,667	0,012	0,168	0,006	0,040	8,240	0,037	0,026	0,012	0,009	0,029	58,735	100,000
EO25vf 0,3, 10	Franz 2 times	Nergerfjellet, Egeøya	Tape	0,226	0,065	0,061	28,004	0,101	8,155	0,002	0,226	0,003	0,043	10,869	0,029	0,057	0,025	0,035	0,000	52,100	100,000
EO25vf 0,3, 12	Franz 2 times	Nergerfjellet, Egeøya	Tape	1,305	0,119	0,203	18,978	0,561	3,870	0,001	0,270	0,000	0,121	17,777	0,115	0,044	0,006	0,000	0,087	56,543	100,000
EO25vf 0,3, 13	Franz 2 times	Nergerfjellet, Egeøya	Tape	4,447	0,281	0,408	16,879	2,145	4,331	0,045	0,174	0,000	0,049	12,898	0,030	0,043	0,032	0,000	0,058	58,184	100,000
EO25vf 0,3, 14	Franz 2 times	Nergerfjellet, Egeøya	Tape	0,991	0,447	0,170	22,933	1,175	0,707	0,038	0,143	0,003	0,105	23,366	0,098	0,115	0,022	0,062	0,068	49,558	100,000
EO25vf 0,3, 16	Franz 2 times	Nergerfjellet, Egeøya	Tape	8,320	0,038	0,037	20,209	0,356	9,728	0,013	0,180	0,000	0,050	8,202	0,059	0,025	0,040	0,014	0,190	52,541	100,000
EO25vf 0,3, 17	Franz 2 times	Nergerfjellet, Egeøya	Tape	10,091	2,010	0,071	29,381	1,323	3,533	0,177	0,439	0,030	0,023	17,043	0,042	0,000	0,110	0,006	0,141	35,581	100,000
EO25vf 0,3, 18	Franz 2 times	Nergerfjellet, Egeøya	Tape	4,064	0,136	0,129	7,213	1,904	4,212	0,031	0,136	0,001	0,432	11,904	0,147	0,011	0,000	0,000	0,073	69,608	100,000
EO25vf 0,3, 19	Franz 2 times	Nergerfjellet, Egeøya	Tape	1,538	0,142	0,025	40,334	0,253	0,572	0,049	0,454	0,000	0,055	37,912	0,032	0,187	0,000	0,000	0,728	17,719	100,000
EO25vf 0,3, 20	Franz 2 times	Nergerfjellet, Egeøya	Tape	0,608	0,013	0,000	0,319	1,304	1,011	0,271	0,939	0,000	0,047	50,320	0,074	0,102	0,000	0,000	0,142	44,849	100,000
FES25mf/map5	Thick section	Festningen, Spitsbergen	Thick section	5,185	0,003	0,026	19,123	0,331	10,931	0,179	0,424	0,000	0,665	62,879	n/a	n/a	n/a	n/a	0,256	n/a	100,000
H-11, 1	Thin section	Iversenfjellet, Hopen	Thin section	19,718	0,028	0,000	28,180	0,624	20,188	0,028	0,395	0,000	0,019	30,339	n/a	n/a	n/a	n/a	0,481	n/a	100,000
H-11, 2	Thin section	Iversenfjellet, Hopen	Thin section	19,270	0,140	0,022	28,851	0,673	20,065	0,000	0,366	0,020	0,082	29,943	n/a	n/a	n/a	n/a	0,565	n/a	99,998
H-11, 3	Thin section	Iversenfjellet, Hopen	Thin section	0,862	0,295	0,045	18,556	2,495	3,966	0,074	13,008	0,000	0,081	58,712	n/a	n/a	n/a	n/a	1,906	n/a	100,000
H-11, 6	Thin section	Iversenfjellet, Hopen	Thin section	5,554	0,063	0,000	43,167	0,316	12,129	0,017	0,670	0,000	0,086	37,560	n/a	n/a	n/a	n/a	0,417	n/a	99,980
H-11, 7	Thin section	Iversenfjellet, Hopen	Thin section	3,131	0,016	0,000	44,160	0,650	7,178	0,041	0,945	0,003	0,036	43,127	n/a	n/a	n/a	n/a	0,709	n/a	99,994
H-11, 10	Thin section	Iversenfjellet, Hopen	Thin section	9,373	0,032	0,041	39,322	0,172	14,597	0,000	0,631	0,004	0,190	35,232	n/a	n/a	n/a	n/a	0,373	n/a	99,967
H30m, 1	Franz 1 time	Iversenfjellet, Hopen	Tape	5,757	0,039	0,017	13,657	0,386	2,263	0,032	0,740	0,000	2,248	26,481	0,425	0,064	0,060	0,096	0,240	47,497	100,000
H30m, 2	Franz 1 time	Iversenfjellet, Hopen	Tape	5,658	0,055	0,010	23,642	0,179	4,368	0,004	0,174	0,000	0,487	11,469	0,138	0,034	0,032	0,092	0,131	53,526	100,000

Sample	Separate Type	Location	Preparate	Al	Na	K	Cr	Si	Mg	Ca	Mn	Y	Ti	Fe	V	Co	Ni	Cu	Zn	O	Total
H30m, 4	Franz 1 time	Iversenfjellet, Hopen	Tape	2,735	0,261	0,057	20,295	2,717	0,681	0,089	2,809	0,000	0,388	29,075	0,062	0,042	0,000	0,215	1,104	39,471	100,000
H30m, 5	Franz 1 time	Iversenfjellet, Hopen	Tape	4,045	0,055	0,022	8,482	0,262	6,488	0,026	0,182	0,032	1,253	16,356	0,282	0,054	0,051	0,160	0,177	62,073	100,000
H30m, 6	Franz 1 time	Iversenfjellet, Hopen	Tape	1,979	0,467	0,050	11,385	2,208	1,312	0,112	0,480	0,016	0,203	14,254	0,061	0,033	0,019	0,237	1,203	65,981	100,000
H30VF, 1	Franz 1 time	Iversenfjellet, Hopen	Tape	4,292	0,041	0,000	20,347	0,180	5,043	0,008	0,170	0,004	0,033	9,197	0,072	0,043	0,026	0,026	0,133	60,386	100,000
H30VF, 2	Franz 1 time	Iversenfjellet, Hopen	Tape	1,261	0,145	0,072	19,695	1,249	7,159	0,042	0,162	0,000	0,186	8,414	0,101	0,046	0,000	0,041	0,272	61,156	100,000
H30VF, 3	Franz 1 time	Iversenfjellet, Hopen	Tape	2,208	0,738	0,042	19,039	2,179	0,610	0,177	1,294	0,000	0,486	18,671	0,075	0,142	0,130	0,091	2,080	52,040	100,000
H30VF, 4	Franz 1 time	Iversenfjellet, Hopen	Tape	6,788	0,514	0,047	14,092	2,029	0,475	0,148	0,279	0,000	1,764	16,163	0,276	0,061	0,045	0,121	3,435	53,766	100,000
H30VF, 5	Franz 1 time	Iversenfjellet, Hopen	Tape	16,492	0,126	0,036	12,107	0,358	6,548	0,026	0,122	0,000	0,329	10,457	0,158	0,022	0,028	0,068	0,102	53,023	100,000
H30VF, 6	Franz 1 time	Iversenfjellet, Hopen	Tape	14,519	0,061	0,035	10,135	0,773	6,181	0,033	0,121	0,000	0,050	12,353	0,107	0,037	0,098	0,081	0,092	55,324	100,000
H30VF, 10	Franz 1 time	Iversenfjellet, Hopen	Tape	5,841	0,221	0,090	20,785	0,875	0,501	0,024	1,345	0,000	0,006	14,007	0,086	0,039	0,000	0,065	0,854	55,262	100,000
H30VF, 11	Franz 1 time	Iversenfjellet, Hopen	Tape	0,385	0,197	0,037	15,696	0,382	3,099	0,044	0,151	0,000	0,015	11,093	0,058	0,043	0,071	0,061	0,666	68,004	100,000
H30VF, 12	Franz 1 time	Iversenfjellet, Hopen	Tape	2,471	0,659	0,093	15,642	1,654	0,678	0,228	1,303	0,000	0,285	28,443	0,076	0,064	0,000	0,084	0,909	47,412	100,000
H30VF, 13	Franz 1 time	Iversenfjellet, Hopen	Tape	4,507	0,244	0,080	16,540	1,885	3,865	0,040	0,249	0,015	0,086	9,643	0,082	0,057	0,000	0,045	0,134	62,529	100,000
H30VF, 14	Franz 1 time	Iversenfjellet, Hopen	Tape	7,053	0,008	0,039	15,408	0,409	8,943	0,039	0,232	0,028	0,014	6,268	0,055	0,020	0,026	0,048	0,065	61,346	100,000
H30VF, 15	Franz 1 time	Iversenfjellet, Hopen	Tape	4,450	0,047	0,041	20,088	1,230	4,743	0,010	0,153	0,005	0,031	8,374	0,068	0,031	0,000	0,000	0,186	60,544	100,000
H30VF, 16	Franz 1 time	Iversenfjellet, Hopen	Tape	15,469	0,027	0,093	12,534	0,877	7,512	0,000	0,137	0,000	0,145	7,727	0,106	0,023	0,039	0,029	0,086	55,196	100,000
H30VF, 17	Franz 1 time	Iversenfjellet, Hopen	Tape	5,534	0,219	0,222	19,486	5,046	0,728	0,320	1,067	0,000	0,649	20,671	0,126	0,142	0,124	0,085	2,767	42,814	100,000
H30VF, 18	Franz 1 time	Iversenfjellet, Hopen	Tape	14,878	0,153	0,144	11,608	1,383	7,846	0,013	0,108	0,002	0,175	6,648	0,112	0,029	0,034	0,042	0,063	56,762	100,000
KTO14m, 1	Franz 1 time	Kapp Toscana, Spitsbergen	Tape	6,895	0,292	0,129	33,344	1,487	2,024	0,169	0,492	0,000	0,117	34,254	0,130	0,128	0,103	0,000	0,187	20,250	100,000
KTO14m, 2	Franz 1 time	Kapp Toscana, Spitsbergen	Tape	3,519	0,685	0,679	23,798	2,463	1,946	0,548	0,541	0,010	0,270	27,177	0,070	0,126	0,151	0,036	0,552	37,429	100,000
KTO14m, 3	Franz 1 time	Kapp Toscana, Spitsbergen	Tape	15,398	0,122	0,538	13,564	1,567	8,874	0,027	0,105	0,000	0,051	7,634	0,063	0,037	0,034	0,009	0,212	51,765	100,000

Sample	Separate Type	Location	Preparate	Al	Na	K	Cr	Si	Mg	Ca	Mn	Y	Ti	Fe	V	Co	Ni	Cu	Zn	O	Total
KTO14m, 4	Franz 1 time	Kapp Toscana, Spitsbergen	Tape	10,796	0,093	0,063	26,651	0,229	4,991	0,074	0,231	0,018	0,372	15,718	0,163	0,002	0,077	0,000	0,320	40,201	100,000
KTO14m, 5	Franz 1 time	Kapp Toscana, Spitsbergen	Tape	1,085	0,338	0,084	15,156	1,106	0,876	0,069	0,294	0,000	0,261	19,754	0,122	0,055	0,088	0,000	1,114	59,598	100,000
KTO14m, 7	Franz 1 time	Kapp Toscana, Spitsbergen	Tape	0,451	0,174	0,073	16,534	0,696	1,738	0,063	0,269	0,000	0,078	24,155	0,074	0,028	0,129	0,000	0,083	55,455	100,000
KTO14m, 9	Franz 1 time	Kapp Toscana, Spitsbergen	Tape	3,816	0,331	0,776	11,736	12,426	0,570	1,657	0,600	0,000	0,113	40,597	0,056	0,125	4,048	0,136	0,000	23,016	100,000
KTO14m, 10	Franz 1 time	Kapp Toscana, Spitsbergen	Tape	3,503	2,675	0,372	12,484	8,744	0,790	0,109	0,229	0,016	0,147	14,078	0,094	0,004	0,034	0,043	0,426	56,251	100,000
KTO14m, 11	Franz 1 time	Kapp Toscana, Spitsbergen	Tape	6,547	1,646	0,312	13,463	4,763	2,069	0,181	1,722	0,010	0,030	26,509	0,008	0,171	0,130	0,013	0,358	42,068	100,000
KTO14m, 12	Franz 1 time	Kapp Toscana, Spitsbergen	Tape	5,967	0,229	0,352	24,278	1,747	4,669	0,049	0,372	0,016	0,072	13,731	0,075	0,041	0,018	0,000	0,159	48,226	100,000
KTO14m, 13	Franz 1 time	Kapp Toscana, Spitsbergen	Tape	1,214	0,258	0,278	13,156	1,635	2,556	0,169	0,336	0,002	0,045	15,057	0,073	0,045	0,037	0,000	0,215	64,926	100,000
KTO14m, 14	Franz 1 time	Kapp Toscana, Spitsbergen	Tape	5,828	0,029	0,081	10,319	0,562	3,092	0,033	0,174	0,106	1,091	21,513	0,202	0,049	0,061	0,025	0,130	56,707	100,000
KTO14m, 15	Franz 1 time	Kapp Toscana, Spitsbergen	Tape	2,426	0,047	0,132	23,795	0,559	4,601	0,024	0,234	0,000	0,027	11,875	0,087	0,041	0,013	0,003	0,158	55,977	100,000
KTO14m, 16	Franz 1 time	Kapp Toscana, Spitsbergen	Tape	5,903	0,124	0,098	10,340	0,797	3,149	0,057	0,168	0,001	1,123	21,797	0,232	0,051	0,045	0,001	0,089	56,025	100,000
KTO14m, 17	Franz 1 time	Kapp Toscana, Spitsbergen	Tape	0,245	0,038	0,017	17,239	0,179	1,193	0,066	0,345	0,000	0,125	25,995	0,079	0,092	0,016	0,008	0,133	54,230	100,000
KTO14m, 18	Franz 1 time	Kapp Toscana, Spitsbergen	Tape	3,228	0,324	0,570	17,847	3,491	0,924	0,129	0,938	0,000	0,460	24,397	0,088	0,092	0,162	0,001	0,298	47,054	100,000
KTO14m, 19	Franz 1 time	Kapp Toscana, Spitsbergen	Tape	8,116	0,208	0,047	18,695	0,644	0,516	0,150	2,379	0,000	0,659	26,098	0,244	0,077	0,090	0,000	0,611	41,467	100,000
KTO14m, 20	Franz 1 time	Kapp Toscana, Spitsbergen	Tape	5,168	0,706	0,400	31,824	1,535	3,236	0,077	0,309	0,000	0,128	17,977	0,045	0,091	0,021	0,000	0,129	38,353	100,000
SV-7-4, 2	Thin section	Blanknuten, Edgeøya	Thin section	7,056	0,035	0,000	41,045	0,766	10,803	0,054	0,759	0,000	0,052	38,959	n/a	n/a	n/a	n/a	0,462	n/a	99,992
SV-7-4, 3	Thin section	Blanknuten, Edgeøya	Thin section	3,393	0,021	0,031	33,710	0,317	5,138	0,086	0,965	0,066	0,233	55,567	n/a	n/a	n/a	n/a	0,466	n/a	99,993
SV-7-4, 4	Thin section	Blanknuten, Edgeøya	Thin section	18,327	0,030	0,026	28,345	0,674	18,569	0,020	0,544	0,000	0,000	33,028	n/a	n/a	n/a	n/a	0,437	n/a	100,000
SV-7-4, 5	Thin section	Blanknuten, Edgeøya	Thin section	6,758	0,084	0,071	14,981	9,839	16,585	0,056	0,963	0,000	0,425	49,389	n/a	n/a	n/a	n/a	0,843	n/a	99,992

6.4.2 Plot generation

By modifying the compositional data as laid out in Barnes and Roeder (2001), comparing chromium spinel data in the same plots become viable. Based on the generalized XY_2O_4 spinel formula, the organized data enables generation of the four discrimination diagrams used in this study;

- Triplot of the major trivalent cations Cr, Fe^{3+} and Al.

- Plot of $Fe^{2+}/(Fe^{2+}+Mg)$ vs $Cr/(Cr+Al)$ ratios.

- Plot of $Fe^{2+}/(Fe^{2+}+Mg)$ vs $Fe^{3+}/(Cr+Al+Fe^{3+})$ ratios.

- Plot of TiO_2 weight % vs $Fe^{3+}/(Cr+Al+Fe^{3+})$ ratios.

The Barnes and Roeder (2001) article also present density distribution plots of the 50th and 90th percentiles of chromium spinels from different petrogenesis. The generated density plots are based on published chromium spinel compositions available at the time of publication, providing a tool to compare chemical composition to petrogenesis. A triplot representing all samples applied in the Barnes and Roeder (2001) article are presented in Figure 6.39, it is compensated for over- sampling.

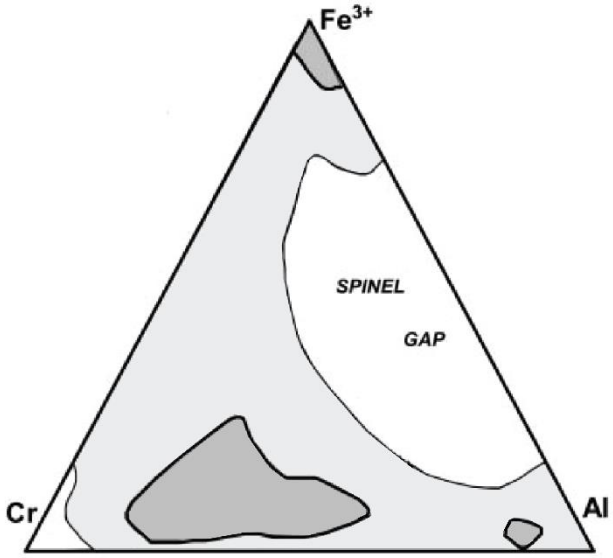

Figure 6.39 *Chemical composition of major trivalent cations in chromium spinel. Plotted with the 95th (dark gray) and 50th (bright gray) procentiles. Modified after Barnes and Roeder (2001).*

6.4.3 Dataset differences

In order to investigate the relevance of the various chromium spinel data sets due to differences in sample location, grain size, way of concentrating grains or preparation before EPMA scanning, the different data sets have been plotted against each other. With only a few data points for several of the data sets statistical relevance is not attainable in most cases.

Comparing the data sets visually can, in spite of the few data points, show disparities. It can disclose provenance sensitive information, or information about biases in the sampling and concentrating process. The following plots and comments presented in this sub-chapter were chosen as they depict datasets relevant for comparison in a visually attainable way. It is also worth noting that discrepancies plotted may be caused by other differences than the one investigated in each figure.

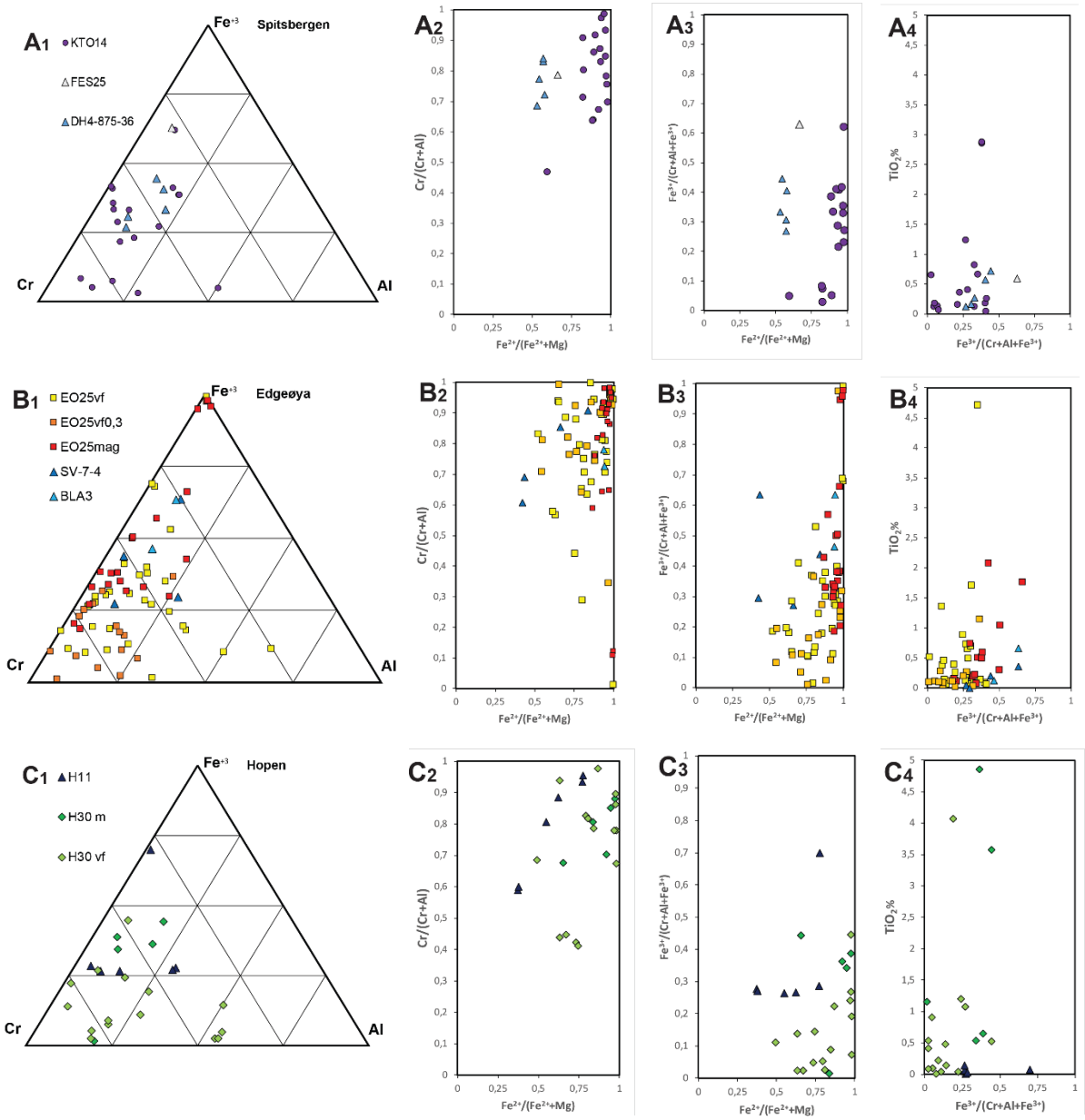

Figure 6.40 *Plots comparing different sampling locations west to east. A diagrams depict Spitsbergen chromium spinel samples, B depict Edgeøya samples and C show Hopen samples. Numbers 1- 4 represent; 1)Triplot of Cr, Fe^{2+}, Al trivalent cation population, 2) $Fe^{2+}/(Fe^{2+}+Mg)$ vs $Cr/(Cr+Al)$, $Fe^{2+}/(Fe^{2+}+Mg)$ vs $Fe^{3+}/(Cr+Al+Fe^{3+})$ and 4) $Fe^{3+}/(Cr+Al+Fe^{3+})$ vs TiO^2 weight percent.*

No clear differences can be observed between sampling locations seen in Figure 6.40. In the triplots (A1, B1, C1) a low aluminium signature, with clustering around a main cluster of 30% Fe^{3+} is observed, although the clustering is somewhat less developed in the Hopen samples (C1), than the others. Samples plotting around the cluster show a similar pattern with both Cr, Fe^{3+} as well as Al enriched members. Similar patterns are observed for all locations in the

discrimination diagrams, although the Hopen samples C show less clustered plots. This may however be a result of fewer data points from Hopen.

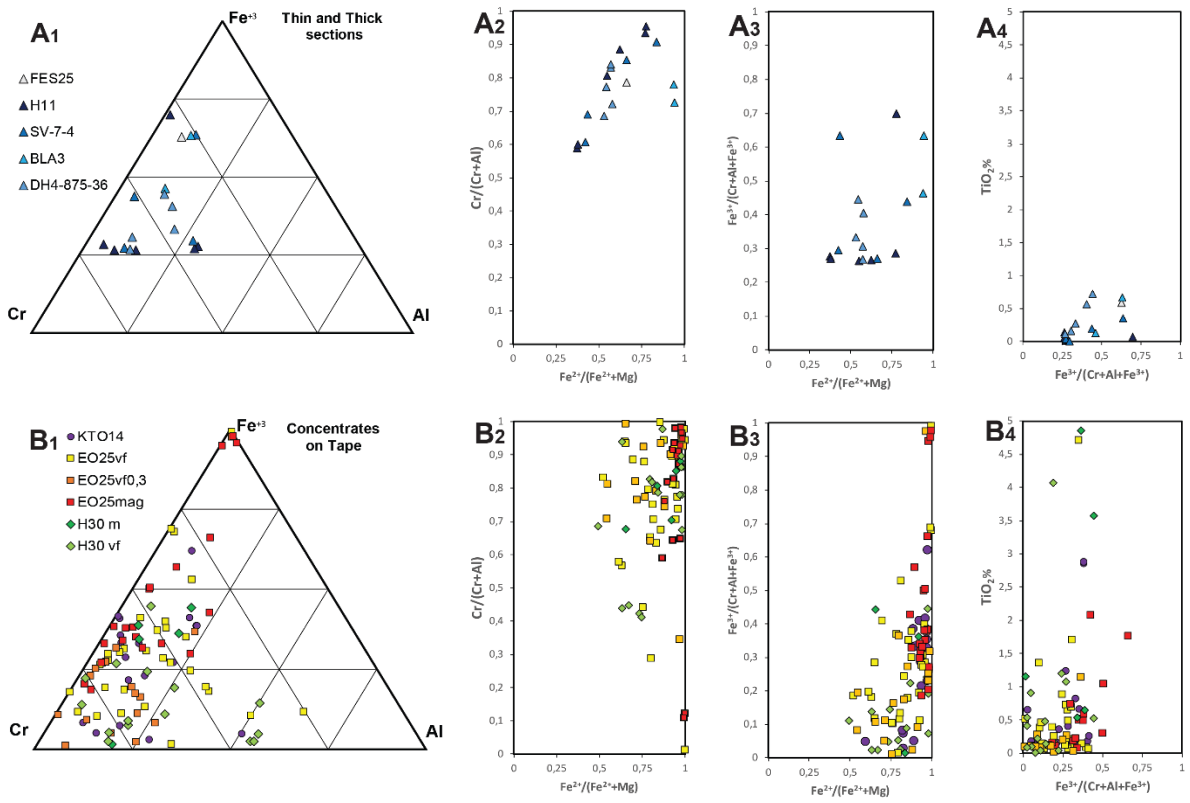

Figure 6.41 *Comparing data from thin sections (A), to samples with topography (B). Numbers 1- 4 represent; 1)Triplot of Cr, Fe^{2+}, Al trivalent cation population, 2) $Fe^{2+}/(Fe^{2+}+Mg)$ vs $Cr/(Cr+Al)$, $Fe^{2+}/(Fe^{2+}+Mg)$ vs $Fe^{3+}/(Cr+Al+Fe^{3+})$ and 4) $Fe^{3+}/(Cr+Al+Fe^{3+})$ vs TiO^2 weight percent.*

The discrimination diagrams in Figure 6.41 plot compositional data from thin sections differently than samples with topography. This is also a comparison of compositional data gathered from unprocessed sandstones (A) vs samples that have undergone steps of concentration and Franz separation (B). The cause of the observed differences cannot with absolute certainty be attributed to only one of the possibilities. The triplot in Figure 6.41 B1 show a wider distribution in the plot, than the data points in the A1 triplot. Both triplots show low Al content for the great majority of the data points, but the B1 selection have both magnetite's (Fe^{3+} end member) and several Cr enriched entries. The complete A1 data set have similar data points found in the B1 data set but with a different central point, B1 having less aluminium.

Differences in the datasets of Figure 6.41 can be best observed in the A2/B2, A3/B3 and A4/B4 plots. The most important observation from these plots are the low Mg content of the B dataset.

A majority of the A2 compositions show a marked higher magnesium content than the B2 selection while still having a similar Cr/Al ratio in the two datasets. The same high magnesium content observed in the thin section data are seen in the A3/B3 data where A3 plots with Mg enriched with higher Fe^{3+} content then chromium spinel of the B dataset. The A4/B4 discrimination diagram show a more concentrated A dataset, and high TiO_2 values only in the B dataset. The Low Fe^{3+} values are also not found in this discrimination diagram. Although plotting close in the triplots, the two datasets A and B show significant differences, especially concerning the Mg content. This call the reliability of the B dataset in question

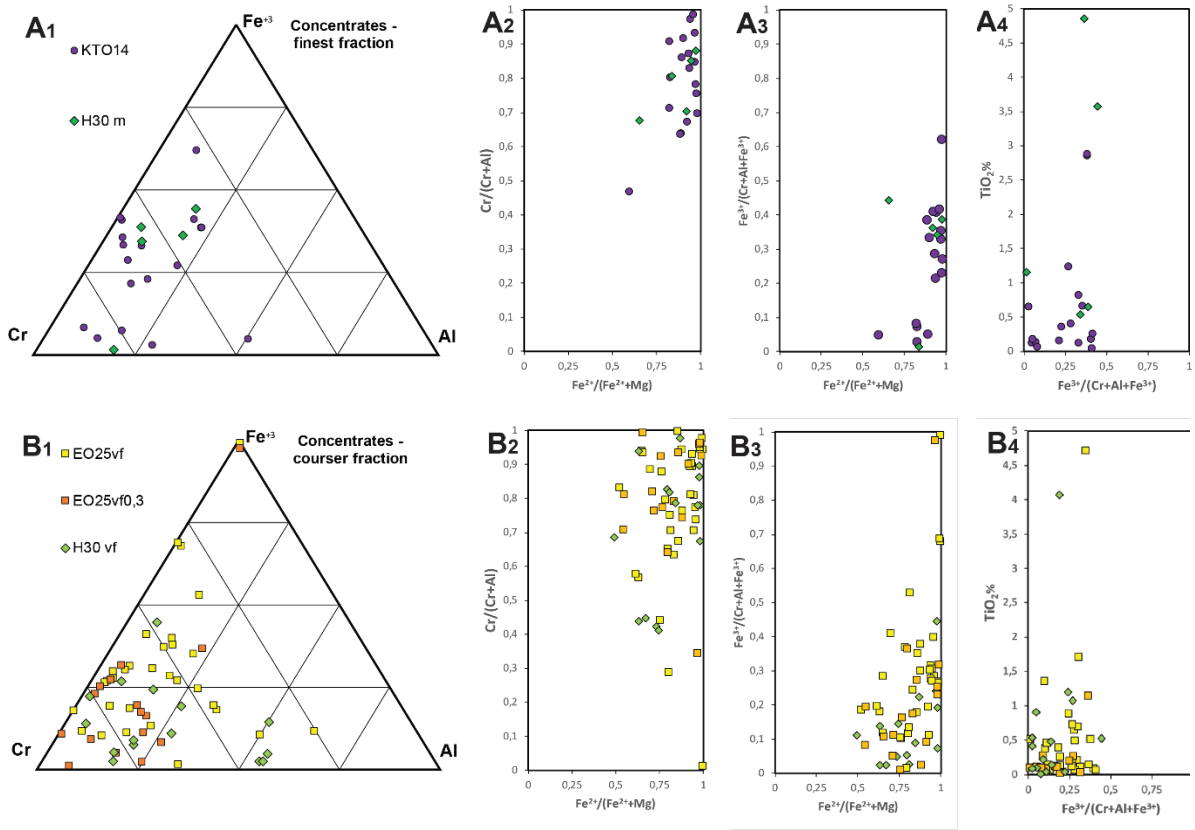

Figure 6.42 *Comparing chromium spinel grains in two different grain size fractions. Silt size fraction grains are plotted in A diagrams. Courser fraction chromium spinel grains are plotted in B diagrams. Numbers 1- 4 represent: 1)Triplot of Cr, Fe^{2+}, Al trivalent cation population, 2) $Fe^{2+}/(Fe^{2+}+Mg)$ vs $Cr/(Cr+Al)$, $Fe^{2+}/(Fe^{2+}+Mg)$ vs $Fe^{3+}/(Cr+Al+Fe^{3+})$ and 4) $Fe^{3+}/(Cr+Al+Fe^{3+})$ vs TiO^2 weight percent.*

Chromium spinel grains are found in different size fractions of the sieved and Franz separated sandstone concentrates. In Figure 6.42 a comparison of the fine, mainly silt size, grains (A) and courser fine to very fine sand sized grains (B) are observed. No definite differences between the datasets are observed, indicating that the grain size parameter on the concentrates do not influence the registered element distribution. When taking the A2 and B2, A3 and B3 and A4

and B4 discrimination diagrams into consideration, the data plot more clearly clustered in the A dataset, but with some points covering roughly the same area as the B dataset. In the A1 and B1 Triplot the same general distribution pattern appears, although here the B dataset has the most pronounced clustering. The B dataset displays a higher Cr vs Fe^{3+} content then the A dataset, but Cr rich samples can also be seen in the A dataset. The faction size of the separates does not show any significant biases.

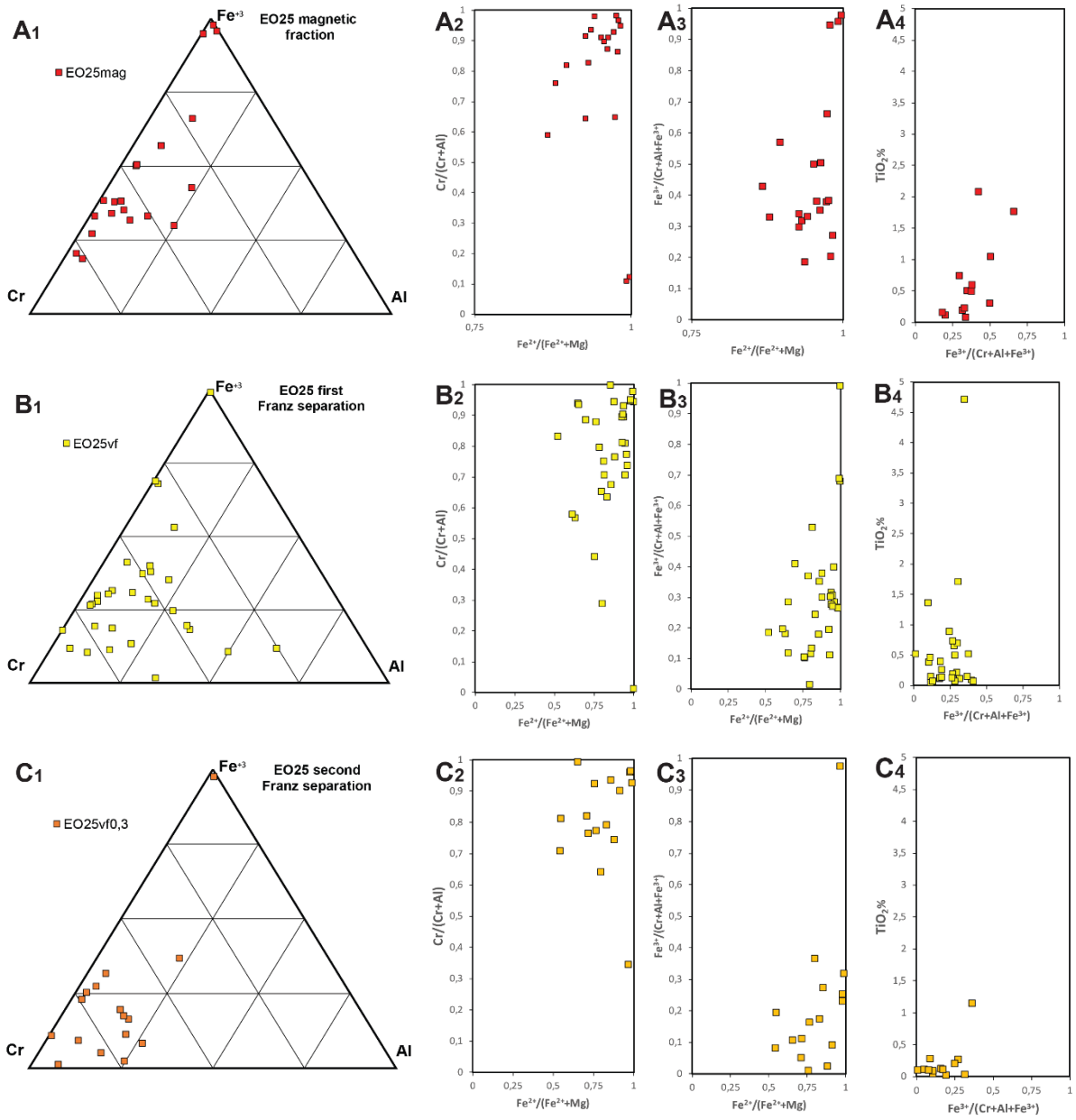

Figure 6. 43 *Comparing the different separates of the same rock sample, EO25. A show the most magnetic fraction, removed by a strong magnet before Franz. B are the samples for the first Franz separation, C are the results after a second Franz separation on the same rock sample. Numbers 1- 4 represent: 1)Triplot of Cr, Fe^{2+}, Al trivalent cation population, 2) $Fe^{2+}/(Fe^{2+}+Mg)$ vs $Cr/(Cr+Al)$, $Fe^{2+}/(Fe^{2+}+Mg)$ vs $Fe^{3+}/(Cr+Al+Fe^{3+})$ and 4) $Fe^{3+}/(Cr+Al+Fe^{3+})$ vs TiO^2 weight percent.*

Figure 6. 43 compares three different separates of the same sandstone sample, EO25. The A1, B1 and C1 plots as well as the A3, B3 and C3 plots clearest show the differences in composition between these datasets. The magnetic (A) sample represent the most magnetic fragments separated before Franz separation. As shown in the dataset of A1 and A3, this way of separation has favoured the Fe^{3+} enriched chromium spinels in the dataset. A standard Franz separation were performed on the B separate, showing a triplot pattern representative of the total De Geerdalen chromium spinel dataset of this study. The C datasets are two times Franz separated samples and clearly showing chromium enrichment. This suggests biased sampling favouring a higher chromium content, possibly because of less magnetic response. The A2, B2 and C2 and A4, B4 and C4 datasets plot similarly, showing a similar magnesium content and low titanium content.

The separates show clear differences, with the magnetic fraction (A) samples being Fe^{3+} enriched, and the two times Franz separated sample (C) being clearly Cr enriched. The one time Franz separated sample (B) can be seen as an average of the two other separates. If the A and C datasets were to be combined, they would produce a similar pattern to the B dataset. A combined E25 dataset is therefore suggested to be representative, while the A and C constituents have clear biases with respect to two of the major trivalent cations in the crystal structure.

6.4.4 Chromium spinel source rock characteristics

The De Geerdalen Formation chromium spinels compositions are quite uniform, suggesting that a considerable majority have the same or similar petrogenic origin. After comparing the dataset to possible source rock density distribution diagrams, a continental intrusion petrogenesis is found a likely source. The more specific petrogenic division into categories such as “Sub –volcanic intrusions in flood basalt provinces”, “flood basalt” and “continental intrusions” (Barnes and Roeder, 2001) are difficult to determine.

A possible bias in the data between polished thin sections and samples on tape is observed in Figure 6.41, and as a consequence several figures in this sub-chapter will cover both complete datasets and the thin section dataset. In the figures, information about the source rock is derived from comparing datasets to Figure 6.41, and the density distribution diagrams of Barnes and

Roeder (2001). In this sub- chapter, discrimination diagrams that provide information excluding or supporting one possible source rock interpretation will be presented.

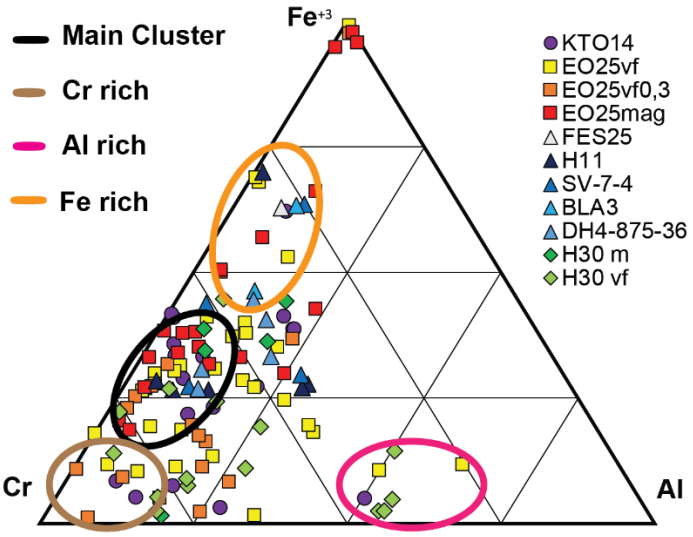

Figure 6.44 *Complete dataset plotted in a triplot with interesting mineral composition clusters indicated.*

As seen in Figure 6.44 a main cluster in the complete data-set can be observed. It has low aluminium content and a Cr/(Cr+Fe^{3+}) ratio of around 0,70. No major rock density distribution diagram covers the entire main cluster, making a straight-forward source interpretation impossible. By inspecting the other areas of interest in Figure 6.44, important petrogenic information can be gained. The low aluminium content, and higher iron content, restricts the possibility of a major ophiolite source, with a possibility of minor input recognized in the Al rich sub- group. The Cr- rich group can possibly be an expression of a minor chromium spinel source rock, or be variations within the main source. The existence of a Fe^{3+} rich cluster proves important to source rock identification, as it limits possible source rocks.

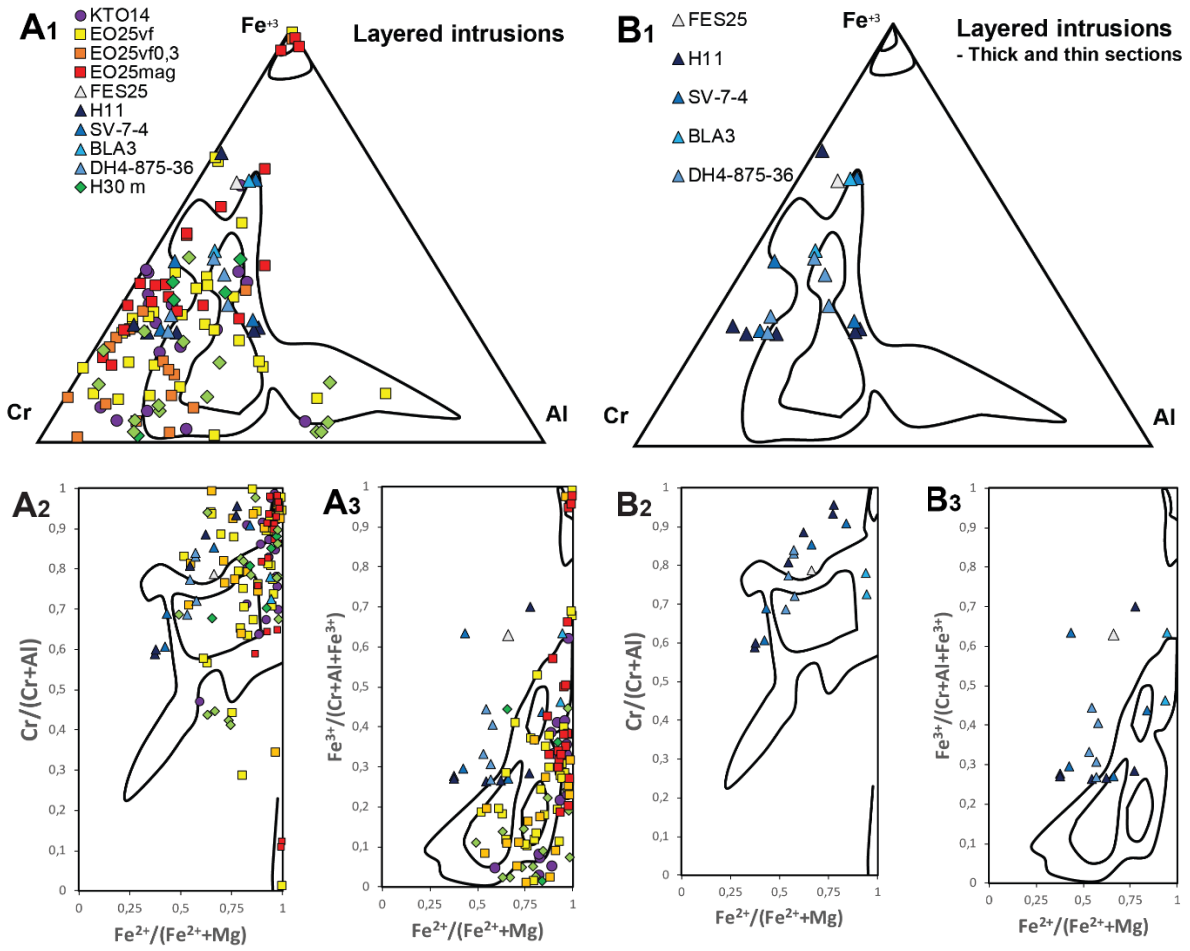

Figure 6.45 *Comparison of the dataset to layered intrusions density distribution diagrams with the 90th (outer curves) and 50th procentiles (inner curves). Complete dataset labelled A, polished thin section dataset labelled B.*

Mafic and sometimes ultra-mafic continental layered intrusions are a category density distribution plots of Barnes and Roeder (2001), covering both the plutonic intrusion, associated chromitites as well as sub volcanic intrusions. Chromium spinels of this origin are often richer in Fe^{3+} and Mg then ophiolites or basalts, except flood basalts. In Figure 6.45 the complete chromium spinel dataset and the polished thin section dataset are compared to layered intrusion density distribution diagrams. A TiO_2 weight percent vs $Fe^{3+}/(Cr+Al + Fe^{3+})$ were not included, as a comparison to the density distribution diagram procentiles does not provide discriminating information.

The triplots of A1/B1 in Figure 6.45 fit many of the chromium spinels with a higher Al content than that of the main cluster in Figure 6.44. The B1 data plot fits reasonably well with this density distribution diagram, better than the complete dataset of A1. The fit observed in B1 weakens in the B2 and B3 density distribution diagrams, only showing vague similarities. The

main cluster of A1 and A2 data generally constitute of too little aluminium to fit the layered intrusions density distribution diagram. In the A2, and more observable in the A3 diagrams, are the Mg content on the low side of a fit, but not by much.

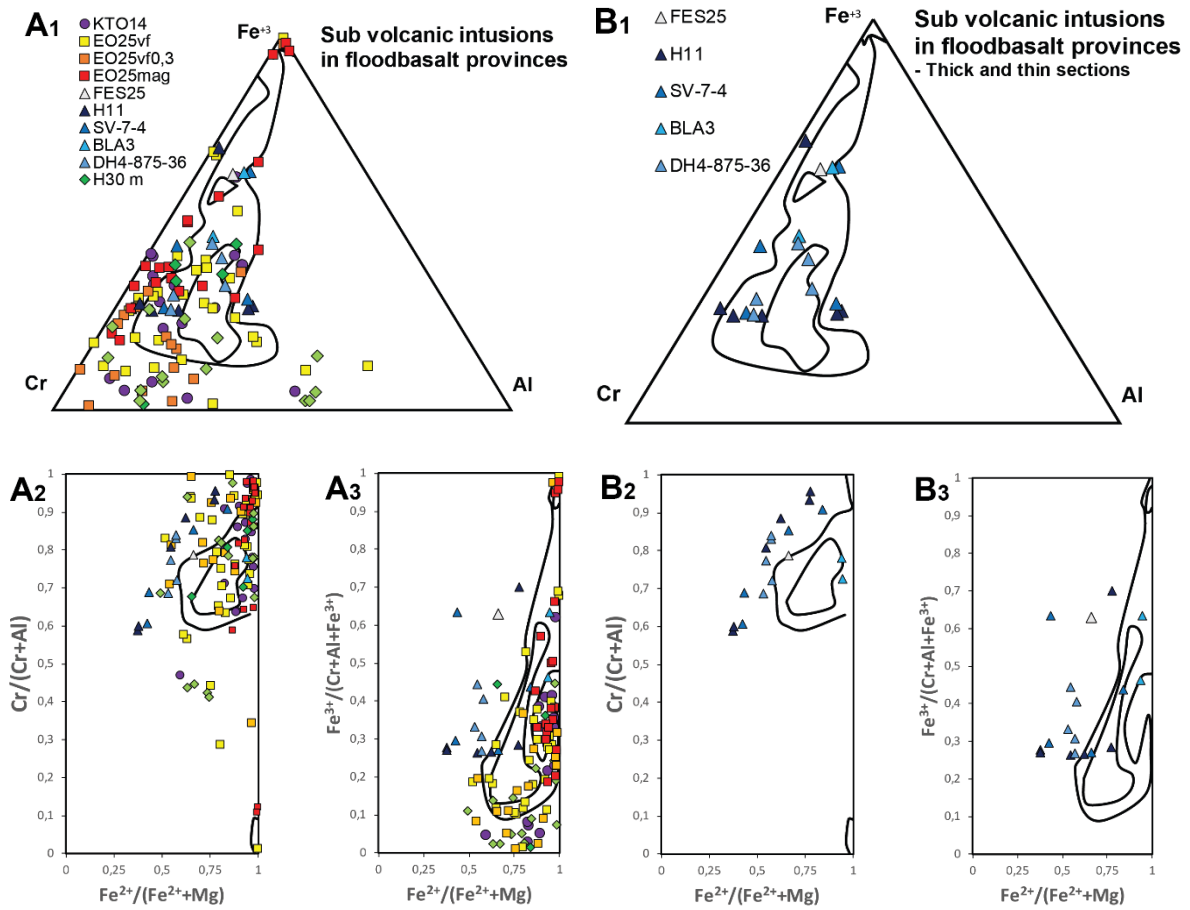

Figure 6.46 *Comparison of the dataset to sub volcanic intrusions in flood basalt provinces density distribution diagrams with the 90th (outer curves) and 50th procentiles (inner curves). Complete dataset labeled A and polished thick and thin section dataset labeled B.*

The density distribution diagram "Sub volcanic intrusions in flood basalt province" is compared to the dataset in Figure 6.46. These are sills and dikes in the proximity of, or originating in flood basalt. Similar to the layered intrusion diagram the origin of the rocks are continental intrusive magmas. The differences are more Fe^{3+} chromium spinels as well as a slightly lower aluminium content in the grains. When comparing to thin and thick section data points, this density distribution diagram proves a good fit, the same data do however not match the B2 and B3 compositions, generally having too high Mg content. In A1 and A2 the sub volcanic intrusions density distribution diagrams cover much of the main cluster data points, although aluminium content is on the low side. The A3 plot fit better than the B3 plots, plotting close to the sub

volcanic intrusion 90th procentiles. TiO_2 weight percent diagram did not add discriminatory information in this case.

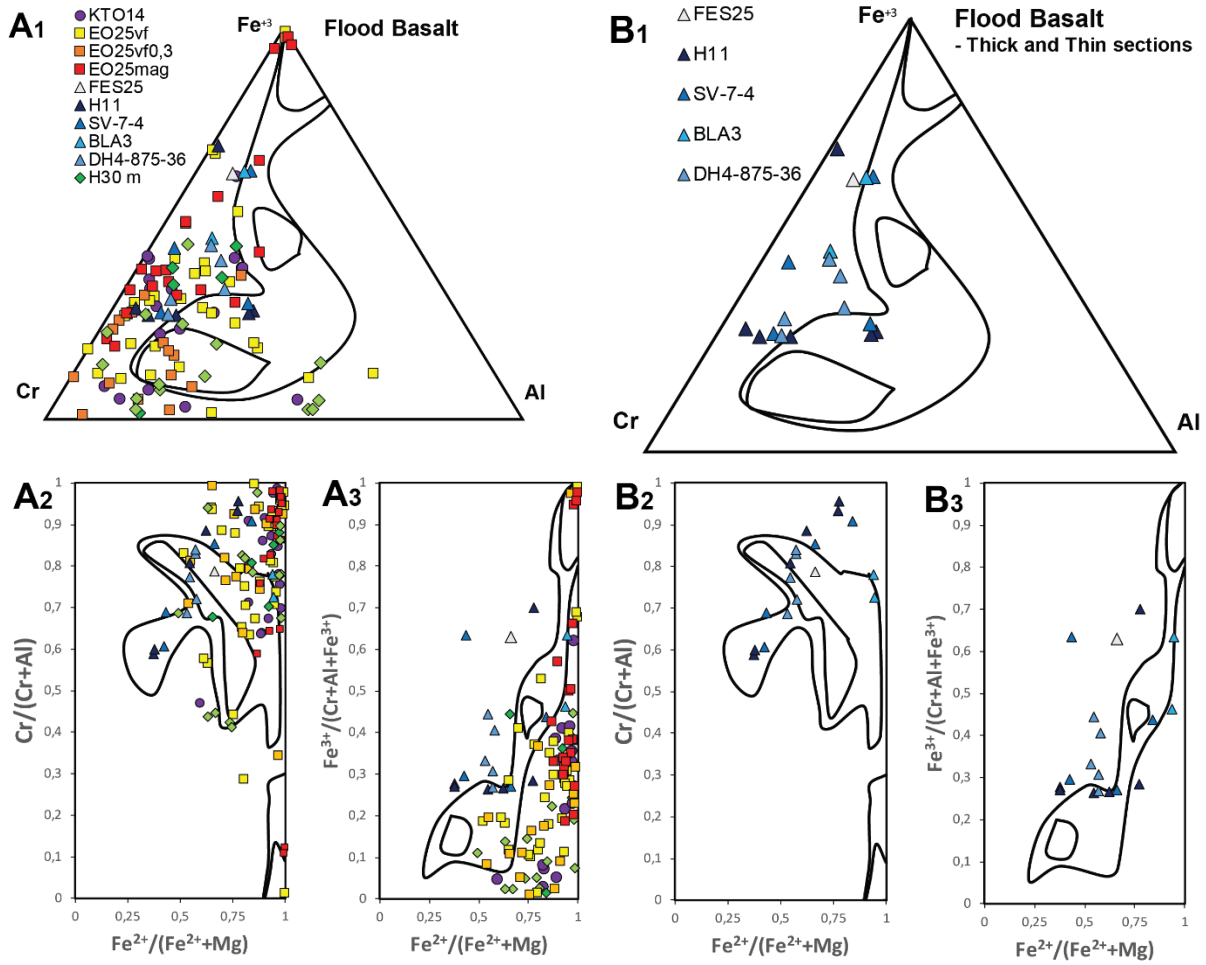

Figure 6.47 *Comparison of the dataset to flood basalt density distribution diagrams with the 90th (outer curves) and 50th procentiles (inner curves). Complete dataset labeled A and polished thick and thin section dataset labeled B.*

Another possible continental chromium spinel source, and associated with the sub volcanic flood basalt province intrusions, are flood basalts as compared to in Figure 6.47. A larger Fe^{3+} - rich population combined with a higher aluminium content than in other continental sources are expected in flood basalt chromium spinel. The B thin section dataset is inconclusive, the B2 plot proves a good fit, while B1 generally contains too little aluminium. The B3 diagram shows a similar trend in the dataset as in the flood basalt distribution, but with a too high Mg content it is not a direct match. The A dataset correlates less than the B dataset, having less aluminium as shown in A1 and A2, and low magnesium as displayed in the A2 and especially in the A3 dataset.

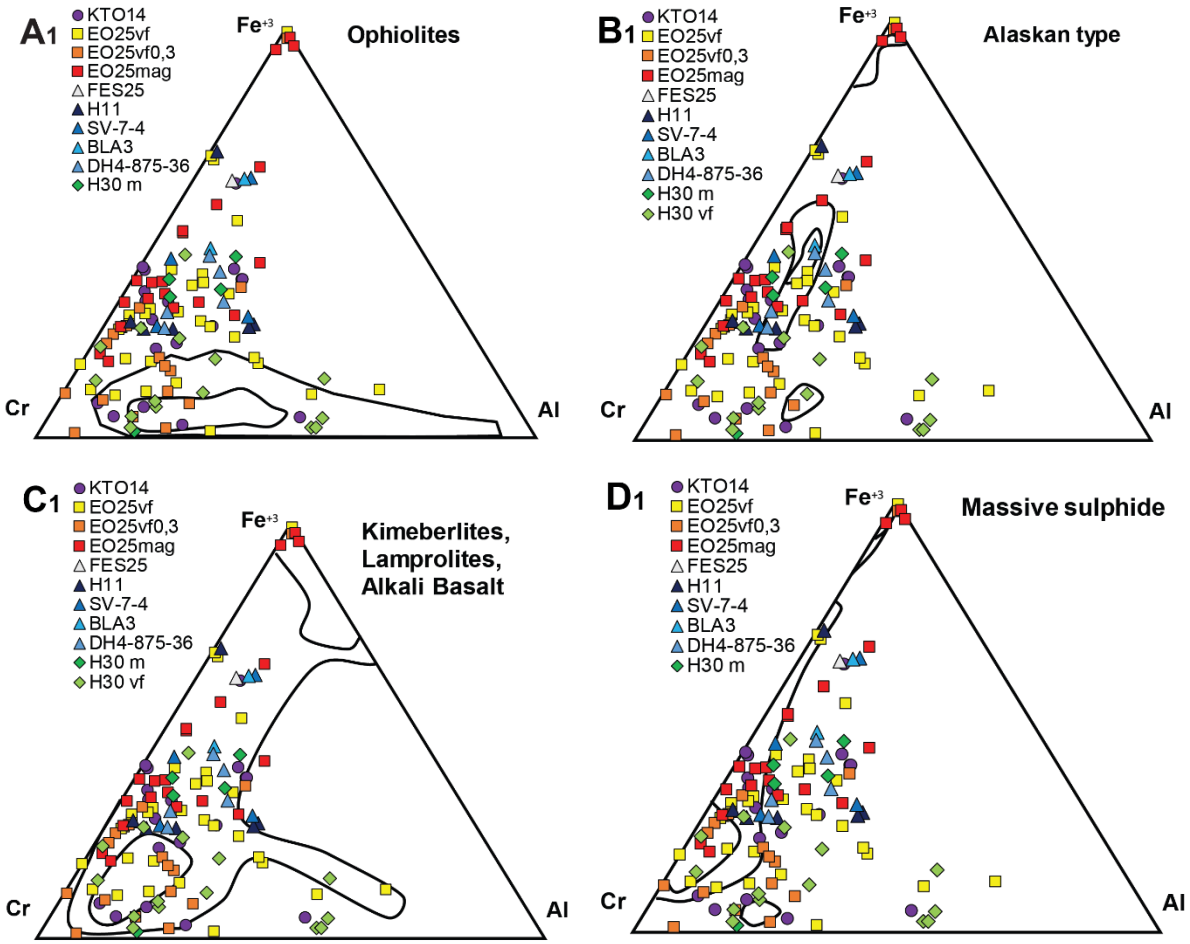

Figure 6.48 *Comparison of the complete dataset to several density distribution diagrams: A – Ophiolites, B – Alaskan type intrusions, C – Kimberlites, Lamprolites and Alkali basalt and D – Massive Fe – Ni sulphides with 90th (outer curves) and 50th procentiles (inner curves).*

In A1 of Figure 6.48 and Figure 6.49, comparisons to ophiolite density distribution diagram percentiles are shown. The ophiolite density distribution diagram is included in the figures, to represent rocks that are of ophiolite associated origin, and show the same trend of low Fe^{3+} and highly varying Cr/Al ratio. The categories “Ocean Floor”, “Ocean Island” and “Island Arc” of Barnes and Roeder (2001) display the same compositional trend as ophiolites. Ophiolittic chromium spinel compositions do not fit well with the chromium spinel of the dataset. In Figure 6.48 some overlapping chromium spinels can be observed, mostly EO25, H30 and KTO14 samples. In Figure 6.49 most of the overlapping data points are thin section samples. Based on this data can ophiolittic or similar rocks not be excluded as minor source to the De Geerdalen Formation chromium spinels. It can, however, not be a major contributor, as the composition does not match for most chromium spinel grains.

Alaskan type ultra-mafic intrusive rocks generate a distinct type of chromium spinel distribution, as compared in the B1 datasets in Figure 6.48 and Figure 6.49. As the Alaskan type chromium spinels constitute of quite specific compositions, as seen in Figure 6.48, this type of rock does not explain the much larger distribution of compositional data found in the plot. In Figure 6.49, some of the thin section data points correspond to Alaskan type origin, the same thin section points that have overlapping plots in the triplot. Based on the dataset can an Alaskan type intrusion possibly be a marginal contributor to the De Geerdalen Formation sediments as there are a few overlapping chromium spinels.

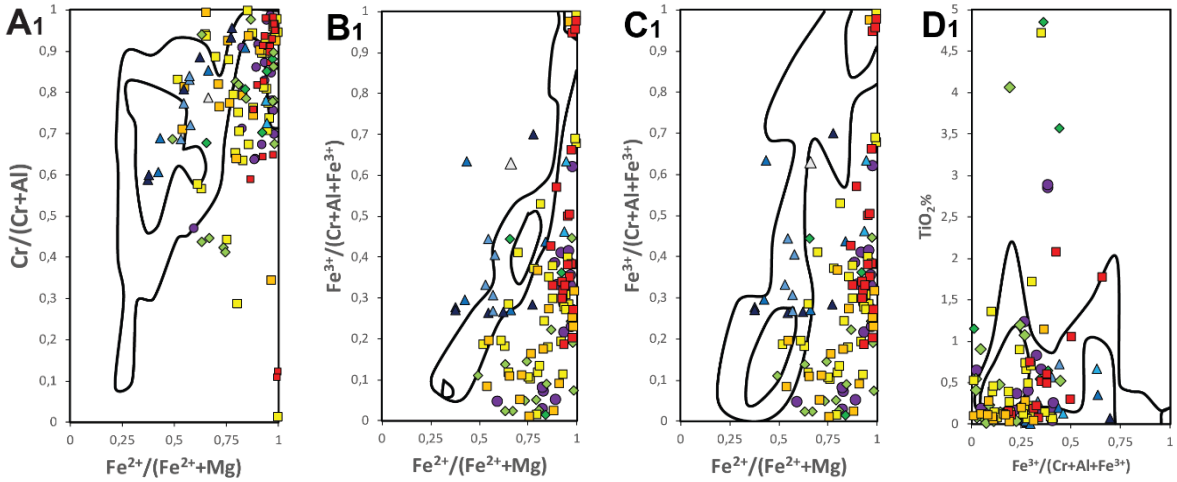

Figure 6.49 *Comparison of the complete dataset to density distribution diagrams for A – Ophiolites, B – Alaskan type intrusions, C – Kimberlites, Lamprolites and Alkali basalt and D – Massive Fe – Ni sulphides with 90th (outer curves) and 50th procentiles (inner curves).*

7 Discussion

When discussing the De Geerdalen Formation provenance, the results of this study will be assessed before taking other authors' work on the De Geerdalen Formation provenance into consideration. The discussion starts with an assessment of the quality of the acquired data. This is necessary because it seems that there is a bias in the dataset related to the mode of acquisition. The results are discussed starting with the source rock lithology based on petrographical observations. Later, the source of the chromium spinels in the De Geerdalen Formation is discussed, based on the differences in chemical composition of the detrital minerals. Finally, a sub- chapter comparing the results of this work to that of other authors' contributions is presented.

7.1 Data quality

Before interpreting and discussing the results, an evaluation of the quality of the data produced in this study is necessary. As the petrographical data were non- quantitative, the presence of minerals, clasts and textures are established by direct visual light microscope or SEM observation. Erroneous identification is possible, but this risk is greatly reduced by repeated observations of the same type, as well as determining chemical compositions by the use of a Scanning Electron Microscope. As pointed out in the results chapter, a bias in the measured chromium spinel composition was present. This bias can have different explanations, but must be taken into consideration before discussing the data further.

7.1.1 Chromium spinel data

The bias in the measured chromium spinel compositions is described in Figure 6.44, where thin section data generally contained more aluminium, trivalent iron and less magnesium than chemical compositions determined on tape attached chromium spinel. Three possible explanations for the bias are suggested:

- Tape attached chromium spinels have a topography. This may have influenced measurements and under-reported or over-reported some of the element concentrations. The low total oxide percent (See Appendix 1) of these datasets suggests flaws in the EPMA measurements.

- Variations in the response to magnetic separation. Degree of magnetic susceptibility may vary between different chromium spinel compositions, possibly over-sampling more magnetic

minerals. In Figure 6.46 the impact of different separation techniques on the same sample is observed, resulting in variations in chemical composition. The observed variations were mainly in the total Fe^{3+} content.

- Variations in sampled rocks.

Of the possible reasons for the bias in the dataset, the most probable explanation is measurements on flat surfaces versus uneven surfaces. Other possibilities do not account for the low total compositional percentages obtained from samples with uneven surfaces. The only magnetically separated sample that is also polished flat, the FES25 sample, has the highest magnesium content of all separated samples. However, compared to thin section chromium spinels, sample FES25 is the fourth lowest in magnesium. This suggests underreporting of magnesium in the separated samples. Because the magnesium content is important to stoichiometrically calculate Fe^{3+} content, correcting this could shift the two datasets closer to each other. Higher magnesium content would influence many of the ratios used in the discrimination diagrams. Correcting for wrong values could, however, be difficult, as it involves modifying the data by adding values based on assumptions of content.

Independent sampling and testing suggest no regional or stratigraphic variation as the source of the differences in the data. The different magnetic separation techniques investigated in Figure 6. 46, do not show variation in aluminium or magnesium content. They do, however, have a highly variable Cr/Fe^{3+} ratio, producing more Fe^{3+} rich chromium spinels when at higher magnetism. As the E25 samples of Figure 6.46 are the only investigated by both the second Franz separation and in the magnetic fraction, it shows the differences in the various magnetic separations. The differences do not explain well the variation between thin sections and the tape attached chromium spinel data, as this variation is observed in magnesium and aluminium content, rather than iron content.

Further on in this discussion, two options will be taken into account each time the chromium spinel data are evaluated:

1st: Assuming tape attached samples are erroneous and should be excluded from any interpretation.

2nd: Assuming tape attached samples yield too low magnesium and possibly other element concentrations. Including the tape attached samples if useful information such as clustering or

diversification can support other observations. The data from the tape attached samples must be considered uncertain, and less reliable than thin section data.

By disregarding the tape attached samples, few chemical analyses from the De Geerdalen Formation chromium spinels remain, which weakens the reliability of the interpretations. The complete data will therefore continue to be taken into consideration if useful information can be derived, such as in the second option listed above.

7.2 Sediment source rock lithology – contributions from this study

By petrographic investigation on thin sections and SEM, several provenance sensitive observations have been made. Regarding the lithology of the De Geerdalen Formation source rock based on this study, different observations support the existence of various and diverse source rocks. Metamorphic, igneous and biogenic sedimentary lithic clasts are proof of this diverse source. The described heavy minerals add additional source information.

7.2.1 Metamorphic source rock

Lithic fragments and polycrystalline clasts, clearly identifiable as metamorphic in origin, can be organized in two different categories. One is labelled mica schist lithic fragments, but in reality used as a general term for all metapelitic rocks of varying metamorphic grade. The other category contains polycrystalline quartz clasts showing different greenschist facies deformation fabrics, originally in quartzite. Together they reflect a metamorphic source rock of greenschist to lower amphibolite facies. Both clast categories are numerous in the sediments and, considering that metapelitic rock fragments are less stable, reflect erosion of a considerable area of metasedimentary source rock. It is likely that the erosion of the metasedimentary rocks recycles a part of the heavy minerals suite in the original sediments.

Metapelitic lithic fragments in the De Geerdalen Formation, such as the one in Figure 6.20, are observed both in West Spitsbergen, Hopen and Edgeøya. This indicates the same lithic fragments being deposited in the entire study area, the same source is a possibility, but this has to be further investigated. There are variations in metamorphic grade between the metapelitic lithic fragments, suggesting erosion of different metapelites.

Different types of greenschist facies deformation fabrics and textures, such as the one in Figure 6.27, are observed in polycrystalline quartz of the De Geerdalen Formation. The types of fabric observed help restrict possible temperatures at the time of deformation.

The possibility that the De Geerdalen Formation constitutes, to a large extent, recycled metasediments, imposes constraints on interpretations of the heavy minerals, and suggests a cause of the high degree of clast rounding in the formation. The most stable heavy minerals, with zircon as an example, could remain unaltered in lower metamorphic facies and mixed with other sediments contribute to a new, more complex zircon population. Different rounding of clasts is observed in the De Geerdalen Formation (Figure 6.39), and a possible explanation of this could be that a proportion of recycled clasts originated from the proposed metasedimentary source.

7.2.2 Volcanic source rock

Volcanic fragments, such as in Figure 6.22, are observed in most samples, typically mafic and often dissolved or partially dissolved. This type of clast is generalized under the name volcanic lithic fragment, but may also derive from shallow intrusive rocks (Mørk 2013). Felsic volcanic clasts may exist in the formation, but definitive identification has not been possible. As there is a considerable contribution of volcanic lithic clasts in the investigated part of the De Geerdalen Formation, the area of the mafic magmatic source must have been considerable.

At least one observation associates the lithic fragments with the accessory mineral apatite. In Figure 6.23 an apatite crystal is positioned in the centre of a volcanic lithic fragment as a phenocryst. Other than this observation the origin of the apatites in the formation is unknown.

7.2.3 Biogenic quartz source

Recognizable spiculite biogenic quartz is found in both the Kapp Toscana location at Spitsbergen (Figure 6.29) and Negerfjellet at Edgeøya (Figure 6.30). The spiculites at Svalbard are associated with the late Permian Kapp Starostin Formation (Siedlecka, 1970). This formation, or a Barents Sea equivalent, are the likely sources to spiculites in the De Geerdalen Formation. The observation of spiculites in the De Geerdalen Formation indicates deposition of eroded Kapp Starostin Formation or equivalent sediments at this time. Observations of

spiculites both in East and West Svalbard indicate that the Kapp Starostin Formation continued as a source of sediments during that time interval.

The Kapp Starostin Formation biogenic silica is recognizable as spiculites in some instances, and locally it can be described as chert (Siedlecka, 1970). Chert of the Kapp Starostin Formation, or equivalents, is a possible source to the large proportion of polycrystalline quartz in the De Geerdalen Formation as e.g. seen in Figure 6.26. The polycrystalline quartz content could also be explained as felsic volcanic fragments (Soloviev, 2015), deformed quartzite or other sedimentary chert sources.

7.2.4 Heavy minerals

The accessory heavy minerals described from different locations in the De Geerdalen Formation add provenance sensitive information. The heavy minerals observed are apatite, chromium spinel, garnet, rutile, tourmaline and zircon. The presence of these minerals reveals provenance sensitive information as they originate in different types of rock. The heavy minerals are organized in the same way as Soloviev et al. (2015) into Sialic minerals: apatite, rutile, tourmaline and zircon, Mafic minerals: chromium spinel, and Cosmopolitan minerals: garnet. In addition, mica can be classified as a Cosmopolitan mineral in the sediments. The chromium spinel contribution to the De Geerdalen Formation is discussed at length in the following chapter.

The origin of the De Geerdalen Formation apatite is uncertain as the mineral is formed both in igneous melts and in sedimentary processes. Where present in a sedimentary rock, the apatite may represent a detrital grain from an igneous, sedimentary or metasedimentary rock that was eroded, or it can precipitate out of sea water on the sea bottom. Euhedral minerals, as the one depicted in Figure 6.9 and Figure 6.10, indicate that at least some of the De Geerdalen Formation apatites crystallized from a melt. The classification as a sialic mineral as in Soloviev et al. (2015), can further be supported by the appearance of the apatite phenocryst in a volcanic lithic fragment found in Figure 6.23. The general chemistry of the volcanic lithic clasts is mafic.

The presence of tourmaline and zircon in the De Geerdalen Formation suggests a felsic source rock. With very stable minerals, like zircon, possible sediment recycling hampers a simple tie to original source rock. The zircons in the De Geerdalen Formation may reflect recycled sedimentary rocks, a felsic crystalline rock being eroded for the first time, or a mix of the two sources.

A metamorphic source rock is indicated by the presence of garnet in the De Geerdalen Formation. Garnet could have been more abundant at deposition than observed in the present sediments, as they are less stable then for example zircon or chromium spinel (Morton and Hallsworth, 1999). Rutile is another mineral that can be associated with high pressure metamorphism.

7.3 De Geerdalen Formation chromium spinel

Of the two chromium spinel datasets that were obtained, the most reliable thin section dataset is used as a basis for discussion here. Input from the complete dataset is considered in light of the more reliable thin section data. Other factors possibly impacting the results, such as sample location, stratigraphic setting of samples and stability of the minerals in sediments, are expanded upon. Different sources to De Geerdalen Formation chromium spinels are considered, supporting one or different types of continental intrusions as the source.

7.3.1 Stability of chromium spinel in sediments

Chromium spinel is typically assumed to be stable in sediments to considerable depths, as suggested in Morton and Hallsworth (1999) and Table 3.1 of this thesis. This is consistent with the grains of the chromium spinel in this study, with one exception depicted in Figure 6.15. The depicted, originally euhedral, mineral was later partially dissolved, resulting in a pattern of partly dissolved patches. As a proof of dissolution in chromium spinels during diagenesis, considerations must be taken when using the mineral in provenance studies.

The cause of the dissolution can have several explanations; mineral element composition, weathering, transportation, deposition, diagenetic alteration by pore fluids or a combination of these. In the case of the chromium spinel shown in Figure 6.15, the alteration is probably caused by post depositional reactions between the mineral and pore fluids. As unaltered chromium spinels were found in the same thin section, this grain may have a composition more likely to react with the fluids. Varying chromium spinel stability in sediments due to differences in composition implies possible biases in provenance or heavy mineral correlation studies towards the more stable element compositions. As partial dissolution has only been observed in one of the samples in the study, and a considerable and diverse chromium spinel population is observed in the De Geerdalen Formation, chromium spinel dissolution can be considered rare, and probably does not generate an important bias.

7.3.2 Variations by location and stratigraphic setting

Variations in chromium spinel chemical composition by sample location or sample type show no clear variation between localities. Comparisons of chromium spinel chemistries between the three Svalbard islands of Hopen, Edgeøya and Spitsbergen can be seen in Figure 6.43. Both the thin sections dataset and the tape attached dataset display a similar pattern for each island, with a cluster of chromium spinel compositions, and a radiating pattern of analyses around the cluster. The low number of data points from reliable thin sections imposes some uncertainty in the comparison. The thin section data plot in accordance to the same broad category of provenance, continental intrusions, suggesting the same provenance for all thin section locations.

As no detailed facies analysis is implemented in this study, comparisons between chromium spinel compositions in different depositional settings have not been carried out. A few chromium spinel grains are found in thin sections of varying grain size, degree of compaction, diagenetic imprint and presumably depositional setting. Variations in chromium spinel compositions for the thin section dataset are small, and plot within the same density distribution diagram of the proposed provenance. Large variations in chrome spinel compositions would be indicative of alternating provenance, or other factors controlling sediment deposition. Few data and little variation in the observed chromium spinels make chromium spinel compositions unreliable for testing changes between depositional environments in this case.

7.3.3 Source of chromium spinel

The chromium spinel compositions described in this thesis can best be explained as originating in an intrusive continental magma. Density distribution diagrams for three different types of continental intrusions presented together with thin section datasets in Figure 6.48 to 9.50 B-plots, support this petrogenetic interpretation. The chromium spinels plot in, or in immediate proximity, of these density distribution diagrams. Chromium spinels containing upwards of 25% Fe^{3+} of the trivalent cations are typically associated with magmas continental intrusive origin. Alaskan type intrusions can also be considered a possibility as they generate relatively Fe^{3+} enriched chromium spinels. When compared in Figure 6.51 and Figure 6.52 B1, the Alaskan type chromium spinel compositions have less compositional variation, and do not cover the variation found in the dataset. Mafic and ultra- mafic rocks uncommon at the surface,

such as kimberlites and komatiites, can generate chromium spinels of the observed compositions. As the number of chromium spinels found in the De Geerdalen Formation in Svalbard implies a large area of chromium spinel source rock, a rare rock such as komatiite and kimberlite/lamproite is considered an unlikely source.

Distinguishing potential source rocks between the three different types of continental intrusions investigated in Figure 6.48 to 9.50 B sets is difficult. When comparing to the Barnes and Roeder (2001) density distribution diagrams for "Continental intrusion", "Sub volcanic intrusion in flood basalt province" and "Flood basalt", best fits vary between the discrimination diagrams.

The trivalent cations diagram of Figure 6.48 to 9.50 B1, match best with "Sub volcanic intrusion in flood basalt provinces", but also quite well with the "Layered intrusion" density distribution diagram percentiles. In Figure 6.48 B1, the Layered intrusion density distribution and the chromium spinel plots correspond well with a majority of the thin section data points, plotting within the 90th percentile. It is noteworthy that the "Layered intrusions" density distribution diagram includes more varied chromium spinel compositions than covered by the thin section dataset of this study. In the complete dataset of Figure 6.48 A1, a more varied chromium spinel contribution plotting in the "Layered intrusion" density distribution diagram is present.

In Figure 6.49 B1, thin section chromium spinel compositions and "Sub volcanic intrusions in flood basalt provinces" overlap quite well, covering most of the data points. The A1 discrimination diagram of Figure 6.49 shows that the majority of the tape attached data also plot in proximity of the sub volcanic intrusion density distribution diagram, adding weight to this lithology as a possible source.

Flood basalts, as described in Figure 6.50 B1, require higher aluminium content than the chromium spinels found in this study. Only the chromium spinels with the highest aluminium content plot within the flood basalt density distribution diagram. Some data points of low trivalent iron content plot within the flood basalt density distribution diagram of Figure 6.50 A1, suggesting flood basalts as a possible origin.

Comparing the B2 diagrams of Figure 6.48 to 9.50, an interpretation of flood basalts is favoured, conflicting with the interpretation from the trivalent cations diagram. A generally higher Fe^{2+} content is needed in order to plot in more coherence with the Figure 6.48 and Figure 6.49 B2 discrimination diagrams of "Layered intrusions" and "Sub- volcanic intrusions". The Layered intrusion diagram matches best of the two, with a few data points shared with the thin

section dataset. The aluminium/chromium ratio is, however, within the fields for all three continental intrusive options.

Comparing the "Flood basalt" density distribution diagram to the thin section dataset in Figure 6.50, a very good match is observed. The chromium spinel data plot along a line of increasing Fe^{2+} and Cr, corresponding to a position within the 90th percentile density distribution diagram. It is noteworthy that the complete dataset, plotted in Figure 6.48 to 9.50 A2, has similar aluminium/chromium ratio as the thin section chromium spinels.

As for the B2 diagrams of Figure 6.48 to 9.50, the B3 diagrams are inconclusive, with several chromium spinel grains plotting outside the density distribution diagrams for each of the possible sources. Small differences between the plots make source rocks difficult to distinguish, although the Figure 6.48 and Figure 6.49 density distribution diagrams plot closer to the 50th percentile. The A3 diagrams, comparing the complete dataset to the different continental intrusions, plot in close proximity to the "sub volcanic intrusion" density distribution diagram, but does not overlap.

A more precise description of a mafic or ultra- mafic continental intrusion source is difficult to establish based on inconclusive plots and conflicting results as well as few data points. Possible reasons can be alteration of chromium spinels by diagenesis or metamorphism. When comparisons rely on density distribution diagrams based on average chromium spinel compositions, they may not be entirely representative of variations in source rock petrogenesis.

When comparing the dataset to compositions of metamorphosed chromium spinel by Barnes and Roeder (2001), some chemical alteration could have taken place, explaining data values. Metamorphic spinel is generally enriched in Fe^{2+} contra magnesium, as well as richer in chromium and Fe^{3+}. This applies to greenschist and amphibolite facies rocks, and may explain some of the data points not covered by density distribution diagrams. In the complete dataset there are many analyses with a high Cr vs Al ratio, as well as low magnesium; features that may be explained by metamorphic alteration. Metamorphism would also preferably alter the outer parts of the mineral, the parts that were most likely to be tested when inspecting tape attached mineral grains. Diagenetic alteration of chromium spinel is possible, as discussed in the stability sub- chapter above. Alteration of chromium spinel, influencing compositions recorded in this study, is possible, but information about the type and stability of alteration is not known.

An attempt to subdivide chromium spinels of continental intrusive origin can be seen as artificial. When applied to provenance, the different possible types of continental intrusions are

related, and would over geological time erode and may contribute sediments to the same system. If the sediment drainage system is of sufficient size and drains sub- volcanic intrusions, layered intrusions and flood basalts, the detrital chromium output will have a mixed signature. The data obtained in this study suggest that such a mix may be represented in the De Geerdalen Formation on Svalbard.

7.4 Earlier work on provenance and this study

In order to understand the provenance of the De Geerdalen Formation, comparisons are made between articles studying De Geerdalen Formation provenance and this thesis.

7.4.1 Petrographical

Previous petrographical work on the De Geerdalen Formation on Svalbard and the Barents Sea Snadd Formation (Mørk (1999), Riis et al., 2008, Mørk, (2013)) are largely supported by the observations of this thesis.

Mineralogy and mineral distributions e.g. of plagioclase and alkali- feldspar in this study are comparable to observations from Svalbard and the Barents Sea (Mørk 1999, Riis et al., 2008 and Mørk, 2013), and Franz Josef Land (Soloviev et al., 2015). Plagioclase and microcline grains with tabular habitus and locally twinning, as described in Soloviev et al., (2015), are similar to rectangular plagioclase observed in this thesis, and the alkali- feldspar content is lower than the plagioclase content as observed in e.g. Riis et al. (2008), supported by observations in this thesis. Explanations can be either unfavourable diagenetic conditions for the preservation of alkali- feldspars or an alkali- feldspar poor source rock.

Different lithic clasts are observed in the De Geerdalen Formation and its equivalents. Volcanic lithic fragments are described by all workers (Mørk 1999, Riis et al., 2008, Mørk, 2013, this thesis and Soloviev et al., 2015), and they are typically partially dissolved or altered to clay minerals. Soloviev et al. (2015) describe both felsitic volcanic fragments and volcanic glass that are typically altered to clay minerals. While Mørk (1999) and Mørk (2013) do not suggest a source of the volcanic lithic fragments, Riis et al. (2008) suggest these sediments were derived from the east. Siberian Plume magmatism is associated with the volcanic lithic clasts on Franz Josef Land (Soloviev et al., 2015). Mica schist lithic fragments are observed throughout the

Barents Sea and Svalbard, including Franz Josef Land (Mørk, 1999), supporting an interpretation of a metasedimentary source rock.

When considering the heavy mineral assemblage in the De Geerdalen Formation, the same minerals are observed in this study as in Mørk (1999), Riis et al. (2008) and Mørk, (2013), with the exception of apatite, which appears to be a common heavy mineral in the De Geerdalen Formation. The heavy mineral assemblage at Franz Josef Land (Soloviev et al., 2015) also includes ilmenite, leucoxene, staurolite and amphibolite. Possible explanations for more diverse mineral compositions in the Franz Josef Land (Soloviev et al., 2015) study are that they were detected after heavy mineral separation by a different approach than in the other works, that they have a different provenance or that they have a different preservation state.

7.4.2 Quartz provenance

Muller and Kneis (2013) have, based on samples from the De Geerdalen Formation at Blanknuten, Edgeøya, described a lower greenschist facies quartzite as the source of 66 -73% of the quartz in the formation. The rest of the quartz is of high metamorphic/igneous origin. The observation of a lower grade metamorphic quartz source rock in Muller and Kneis (2013) is supported by observations in this thesis of polycrystalline quartz clasts with greenschist facies deformation fabrics.

Polycrystalline quartz in the De Geerdalen Formation can be of metamorphic origin or possibly chert. Polycrystalline quartz aggregates are described throughout the De Geerdalen Formation (Mørk 1999, Riis et al., 2008, Mørk, 2013, this thesis and Soloviev et al., 2015). Riis et al. (2008) suggest that the clasts are chert, possibly eroded from the Kapp Starostin Formation, or equivalent. In this thesis, visual evidence for detrital spiculites at both East and West Svalbard supports this hypothesis, as at least a part of the chert in the De Geerdalen Formation is derived from the Kapp Starostin Formation or equivalents.

7.4.3 Chromium spinel

No attempt at defining chromium spinel source rock for the De Geerdalen Formation sandstones has been done before this thesis. By noticing the presence of a chromium spinel in the sandstones, works such as Riis et al. (2008), have suggested a mafic or ultra- mafic source amongst the proposed source rocks.

7.5 Evaluation of the De Geerdalen Formation provenance

After evaluating all data and articles so far, an easterly source to the De Geerdalen Formation is supported.

7.5.1 Local variations

When comparing sample locations, no discriminatory differences between different locations were observed. The heavy mineral component to the sandstones is the same on the islands of Hopen and Edgeøya, while the same heavy minerals are observed, except tourmaline, at Spitsbergen. Mørk (2013) has, however, observed it in samples from this island. Applicable chromium spinel data are few, but compositional data indicate the same petrogenesis for all grains. Bue and Andresen (2013) have published detrital zircon age data from three different De Geerdalen Formation locations, showing similar age peaks and origin. No considerable differences in provenance are observed the in the entire De Geerdalen Formation.

7.5.2 Zircon data

Detrital zircon geochronological ages are published from both Svalbard (Bue and Andresen, 2013) and Franz Josef Land (Soloviev et al., 2015) and other locations fringing the Arctic ocean (Zhang et al., 2016). The detrital zircon distributions of De Geerdalen Formation equivalents display a markedly different age distribution than the underlying formations (Bue and Andresen, 2013, Soloviev et al., 2015, Zhang et al., 2016).

The De Geerdalen Formation zircon age peaks are organized in four categories based on time associated rock forming events (Soloviev et al., 2015). Mesoproterozoic and older age peaks are excluded.

- Timanide 650 – 500 Ma
- Caledonian 500 – 390 Ma
- Uralide 370 – 270 Ma
- Siberian plume magmatism 250 – 230 Ma

Soloviev et al. (2015) suggest that Caledonian age zircons are derived from the Baltica craton, possibly Timanides or Severnaya Zemlya, while younger zircons are suggested to originate in

the northern Uralian foldbelt, Taimyr or Siberian plume (Soloviev et al., 2015). An east to southeast source is supported (Soloviev et al., 2015). The zircons are, based on mineral morphology, described as originating in granitoid melts. Bue and Andresen (2013) suggest a north Uralid, possibly with minor Timanide input, source of the De Geerdalen Formation. A relatively small proportion of Timanide aged zircons weaken claims to a provenance southeast of Svalbard (Lundschien et al., 2014).

The zircon age distribution of the De Geerdalen Formation at Svalbard (Bue and Andresen, 2013), and the age distribution in the Franz Josef Land samples (Soloviev et al., 2015) display a similar pattern, suggesting similar sediment provenance (Soloviev et al., 2015, Zhang et al., 2016). Zircon age distributions from several Arctic locations of Middle and Late Triassic also show this pattern, indicating a large area of Uralide and Siberian Plume related provenance ages (Zhang et al., 2016).

With a probable metasedimentary source rock for considerable parts of the De Geerdalen Formation, some degree of zircon recycling is likely to have taken place. As recycled zircons have a longer and more complex sedimentary history, they are progressively likelier to represent older zircon ages. Taking zircon recycling into consideration, the older zircon age peaks could represent the older e.g. Caledonian age zircons being deposited over a large area, later becoming the De Geerdalen Formation source rock. This complicates a direct comparison of zircons age to high grade metamorphic or igneous rocks.

7.5.3 Prograding shoreline

Based on the Snadd Formation seismic interpretation in the northern Barents Sea east of Svalbard, a nortwestwardly prograding shoreline is found, suggesting a nortwestwardly sediment transport direction (Riis et al., 2008, Høy and Lundschien, 2011, Lundschien et al., 2014, Klausen et al., 2015). Shoreline progradation was stable throughout the Middle and Late Triassic, ultimately covering the area of present day Svalbard itself (Klausen et al., 2015).

When comparing the suggested provenance to the southeast of present day Svalbard (Lundschien et al., 2014, Klausen et al., 2015) to other provenance relevant observations, the data become conflicted. Timanide zircon ages are not predominant in the De Geerdalen Formation, although the Timanides are located to the southeast of Svalbard. It is difficult to include Siberian plume zircon ages, common volcanic lithic clasts and chromium spinels of a continental intrusive origin in the sediments without adding a long sediment transport distance.

This is because, as seen in Figure 7.1, sediments from the Siberian plume would first have to be transported to the west of the Uralides, before continuing north-westward to Svalbard.

Assuming sediments are not added perpendicular to the mapped prograding shorelines makes it possible to evaluate alternative sediment transport directions. A shoreline influenced by strong alongshore currents can redistribute sediments, generating shorelines oblique to sediment input.

7.5.4 Source rock lithology

Four different types of source rock can be described for the De Geerdalen Formation.

A metasedimentary source can be deduced from abundant metapelitic lithic fragments, lower greenschist facies deformed quartzite clasts and the heavy mineral garnet. The quartzite is suggested to contribute about 66% or more of the De Geerdalen Formation quartz, based on samples from Blanknuten, Edgeøya (Muller and Knies, 2013). No specific location can be tied to the metasedimentary source, as greenschist facies metasedimentary rocks are found several places in the region.

The abundant volcanic lithic fragments described throughout the De Geerdalen Formation are likely derived from extrusive or shallow intrusive predominantly mafic igneous activity. The De Geerdalen Formation chromium spinels have chemical compositions corresponding to chromium spinels formed from continental intrusive melts. At the time the De Geerdalen Formation was deposited, there was active volcanism in Taimyr (Zhang et al., 2016). It represented the final stages of the Siberian Traps Large Igneous Province. The volcanic lithic fragments and chromium spinels of the De Geerdalen Formation may originate from this massive magmatic province.

A source of felsic composition must be present based on the presence heavy minerals like zircon and rutile described in the De Geerdalen Formation. Alkali- feldspars are also present, suggesting a more felsic source.

The biogenic spiculites and abundant chert fragments observed in the De Geerdalen Formation probably reflect erosion of chert rich, underlying sediments. Spiculites and chert are known from the Kapp Starostin Formation at Svalbard (Siedlecka, 1970), and erosion of this or equivalent formations could represent parts of the chert contribution in the De Geerdalen Formation. Supposing erosion of chert, other strata will also erode and contribute to the De

Geerdalen Formation sediments. A specific source cannot be established, but is likely to be somewhere in the Barents Sea and infringing areas.

7.5.5 Tectonic setting and location of source rock

When evaluating the chromium spinel compositions deemed of reliable quality (the thin section dataset), a continental intrusive origin is suggested. The relatively small dataset is difficult to explain originating in another magmatic environment, considering common rocks in the earth's crust. Considering location of the closest continental intrusive rocks at the time of deposition of the De Geerdalen Formation, the last stages of the Siberian Plume were active in present day Taimyr. The magmatic activity is located as seen in Figure 7.1, and contributed to large scale magmatism. The heat from the Siberian Plume also led to uplift and higher topography in Taimyr at this time (Zhang et al., 2016). As the Siberian Traps consist of continental intrusive mafic rocks such as flood basalts, shallow intrusions and layered intrusions, these correspond well with the De Geerdalen chromium spinel compositions. As Siberian Traps zircon ages are reported in the De Geerdalen Formation, an interpretation of the Siberian Traps as a source to the De Geerdalen Formation chromium spinels is suggested.

If considering the entire chromium spinel composition dataset, a greater variation in chromium spinel compositions becomes apparent. In this dataset, a continental intrusive mafic or ultra-mafic rock is the most probable origin, although a few chromium spinels also suggest other origins, such as ophiolites. Siberian Trap magmatism is, however, a more probable source.

7.5.6 Regional implications

The De Geerdalen Formation is suggested by several (Mørk, 1999, Riis et al., 2008, Bue and Andresen, 2013, Lundschien et al., 2014, Klausen et al., 2015) to have a provenance from the east. The area suggested as provenance is the present day northern Urals (Riis et al., 2008, Bue and Andresen, 2013) in general. Two transport directions to Svalbard have been suggested; one from the southeast, based on seismic interpretation of shoreline progradation, and another from the northeast, or direct east, as supported by petrographical studies (Mørk 1999, Riis et al., 2008). When comparing suggested sediment origin as discussed prior to the suggested provenance directions, a northeasterly or directly easterly source seems more probable.

In Figure 7.1, possible ways of transporting sediments from the Siberian Traps to Svalbard are laid out. Accepting that the chromium spinels of the De Geerdalen Formation most likely derived from continental intrusions, and supported by zircon ages of Siberian plume age, the sediments were most likely transported from the Taimyr area. The shortest possible distance of transporting sediments to Svalbard from Taimyr would imply an east-northeast provenance. A southern route, as indicated in Figure 7.1, implies a much longer transportation of sediments and a higher probability of Timanide associated zircon age peaks.

A Uralide impact on De Geerdalen Formation sediments is seen in zircon age data. With an ultimate sediment source suggested east of the assumed Uralid orogeny, a Uralid contribution to De Geerdalen sediments is expected. The metasedimentary source rock for the De Geerdalen Formation could be regionally metamorphosed rocks of this orogen, although other sources cannot be excluded.

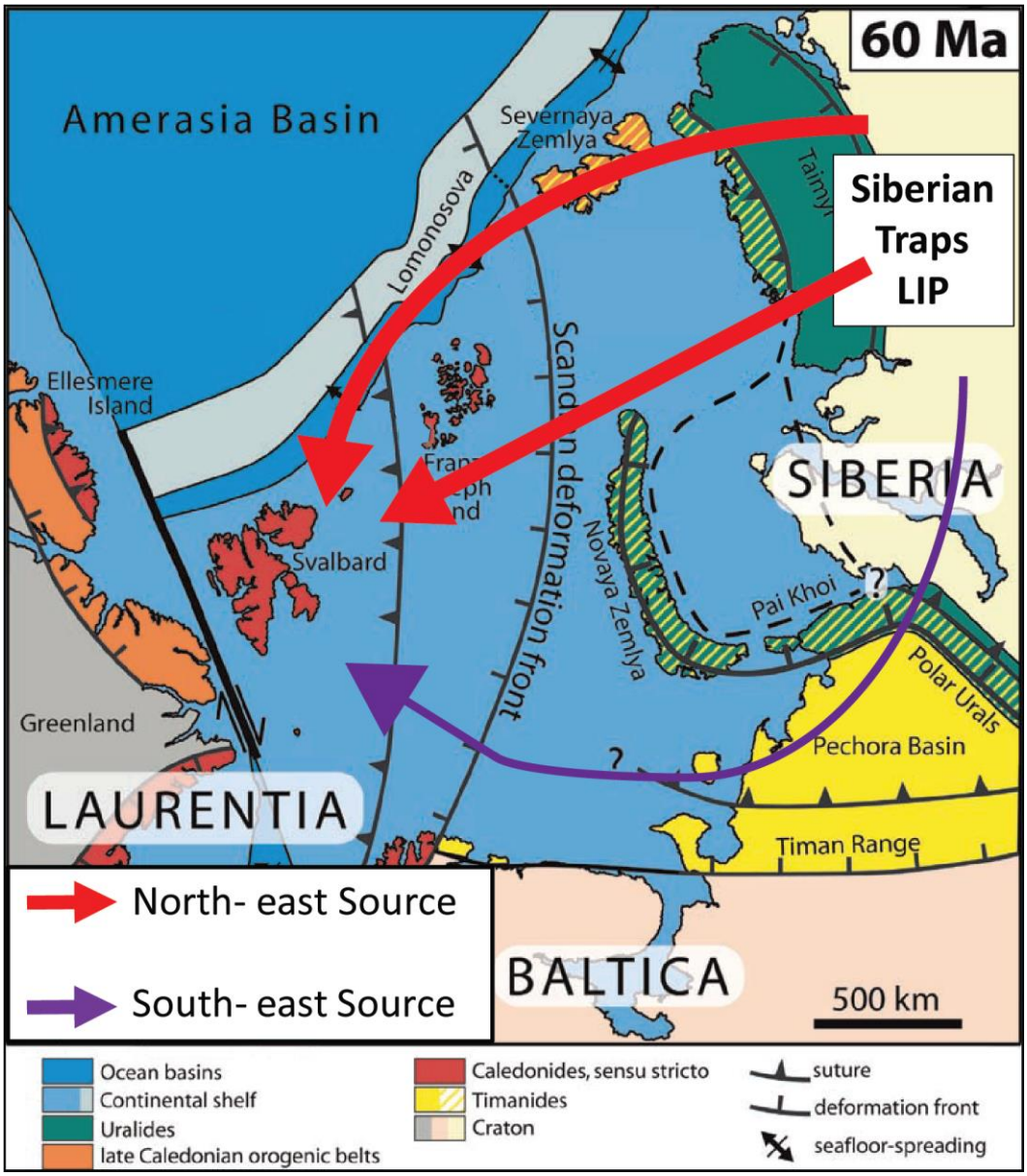

Figure 7.1 *Arrows indicating possible sources to the De Geerdalen Formation at Svalbard. The south east source is supported by works such as Lundschien et al. (2014) and Klausen et al. (2015). The north east source interpretation is supported by petrographical and zircon age observations, as well as chrome spinel compositions. Map modified after Gee et al. (2006) showing a suggested tectonic setting of 60 Ma.*

8 Conclusion and further work

8.1 Conclusion

Based on the results of this study and published work on the De Geerdalen Formation provenance, a list of conclusions is suggested:

1) No discriminatory differences between the various samples and locations of the De Geerdalen Formation were observed. This implies that the same or similar provenance for the formation cannot be excluded. The conclusion is based on chromium spinel compositions indicating the same type of source for all samples, similar heavy mineral composition in investigated samples, and similar zircon age distributions (Bue and Andresen, 2013) for different locations on Svalbard.

2) Chromium spinel chemical compositions consistently suggest a continental intrusive mafic to ultra- mafic source rock. A sub- division into shallow intrusion, layered intrusion or flood basalt could not be accomplished. Abundant volcanic lithic fragments in the sandstones support the existence of volcanic source rocks.

3) Active volcanism in Taimyr associated with the Siberian Traps Large Igneous Province is suggested as the source of the chromium spinel and volcanic lithic fragments in the De Geerdalen Formation. Mafic continental intrusive rocks of the Siberian Traps produced large volumes of volcanic material, active around the same time as the De Geerdalen Formation deposition. Chromium spinel chemical compositions, abundant volcanic fragments in the De Geerdalen Formation, and Svalbard zircon age peaks corresponding to Siberian Traps rock ages, support this.

4) Abundant clasts in the De Geerdalen Formation of greenschist facies quartzites and greenschist to lower amphibolite facies metapelites suggest a considerable contribution from metasedimentary source rocks.

5) Biogenic spiculites are observed in two De Geerdalen Formation samples from Negerfjellet, Edgeøya and Kapp Toscana on Spitsbergen. This suggests erosion of the late Permian Kapp Starostin Formation or equivalents, recognized for its high spiculite and chert content (Siedlecka, 1970). This indicates a similar source to the abundant chert in the De Geerdalen Formation.

6). Assuming a sediment source in Taimyr, the shortest transport direction to Svalbard indicates a provenance northeast or east of Svalbard. Zircon age distributions and heavy mineral

assemblages do not contradict this, being similar to observations from Franz Josef Land (Bue and Andresen, 2013, Soloviev et al., 2015).

7) Chromium spinels cannot be assumed completely stable during diagenesis as one partially dissolved chromium spinel grain is observed.

8.2 Further work

Expanding upon the work of this thesis implies both improving the methods used to retrieve data, as well as investigating other aspects of the De Geerdalen Formation provenance both on a detailed and regional level. A list of possible measures follows:

1) Expanding the chromium spinel chemical composition dataset. As interpretation of detrital chromium spinel source rock was based on rather few data points, an expanded dataset would add certainty or new information to this study's conclusions and results. This can possibly be achieved through heavy minerals separation based on heavy liquids, or handpicking of Franz separated samples.

2) Expanding the database for comparing chromium spinel compositions and including the elements Mn, Zn, Cu and Co in discrimination diagrams. In order to use chromium spinel compositions in a provenance study, reliable and multiple discrimination diagrams would improve the probability of distinguishing different petrogeneses.

3) Collecting samples in suggested source areas to possibly identify mineral compositional relationships could confirm or dispute suggestions made in this thesis.

4) Regional scale sampling and analysing of De Geerdalen Formation detrital chromium spinel to establish regional extent and variations of sources over time. This could be used together with detrital zircon age distributions in provenance studies, as zircons represent a more felsic source, and chromium spinels represent mafic and ultra- mafic sources.

5) Factors controlling the stability of chromium spinel in sediments can be investigated. As chromium spinel is observed as partially dissolved in this thesis, the stability of the mineral in sediments can be evaluated before applying the mineral to provenance studies.

6) In- depth investigations of other De Geerdalen Formation heavy minerals as e.g. apatite or garnet. Detailed compositional data could add significant information in our understanding of the De Geerdalen Formation provenance.

7) In- depth investigation of De Geerdalen Formation polycrystalline quartz component. A better understanding of the chert component in particular can help identify eroded areas in Late Triassic, expanding regional understanding.

9 References

ARAI, S. 1992. Chemistry of chromian spinel in volcanic rocks as a potential guide to magma chemistry. *Mineralogical Magazine,* 56**,** 173-184.

BARNES, S. J. & ROEDER, P. L. 2001. The range of spinel compositions in terrestrial mafic and ultramafic rocks. *Journal of Petrology,* 42**,** 2279-2302.

BIAGIONI, C. & PASERO, M. 2014. The systematics of the spinel-type minerals: An overview. *American Mineralogist,* 99**,** 1254-1264.

BUE, E. P. & ANDRESEN, A. 2013. Constraining depositional models in the Barents Sea region using detrital zircon U–Pb data from Mesozoic sediments in Svalbard. *Geological Society, London, Special Publications*, 386 261-279

COOKENBOO, H., BUSTIN, R. & WILKS, K. 1997. Detrital chromian spinel compositions used to reconstruct the tectonic setting of provenance: implications for orogeny in the Canadian Cordillera. *Journal of Sedimentary Research,* 67 (1) 116-123.

DALLMANN, W., OHTA, Y., ELVEVOLD, S. & BLOMEIER, D., (EDS) 2002. Bedrock Map of Svalbard and Jan Mayen. Temakart No. 33. *Norsk Polarinstitutt, Tromsø*.

DALLMANN, W. 1999. Lithostratigraphic lexicon of Svalbard. Upper Paleozoic to Quaternary Bedrock. Review and Recommendations for Nomenclature Use. Norsk Polarinstitutt, Tromsø.

FOSSEN, H., DALLMAN, W., ANDERSEN, T., RAMBERG, I., BRYHNI, I. & NØTTVEDT, A. E. 2006. Fjellkjeden går til grunne Landet blir til. Norges geologi. *Norsk Geologisk Forening***,** 230-258.

GEE, D., BOGOLEPOVA, O. & LORENZ, H. 2006. The Timanide, Caledonide and Uralide orogens in the Eurasian high Arctic, and relationships to the palaeo-continents Laurentia, Baltica and Siberia. *Geological Society, London, Memoirs,* 32**,** 507-520.

GROGAN, P., NYBERG, K., FOTLAND, B., MYKLEBUST, R., DAHLGREN, S. & RIIS, F. 2000. Cretaceous magmatism south and east of Svalbard: evidence from seismic reflection and magnetic data. *Polarforschung,* 68**,** 25-34.

HIRTH, G. & TULLIS, J. 1992. Dislocation creep regimes in quartz aggregates. *Journal of Structural Geology,* 14**,** 145-159.

HUGHES, J. M., KOHN, M. J. & RAKOVAN, J. F. 2002. Phosphates: Geochemical, geobiological, and materials importance.

HØY, T. & LUNDSCHIEN, B. 2011. Triassic deltaic sequences in the northern Barents Sea. *Geological Society, London, Memoirs,* 35**,** 249-260.

KAMENETSKY, V. S., CRAWFORD, A. J. & MEFFRE, S. 2001. Factors controlling chemistry of magmatic spinel: an empirical study of associated olivine, Cr-spinel and melt inclusions from primitive rocks. *Journal of Petrology,* 42**,** 655-671.

KLAUSEN, T. & MØRK, A. 2014. The Upper Triassic paralic deposits of the De Geerdalen Formation on Hopen: outcrop analog to the subsurface Snadd Formation in the Barents Sea. *AAPG Bulletin,* 98**,** 1911-1941.

KLAUSEN, T. G., RYSETH, A. E., HELLAND-HANSEN, W., GAWTHORPE, R. & LAURSEN, I. 2015. Regional development and sequence stratigraphy of the Middle to Late Triassic Snadd Formation, Norwegian Barents Sea. *Marine and Petroleum Geology,* 62**,** 102-122.

KNARUD, R. 1980. En sedimentologisk og diagenetisk undersøkelse av Kapp Toscana Formasjonens sedimenter på Svalbard.(A sedimentological and diagenetic study of the sediments of the Kapp Toscana Formation in Svalbard). *University of Oslo*.

KUZNETSOV, N., SOBOLEVA, A., UDORATINA, O., HERTSEVA, M. & ANDREICHEV, V. 2007. Pre-Ordovician tectonic evolution and volcano–plutonic associations of the Timanides and northern Pre-Uralides, northeast part of the East European Craton. *Gondwana Research,* 12**,** 305-323.

LARSSEN, G., ELVEBAKK, G., HENRIKSEN, L., KRISTENSEN, E., NILSSON, I., SAMUELSBERG, T. & STEMMERIK, L. 2005. Upper Palaeozoic lithostratigraphy of the southern Norwegian Barents Sea. Norges Geologiske Undersøkelser Bulletin 444. *Trondheim: Geological Survey of Norway*.

LORD, G. S., SOLVI, K. H., KLAUSEN, T. G. & MØRK, A. 2014. Triassic channel bodies on Hopen, Svalbard: Their facies, stratigraphic significance and spatial distribution. *Norwegian Petroleum Directorate Bulletin*, 11, 41-59.

LUNDSCHIEN, B. A., HØY, T. & MØRK, A. 2014. Triassic hydrocarbon potential in the Northern Barents Sea; integrating Svalbard and stratigraphic core data. *Norwegian Petroleum Directorate Bulletin,* 11**,** 3-20.

MORTON, A. C. 1991. Geochemical studies of detrital heavy minerals and their application to provenance research. *Geological Society, London, Special Publications,* 57**,** 31-45.

MORTON, A. C. & HALLSWORTH, C. R. 1999. Processes controlling the composition of heavy mineral assemblages in sandstones. *Sedimentary Geology,* 124**,** 3-29.

MULLER, A. & KNIES, J. 2013. Trace elements and cathodoluminescence of detrital quartz in Arctic marine sediments-a new ice-rafted debris provenance proxy. *Climate of the Past,* 9. 2615-2630.

MØRK, A., VIGRAN, J., KORCHINSKAYA, M., PCHELINA, T., FEFILOVA, L., VAVILOV, M. & WEITSCHAT, W. 2013. Triassic rocks in Svalbard, the Arctic Soviet islands and the Barents Shelf: bearing on their correlations. *Arctic Geology and Petroleum Potential, Norwegian Petroleum Society (NPF), Special Publication,* 2**,** 457-479.

MØRK, M. B. E. 1999. Compositional variations and provenance of Triassic sandstones from the Barents Shelf. *Journal of Sedimentary Research,* 69**,** 690-710.

MØRK, M. B. E. 2013. Diagenesis and quartz cement distribution of low-permeability Upper Triassic–Middle Jurassic reservoir sandstones, Longyearbyen CO2 lab well site in Svalbard, Norway. *AAPG bulletin,* 97**,** 577-596.

PUCHKOV, V. 2012. Dike swarms and related igneous complexes in the Urals. *Geotectonics,* 46**,** 37-46.

PUCHKOV, V. 2013. Structural stages and evolution of the Urals. *Mineralogy and Petrology,* 107**,** 3-37.

PUCHKOV, V. N. 2009. The evolution of the Uralian orogen. *Geological Society, London, Special Publications,* 327**,** 161-195.

RIIS, F., LUNDSCHIEN, B. A., HØY, T., MØRK, A. & MØRK, M. B. E. 2008. Evolution of the Triassic shelf in the northern Barents Sea region. *Polar Research,* 27**,** 318-338.

ROBERTS, D. 2003. The Scandinavian Caledonides: event chronology, palaeogeographic settings and likely modern analogues. *Tectonophysics,* 365**,** 283-299.

RØD, R. S., HYNNE, I. B. & MØRK, A. 2014. Depositional environment of the Upper Triassic De Geerdalen Formation–An EW transect from Edgeøya to Central Spitsbergen, Svalbard. *Norwegian Petroleum Directorate Bulletin,* 11**,** 21-40.

SIEDLECKA, A. 1970. Investigations of Permian cherts and associated rocks in Southern Spitsbergen. *Norsk Polarinstitutt Skr,* 147, 5-87

SMELROR, M., PETROV, O., LARSSEN, G. B. & WERNER, S. 2009. Geological history of the Barents Sea. *Norges Geol. undersøkelse***,** 1-135.

SOLOVIEV, A., ZAIONCHEK, A., SUPRUNENKO, O., BREKKE, H., FALEIDE, J., ROZHKOVA, D., KHISAMUTDINOVA, A., STOLBOV, N. & HOURIGAN, J. 2015. Evolution of the provenances of Triassic rocks in Franz Josef Land: U/Pb LA-ICP-MS dating of the detrital zircon from Well Severnaya. *Lithology and Mineral Resources,* 50**,** 102-116.

VIGRAN, J., MANGERUD, G., MØRK, A., WORSLEY, D. & HOCHULI, P. A. 2014. Palynology and geology of the Triassic succession of Svalbard and the Barents Sea. *Geological Survey of Norway Special Publication,* 14**,** 1 - 247.

WORDEN, R. & BURLEY, S. 2003. Sandstone diagenesis: the evolution of sand to stone. *Sandstone Diagenesis: Recent and Ancient,* 4**,** 3-44.

WORSLEY, D. 2008. The post-Caledonian development of Svalbard and the western Barents Sea. *Polar Research,* 27**,** 298-317.

WORSLEY, D., JOHANSEN, R. & KRISTENSEN, S. 1988. The Mesozoic and Cenozoic succession of Tromsøflaket. *A lithostratigraphic scheme for the Mesozoic and Cenozoic succession offshore mid-and northern Norway. Norwegian Petroleum Directorate Bulletin,* 4**,** 42-65.

ZHANG, X., PEASE, V., SKOGSEID, J. & WOHLGEMUTH-UEBERWASSER, C. 2016. Reconstruction of tectonic events on the northern Eurasia margin of the Arctic, from U-Pb detrital zircon provenance investigations of late Paleozoic to Mesozoic sandstones in southern Taimyr Peninsula. *Geological Society of America Bulletin,* 128**,** 29-46.

Appendix 1

Table 1 *The complete chromium spinel chemical composition data set in mass oxide.*

Sample	Separate	Location	Pereparate	Al2O3	Na2O	K2O	Cr2O3	SiO2	MgO	CaO	MnO	Y2O3	TiO2	FeO	V2O3	CoO	NiO	CuO	ZnO	Total
BLA-3,1	Thin Section	Blanknuten, Edgeøya	Thin Section	11,429	0,31	0,164	23,387	5,703	1,021	0,835	1,568	0	0,665	37,019	n/a	n/a	n/a	n/a	4,886	**86,987**
BLA-3,3	Thin Section	Blanknuten, Edgeøya	Thin Section	15,186	0,036	0	41,451	0,063	1,698	0,186	0,26	0	0,127	39,974	n/a	n/a	n/a	n/a	0,511	**99,492**
DH4-875-36,1	Thin Section	Adventdalen, Spitsbergen	Thin Section	23,972	0,025	0,024	40,572	0,16	11,482	0,02	0,288	0	0,271	23,209	n/a	n/a	n/a	n/a	0,234	**100,257**
DH4-875-36,2	Thin Section	Adventdalen, Spitsbergen	Thin Section	14,15	0,048	0,035	53,739	0,287	10,57	0,025	0,358	0	0,123	21,343	n/a	n/a	n/a	n/a	0,11	**100,788**
DH4-875-36,3	Thin Section	Adventdalen, Spitsbergen	Thin Section	15,432	0,037	0,022	40,703	0,27	12,068	0,018	0,418	0,027	0,723	30,131	n/a	n/a	n/a	n/a	0,071	**99,92**
DH4-875-36,5	Thin Section	Adventdalen, Spitsbergen	Thin Section	19,72	0,075	0,003	39,296	0,515	10,847	0	0,339	0	0,568	28,153	n/a	n/a	n/a	n/a	0,101	**99,617**
DH4-875-36,6	Thin Section	Adventdalen, Spitsbergen	Thin Section	12,754	0,032	0,005	52,027	0,436	10,674	0,002	0,36	0,003	0,161	23,096	n/a	n/a	n/a	n/a	0,062	**99,612**
EO25mag.1	Initial magnetic	Negerfjellet, Edgeøya	Tape	5,464	0,074	0,139	25,551	1,592	2,965	0,178	0,941	0	0,222	32,647	0,152	0,178	0,144	0,035	1,034	**71,316**
EO25mag.10	Initial magnetic	Negerfjellet, Edgeøya	Tape	1,622	0,503	0,28	24,133	1,761	1,506	0,058	1,022	0	0,299	46,872	0,163	0,098	0,187	0,051	0,106	**78,661**
EO25mag.11	Initial magnetic	Negerfjellet, Edgeøya	Tape	0,454	0,116	0,067	35,597	0,568	0,755	0,09	1,324	0	0,597	46,332	0,177	0,055	0,012	0,096	1,217	**87,457**
EO25mag.13	Initial magnetic	Negerfjellet, Edgeøya	Tape	9,837	0,109	1,65	26,626	8,574	2,463	0,09	0,547	0	0,743	40,063	0,137	0,074	0,064	0	0,319	**91,296**
EO25mag.14	Initial magnetic	Negerfjellet, Edgeøya	Tape	3,169	0,132	0,133	8,723	13,843	0,721	14,363	0,994	0	1,766	40,65	0,23	0,139	2,81	0,116	0	**87,789**
EO25mag.15	Initial magnetic	Negerfjellet, Edgeøya	Tape	1,472	0	0,081	22,383	0,231	0,964	0,057	1,539	0	1,048	47,732	1,059	0,132	0,227	0,051	0,03	**77,006**
EO25mag.16	Initial magnetic	Negerfjellet, Edgeøya	Tape	1,927	0,106	0,082	31,219	1,273	1,612	0,079	0,232	0,042	0,077	37,669	0,133	0,129	0,088	0,129	0,306	**75,103**
EO25mag.17	Initial magnetic	Negerfjellet, Edgeøya	Tape	1,867	0,136	0,154	39,759	1,555	1,833	0,074	0,216	0,006	0,15	29,96	0,11	0,247	0,06	0,024	0,691	**76,842**
EO25mag.18	Initial magnetic	Negerfjellet, Edgeøya	Tape	0,448	0,044	0,179	31,512	0,473	1,496	0,175	1,349	0,029	0,22	32,963	0,099	0,121	0,049	0,088	1,155	**70,4**
EO25mag.2	Initial magnetic	Negerfjellet, Edgeøya	Tape	10,356	0	0,025	21,739	1,084	5,046	0,082	0,381	0,018	2,077	51,311	0,857	0,098	0,212	0,048	0,39	**93,724**
EO25mag.20	Initial magnetic	Negerfjellet, Edgeøya	Tape	2,432	0,191	0,083	32,19	1,675	1,129	0,074	1,731	0,081	0,494	44,637	0,22	0,153	0,024	0,05	0,54	**85,704**
EO25mag.3	Initial magnetic	Negerfjellet, Edgeøya	Tape	4,869	0,083	0,161	34,735	3,811	2,144	0,245	1,428	0	0,186	41,634	0,159	0,217	0,091	0,062	1,06	**90,885**

Sample	Separate	Location	Pereparate	Al2O3	Na2O	K2O	Cr2O3	SiO2	MgO	CaO	MnO	Y2O3	TiO2	FeO	V2O3	CoO	NiO	CuO	ZnO	Total
EO25mag.5	Initial magnetic	Negerfjellet, Edgeøya	Tape	0,947	0,155	0,022	38,66	0	0,602	0,021	0,425	0	0,106	31,783	0,047	0,135	0,187	0	0,12	**73,21**
EO25mag.8	Initial magnetic	Negerfjellet, Edgeøya	Tape	3,204	0,108	0,166	33,291	3,493	0,901	0,105	1,116	0,014	0,507	44,474	0,185	0,039	0	0,001	1,14	**88,744**
EO25vf 0,3.1	Franz 2 times	Negerfjellet, Edgeøya	Tape	2,816	0,038	0,062	51,405	0,368	5,734	0,096	1,847	0,016	0,095	14,937	0,085	0,074	0,013	0	0,417	**78,003**
EO25vf 0,3.10	Franz 2 times	Negerfjellet, Edgeøya	Tape	0,285	0,05	0,071	53,244	0,151	8,137	0,003	0,4	0,008	0,086	19,501	0,054	0,107	0,047	0,069	0	**82,213**
EO25vf 0,3.11	Franz 2 times	Negerfjellet, Edgeøya	Tape	12,49	0,064	0,148	50,707	2,788	0,394	0,044	0,718	0	0,154	21,676	0,375	0,091	0,024	0,065	0,41	**90,148**
EO25vf 0,3.12	Franz 2 times	Negerfjellet, Edgeøya	Tape	1,861	0,103	0,267	40,225	0,943	4,364	0,001	0,534	0	0,27	35,635	0,241	0,091	0,013	0	0,198	**84,746**
EO25vf 0,3.13	Franz 2 times	Negerfjellet, Edgeøya	Tape	6,18	0,237	0,522	34,827	3,513	4,76	0,068	0,335	0	0,106	25,175	0,061	0,087	0,064	0	0,128	**76,063**
EO25vf 0,3.14	Franz 2 times	Negerfjellet, Edgeøya	Tape	1,17	0,319	0,188	40,939	1,639	0,658	0,05	0,238	0,007	0,198	39,352	0,173	0,202	0,038	0,116	0,13	**85,417**
EO25vf 0,3.16	Franz 2 times	Negerfjellet, Edgeøya	Tape	10,848	0,03	0,044	39,669	0,546	10,048	0,018	0,33	0	0,104	15,198	0,114	0,048	0,077	0,029	0,399	**77,502**
EO25vf 0,3.18	Franz 2 times	Negerfjellet, Edgeøya	Tape	7,169	0,147	0,204	18,144	3,954	5,871	0,057	0,321	0,005	1,143	28,462	0,365	0,027	0	0	0,196	**66,065**
EO25vf 0,3.2	Franz 2 times	Negerfjellet, Edgeøya	Tape	3,42	0,061	0,02	53,342	0,195	4,855	0,044	0,459	0	0	15,862	0,175	0,091	0,056	0,003	0,565	**79,148**
EO25vf 0,3.21	Franz 2 times	Negerfjellet, Edgeøya	Tape	3,355	0,032	0,046	54,911	0,817	5,015	0	0,484	0,105	0,084	11,351	0	0,066	0	0,025	0,173	**76,464**
EO25vf 0,3.3	Franz 2 times	Negerfjellet, Edgeøya	Tape	7,96	0,072	0,113	39,069	1,21	6,488	0,026	0,639	0	0,048	20,932	0,16	0,121	0,132	0	0,236	**77,206**
EO25vf 0,3.4	Franz 2 times	Negerfjellet, Edgeøya	Tape	1,871	0,067	0,022	36,773	1,015	0,163	0,184	0,789	0,022	0,035	43,476	0,19	0,118	0,121	0,039	0,385	**85,27**
EO25vf 0,3.5	Franz 2 times	Negerfjellet, Edgeøya	Tape	3,828	0,254	0,093	51,687	1,475	3,161	0,053	0,465	0	0,277	29,158	0,075	0,118	0,074	0,02	0,367	**91,105**
EO25vf 0,3.6	Franz 2 times	Negerfjellet, Edgeøya	Tape	5,2	0,031	0,476	32,218	3,942	9,681	0,04	0,348	0	0,023	15,441	0,114	0,116	0,04	0	0,146	**67,816**
EO25vf 0,3.7	Franz 2 times	Negerfjellet, Edgeøya	Tape	6,29	0,003	0,184	32,273	0,552	5,014	0,027	0,336	0	0,122	21,96	0,125	0,119	0,027	0,029	0,316	**67,377**
EO25vf 0,3.9	Franz 2 times	Negerfjellet, Edgeøya	Tape	8,449	0,016	0,029	57,029	0,388	9,575	0,024	0,423	0,024	0,114	21,014	0,097	0,07	0,031	0,024	0,085	**97,392**
EO25vf.1	Franz 1 time	Negerfjellet, Edgeøya	Tape	3,142	0,061	0,042	39,535	0,978	2,067	0,107	0,618	0	0,111	45,095	0,16	0,142	0,173	0	0,682	**92,913**

Sample	Separate	Location	Pereparate	Al2O3	Na2O	K2O	Cr2O3	SiO2	MgO	CaO	MnO	Y2O3	TiO2	FeO	V2O3	CoO	NiO	CuO	ZnO	Total
EO25vf.10	Franz 1 time	Negerfjellet, Edgeøya	Tape	5,891	0,059	0,226	30,585	3,348	1,405	0,099	1,01	0,013	0,083	52,25	0,193	0,097	0,12	0,019	0,336	**95,734**
EO25vf.11	Franz 1 time	Negerfjellet, Edgeøya	Tape	3,722	0,021	0,244	39,426	0,663	5,867	0,061	0,274	0	1,353	19,223	0,234	0,072	0,11	0,003	0,482	**71,755**
EO25vf.13	Franz 1 time	Negerfjellet, Edgeøya	Tape	11,515	0,162	0,162	40,374	0,917	4,918	0	0,332	0	0,315	16,631	0,084	0,078	0,117	0,001	0,675	**76,281**
EO25vf.14	Franz 1 time	Negerfjellet, Edgeøya	Tape	1,499	0,203	0,062	36,892	1,331	3,539	0,078	1,938	0,034	0,215	33,236	0	0,104	0,095	0	0,812	**80,038**
EO25vf.15	Franz 1 time	Negerfjellet, Edgeøya	Tape	6,875	0,011	0,359	40,899	1,613	0,057	0,059	0,402	0,028	0,179	21,318	0,058	0,124	0,014	0,003	0,169	**72,168**
EO25vf.16	Franz 1 time	Negerfjellet, Edgeøya	Tape	2,987	0,443	0,079	34,969	3,09	6,845	0,111	3,939	0	0,064	39,567	0,017	0,289	0,502	0,013	0,971	**93,886**
EO25vf.17	Franz 1 time	Negerfjellet, Edgeøya	Tape	12,106	0,137	0,158	53,024	2,965	4,831	0,022	0,402	0,101	0,11	18,764	0,192	0,058	0,005	0	0,432	**93,307**
EO25vf.18	Franz 1 time	Negerfjellet, Edgeøya	Tape	16,096	0,161	0,147	45,858	3,684	6,148	0,04	0,569	0,043	0,517	23,501	0,168	0,134	0,04	0,045	0,263	**97,414**
EO25vf.19	Franz 1 time	Negerfjellet, Edgeøya	Tape	10,638	0,077	1,004	35,368	12,545	0,366	0,077	0,229	0	0,284	13,965	0,122	0,05	0,01	0	0,115	**74,85**
EO25vf.2	Franz 1 time	Negerfjellet, Edgeøya	Tape	3,309	0,129	0,221	40,978	2,184	2,784	0,171	0,774	0,086	0,26	30,617	0,155	0,142	0,041	0	1,857	**83,708**
EO25vf.20	Franz 1 time	Negerfjellet, Edgeøya	Tape	26,051	0,054	0,04	30,523	0,828	8,87	0,05	0,527	0	0,384	27,975	0,077	0,162	0,073	0,008	0,384	**96,006**
EO25vf.21	Franz 1 time	Negerfjellet, Edgeøya	Tape	7,165	0,139	0,025	31,832	1,398	0,724	0,205	0,529	0,08	0,489	42,561	0,238	0,118	0,269	0	0,943	**86,715**
EO25vf.22	Franz 1 time	Negerfjellet, Edgeøya	Tape	8,322	0,063	0,039	25,638	0,942	4,433	0,048	0,413	0,05	4,715	46,022	1,082	0,153	0,22	0,005	0,315	**92,46**
EO25vf.23	Franz 1 time	Negerfjellet, Edgeøya	Tape	1,812	0,314	0,042	36,195	2,527	1,714	0,483	1,866	0	0,652	34,356	0,443	0,163	0,063	0,098	2,215	**82,943**
EO25vf.24	Franz 1 time	Negerfjellet, Edgeøya	Tape	6,556	0,112	0,128	31,01	3,781	4,633	0,074	0,534	0	0,519	46,479	0,229	0,179	0,077	0,015	0,3	**94,626**
EO25vf.26	Franz 1 time	Negerfjellet, Edgeøya	Tape	1,587	0,099	0,042	41,214	0,951	0,536	0,029	0,502	0	0,193	41,595	0,186	0,157	0,302	0	0,451	**87,844**
EO25vf.27	Franz 1 time	Negerfjellet, Edgeøya	Tape	1,439	0,073	0,193	41,785	0,851	0,516	0,013	0,538	0	0,117	41,226	0,146	0,204	0,311	0	0,533	**87,945**
EO25vf.28	Franz 1 time	Negerfjellet, Edgeøya	Tape	18,937	0,355	0,643	11,322	14,381	5,334	0,179	0,16	0,077	0,144	16,472	0,054	0,068	0,024	0	0,128	**68,278**
EO25vf.29	Franz 1 time	Negerfjellet, Edgeøya	Tape	5,749	0	0,311	41,531	2,004	11,419	0,025	0,277	0	0,389	19,93	0,109	0,084	0,082	0	0,03	**81,94**
EO25vf.3	Franz 1 time	Negerfjellet, Edgeøya	Tape	2,22	0,068	0,073	50,885	1,031	9,671	0,031	0,42	0	0,045	18,604	0,089	0,093	0,034	0,016	0,046	**83,326**
EO25vf.30	Franz 1 time	Negerfjellet, Edgeøya	Tape	11,457	0,15	0,131	29,531	14,019	5,982	0,067	0,486	0	0,89	33,161	0,132	0,065	0,131	0	0,1	**96,302**

Sample	Separate	Location	Pereparate	Al2O3	Na2O	K2O	Cr2O3	SiO2	MgO	CaO	MnO	Y2O3	TiO2	FeO	V2O3	CoO	NiO	CuO	ZnO	Total
EO25vf.30	Franz 1 time	Negerfjellet, Edgeøya	Tape	11,457	0,15	0,131	29,531	14,019	5,982	0,067	0,486	0	0,89	33,161	0,132	0,065	0,131	0	0,1	**96,302**
EO25vf.31	Franz 1 time	Negerfjellet, Edgeøya	Tape	9,261	0,112	0,126	41,193	4,955	6,697	0,116	0,417	0,013	0,068	26,08	0,183	0,088	0,009	0	0,236	**89,554**
EO25vf.32	Franz 1 time	Negerfjellet, Edgeøya	Tape	9,483	0,342	0,255	60,265	4,568	4,363	0,06	0,986	0	0	10,251	0,077	0,087	0	0,027	6,706	**97,47**
EO25vf.33	Franz 1 time	Negerfjellet, Edgeøya	Tape	4,465	0,485	0,281	25,686	6,198	5,535	0,183	0,32	0,033	0,14	32,158	0,108	0,135	0,077	0,044	0,159	**76,007**
EO25vf.35	Franz 1 time	Negerfjellet, Edgeøya	Tape	9,056	0,367	0,169	52,036	2,153	7,013	0,034	0,462	0	0,079	13,694	0,111	0,105	0,036	0	0,316	**85,631**
EO25vf.36	Franz 1 time	Negerfjellet, Edgeøya	Tape	9,957	0,031	0,028	53,327	0,638	5,946	0,015	0,421	0,13	0,026	16,371	0,237	0,076	0,014	0	0,403	**87,62**
EO25vf.37	Franz 1 time	Negerfjellet, Edgeøya	Tape	2,985	0,049	0,039	41,724	0,989	2,019	0,036	1,747	0	0,697	45,214	0,137	0,139	0,018	0,116	0,38	**96,289**
EO25vf.38	Franz 1 time	Negerfjellet, Edgeøya	Tape	8,979	0,476	0,313	32,206	6,355	1,884	0,27	1,087	0,041	0,732	40,713	0,394	0,11	0,077	0,091	2,397	**96,125**
EO25vf.39	Franz 1 time	Negerfjellet, Edgeøya	Tape	7,032	0,319	0,153	46,04	3,282	1,937	0,154	0,577	0	0,458	28,959	0,018	0,035	0,092	0	4,723	**93,779**
EO25vf.4	Franz 1 time	Negerfjellet, Edgeøya	Tape	0,071	0,052	0,051	49,328	0,157	3,355	0	0,502	0,02	0,115	31,825	0,128	0,137	0,107	0,007	0,289	**86,144**
EO25vf.5	Franz 1 time	Negerfjellet, Edgeøya	Tape	2,172	0,049	0,118	47,324	0,754	8,922	0,034	2,04	0,013	0,066	33,417	0,028	0,22	0,237	0,002	0,484	**95,88**
EO25vf.7	Franz 1 time	Negerfjellet, Edgeøya	Tape	4,6	1,044	0,109	28,699	4,929	1,607	0,213	1,806	0	1,71	34,685	0,253	0,119	0	0,011	2,324	**82,109**
EO25vf.8	Franz 1 time	Negerfjellet, Edgeøya	Tape	15,153	0,141	0,321	29,41	8,198	9,984	0,043	0,374	0	0,126	22,971	0,17	0,044	0,124	0,028	0,301	**87,388**
EO25vf.9	Franz 1 time	Negerfjellet, Edgeøya	Tape	14,771	0,068	0,137	29,98	6,73	10,297	0,029	0,415	0,066	0,136	23,758	0,148	0,146	0,086	0,026	0,373	**87,166**
FES25mf	Thick Section	Festningen, Spitsbergen	Thick Section	10,498	0,004	0,033	29,951	0,379	9,712	0,134	0,293	0	0,594	43,343	0,139	0,099	0,157	0	0,171	**95,507**
H-11,1	Thin Section	Iversenfjellet, Hopen	Thin Section	32,615	0,033	0	36,055	0,584	14,653	0,017	0,223	0	0,014	17,084	n/a	n/a	n/a	n/a	0,262	**101,54**
H-11,10	Thin Section	Iversenfjellet, Hopen	Thin Section	15,863	0,039	0,044	51,477	0,165	10,841	0	0,365	0,004	0,142	20,299	n/a	n/a	n/a	n/a	0,208	**99,447**
H-11,2	Thin Section	Iversenfjellet, Hopen	Thin Section	31,561	0,164	0,023	36,551	0,624	14,421	0	0,205	0,022	0,059	16,695	n/a	n/a	n/a	n/a	0,305	**100,63**
H-11,3	Thin Section	Iversenfjellet, Hopen	Thin Section	1,836	0,448	0,061	30,566	3,007	3,706	0,058	9,465	0	0,076	42,563	n/a	n/a	n/a	n/a	1,337	**93,123**
H-11,6	Thin Section	Iversenfjellet, Hopen	Thin Section	9,628	0,078	0	57,88	0,31	9,226	0,011	0,397	0	0,066	22,165	n/a	n/a	n/a	n/a	0,238	**99,999**

Sample	Separate	Location	Pereparate	Al2O3	Na2O	K2O	Cr2O3	SiO2	MgO	CaO	MnO	Y2O3	TiO2	FeO	V2O3	CoO	NiO	CuO	ZnO	Total
EO25vf.30	Franz 1 time	Negerfjellet, Edgeøya	Tape	11,457	0,15	0,131	29,531	14,019	5,982	0,067	0,486	0	0,89	33,161	0,132	0,065	0,131	0	0,1	**96,302**
EO25vf.31	Franz 1 time	Negerfjellet, Edgeøya	Tape	9,261	0,112	0,126	41,193	4,955	6,697	0,116	0,417	0,013	0,068	26,08	0,183	0,088	0,009	0	0,236	**89,554**
EO25vf.32	Franz 1 time	Negerfjellet, Edgeøya	Tape	9,483	0,342	0,255	60,265	4,568	4,363	0,06	0,986	0	0	10,251	0,077	0,087	0	0,027	6,706	**97,47**
EO25vf.33	Franz 1 time	Negerfjellet, Edgeøya	Tape	4,465	0,485	0,281	25,686	6,198	5,535	0,183	0,32	0,033	0,14	32,158	0,108	0,135	0,077	0,044	0,159	**76,007**
EO25vf.35	Franz 1 time	Negerfjellet, Edgeøya	Tape	9,056	0,367	0,169	52,036	2,153	7,013	0,034	0,462	0	0,079	13,694	0,111	0,105	0,036	0	0,316	**85,631**
EO25vf.36	Franz 1 time	Negerfjellet, Edgeøya	Tape	9,957	0,031	0,028	53,327	0,638	5,946	0,015	0,421	0,13	0,026	16,371	0,237	0,076	0,014	0	0,403	**87,62**
EO25vf.37	Franz 1 time	Negerfjellet, Edgeøya	Tape	2,985	0,049	0,039	41,724	0,989	2,019	0,036	1,747	0	0,697	45,214	0,137	0,139	0,018	0,116	0,38	**96,289**
EO25vf.38	Franz 1 time	Negerfjellet, Edgeøya	Tape	8,979	0,476	0,313	32,206	6,355	1,884	0,27	1,087	0,041	0,732	40,713	0,394	0,11	0,077	0,091	2,397	**96,125**
EO25vf.39	Franz 1 time	Negerfjellet, Edgeøya	Tape	7,032	0,319	0,153	46,04	3,282	1,937	0,154	0,577	0	0,458	28,959	0,018	0,035	0,092	0	4,723	**93,779**
EO25vf.4	Franz 1 time	Negerfjellet, Edgeøya	Tape	0,071	0,052	0,051	49,328	0,157	3,355	0	0,502	0,02	0,115	31,825	0,128	0,137	0,107	0,007	0,289	**86,144**
EO25vf.5	Franz 1 time	Negerfjellet, Edgeøya	Tape	2,172	0,049	0,118	47,324	0,754	8,922	0,034	2,04	0,013	0,066	33,417	0,028	0,22	0,237	0,002	0,484	**95,88**
EO25vf.7	Franz 1 time	Negerfjellet, Edgeøya	Tape	4,6	1,044	0,109	28,699	4,929	1,607	0,213	1,806	0	1,71	34,685	0,253	0,119	0	0,011	2,324	**82,109**
EO25vf.8	Franz 1 time	Negerfjellet, Edgeøya	Tape	15,153	0,141	0,321	29,41	8,198	9,984	0,043	0,374	0	0,126	22,971	0,17	0,044	0,124	0,028	0,301	**87,388**
EO25vf.9	Franz 1 time	Negerfjellet, Edgeøya	Tape	14,771	0,068	0,137	29,98	6,73	10,297	0,029	0,415	0,066	0,136	23,758	0,148	0,146	0,086	0,026	0,373	**87,166**
FES25mf	Thick Section	Festningen, Spitsbergen	Thick Section	10,498	0,004	0,033	29,951	0,379	9,712	0,134	0,293	0	0,594	43,343	0,139	0,099	0,157	0	0,171	**95,507**
H-11,1	Thin Section	Iversenfjellet, Hopen	Thin Section	32,615	0,033	0	36,055	0,584	14,653	0,017	0,223	0	0,014	17,084	n/a	n/a	n/a	n/a	0,262	**101,54**
H-11,10	Thin Section	Iversenfjellet, Hopen	Thin Section	15,863	0,039	0,044	51,477	0,165	10,841	0	0,365	0,004	0,142	20,299	n/a	n/a	n/a	n/a	0,208	**99,447**
H-11,2	Thin Section	Iversenfjellet, Hopen	Thin Section	31,561	0,164	0,023	36,551	0,624	14,421	0	0,205	0,022	0,059	16,695	n/a	n/a	n/a	n/a	0,305	**100,63**
H-11,3	Thin Section	Iversenfjellet, Hopen	Thin Section	1,836	0,448	0,061	30,566	3,007	3,706	0,058	9,465	0	0,076	42,563	n/a	n/a	n/a	n/a	1,337	**93,123**
H-11,6	Thin Section	Iversenfjellet, Hopen	Thin Section	9,628	0,078	0	57,88	0,31	9,226	0,011	0,397	0	0,066	22,165	n/a	n/a	n/a	n/a	0,238	**99,999**

Sample	Separate	Location	Pereparate	Al2O3	Na2O	K2O	Cr2O3	SiO2	MgO	CaO	MnO	Y2O3	TiO2	FeO	V2O3	CoO	NiO	CuO	ZnO	Total
KTO14m.1	Franz 1 time	Kapp Toscana, Spitsbergen	Tape	5,587	0,142	0,101	42,655	1,426	1,287	0,158	0,586	0	0,158	41,076	0,164	0,16	0,128	0	0,256	**93,884**
KTO14m.10	Franz 1 time	Kapp Toscana, Spitsbergen	Tape	5,49	2,547	0,54	29,248	16,156	0,979	0,188	0,502	0,056	0,361	31,17	0,217	0,009	0,079	0,104	1,069	**88,715**
KTO14m.11	Franz 1 time	Kapp Toscana, Spitsbergen	Tape	5,89	0,895	0,264	18,569	5,057	1,467	0,183	2,213	0,021	0,043	34,45	0,011	0,232	0,175	0,019	0,528	**70,017**
KTO14m.12	Franz 1 time	Kapp Toscana, Spitsbergen	Tape	7,173	0,167	0,396	44,334	2,477	4,435	0,066	0,633	0,044	0,138	23,635	0,134	0,073	0,032	0	0,31	**84,047**
KTO14m.13	Franz 1 time	Kapp Toscana, Spitsbergen	Tape	2,094	0,272	0,433	32,892	3,311	3,499	0,313	0,784	0,007	0,119	35,725	0,181	0,111	0,091	0	0,576	**80,408**
KTO14m.14	Franz 1 time	Kapp Toscana, Spitsbergen	Tape	9,748	0,029	0,125	25,625	1,107	4,091	0,06	0,403	0,391	2,849	50,53	0,495	0,12	0,148	0,065	0,346	**96,132**
KTO14m.15	Franz 1 time	Kapp Toscana, Spitsbergen	Tape	3,768	0,045	0,19	55,194	1,023	5,649	0,041	0,506	0	0,067	26,034	0,2	0,094	0,029	0,008	0,392	**93,24**
KTO14m.16	Franz 1 time	Kapp Toscana, Spitsbergen	Tape	9,686	0,124	0,148	25,234	1,542	4,087	0,102	0,383	0,002	2,882	50,303	0,558	0,122	0,108	0,003	0,233	**95,517**
KTO14m.17	Franz 1 time	Kapp Toscana, Spitsbergen	Tape	0,317	0,03	0,021	33,235	0,273	1,219	0,094	0,621	0	0,254	47,374	0,15	0,176	0,029	0,015	0,274	**84,082**
KTO14m.18	Franz 1 time	Kapp Toscana, Spitsbergen	Tape	3,609	0,219	0,597	30,33	4,611	0,814	0,161	1,487	0	0,822	39,099	0,147	0,154	0,27	0,001	0,542	**82,863**
KTO14m.19	Franz 1 time	Kapp Toscana, Spitsbergen	Tape	9,423	0,145	0,051	33,295	0,882	0,472	0,196	3,948	0	1,234	43,783	0,428	0,135	0,157	0	1,164	**95,313**
KTO14m.2	Franz 1 time	Kapp Toscana, Spitsbergen	Tape	3,184	0,374	0,584	33,27	2,638	1,386	0,561	0,705	0,02	0,397	35,749	0,097	0,173	0,207	0,052	0,826	**80,223**
KTO14m.20	Franz 1 time	Kapp Toscana, Spitsbergen	Tape	4,518	0,373	0,332	42,965	1,586	2,229	0,077	0,39	0	0,182	22,81	0,06	0,12	0,028	0	0,186	**75,856**
KTO14m.3	Franz 1 time	Kapp Toscana, Spitsbergen	Tape	22,362	0,108	0,727	29,666	2,669	10,223	0,043	0,214	0	0,118	15,763	0,136	0,079	0,073	0,02	0,497	**82,698**
KTO14m.4	Franz 1 time	Kapp Toscana, Spitsbergen	Tape	11,577	0,061	0,064	43,994	0,289	4,226	0,09	0,356	0,043	0,647	24,405	0,265	0,003	0,124	0	0,566	**86,71**
KTO14m.5	Franz 1 time	Kapp Toscana, Spitsbergen	Tape	1,773	0,337	0,126	36,482	2,126	1,135	0,123	0,661	0	0,661	45,027	0,29	0,13	0,209	0	2,873	**91,953**
KTO14m.7	Franz 1 time	Kapp Toscana, Spitsbergen	Tape	0,66	0,155	0,099	36,012	1,201	2,012	0,102	0,547	0	0,179	49,752	0,159	0,06	0,276	0	0,193	**91,407**
SV-7-4,2	Thin Section	Blanknuten, Edgeøya	Thin Section	12,279	0,043	0	55,248	0,755	8,249	0,035	0,451	0	0,04	23,079	n/a	n/a	n/a	n/a	0,265	**100,444**
SV-7-4,3	Thin Section	Blanknuten, Edgeøya	Thin Section	6,472	0,028	0,038	49,74	0,342	4,301	0,061	0,629	0,084	0,196	36,085	n/a	n/a	n/a	n/a	0,293	**98,269**
SV-7-4,4	Thin Section	Blanknuten, Edgeøya	Thin Section	30,443	0,035	0,028	36,421	0,634	13,535	0,012	0,309	0	0	18,677	n/a	n/a	n/a	n/a	0,239	**100,333**
SV-7-4,5	Thin Section	Blanknuten, Edgeøya	Thin Section	12,757	0,113	0,086	21,876	10,514	13,739	0,039	0,621	0	0,354	31,741	n/a	n/a	n/a	n/a	0,524	**92,364**

Appendix 2

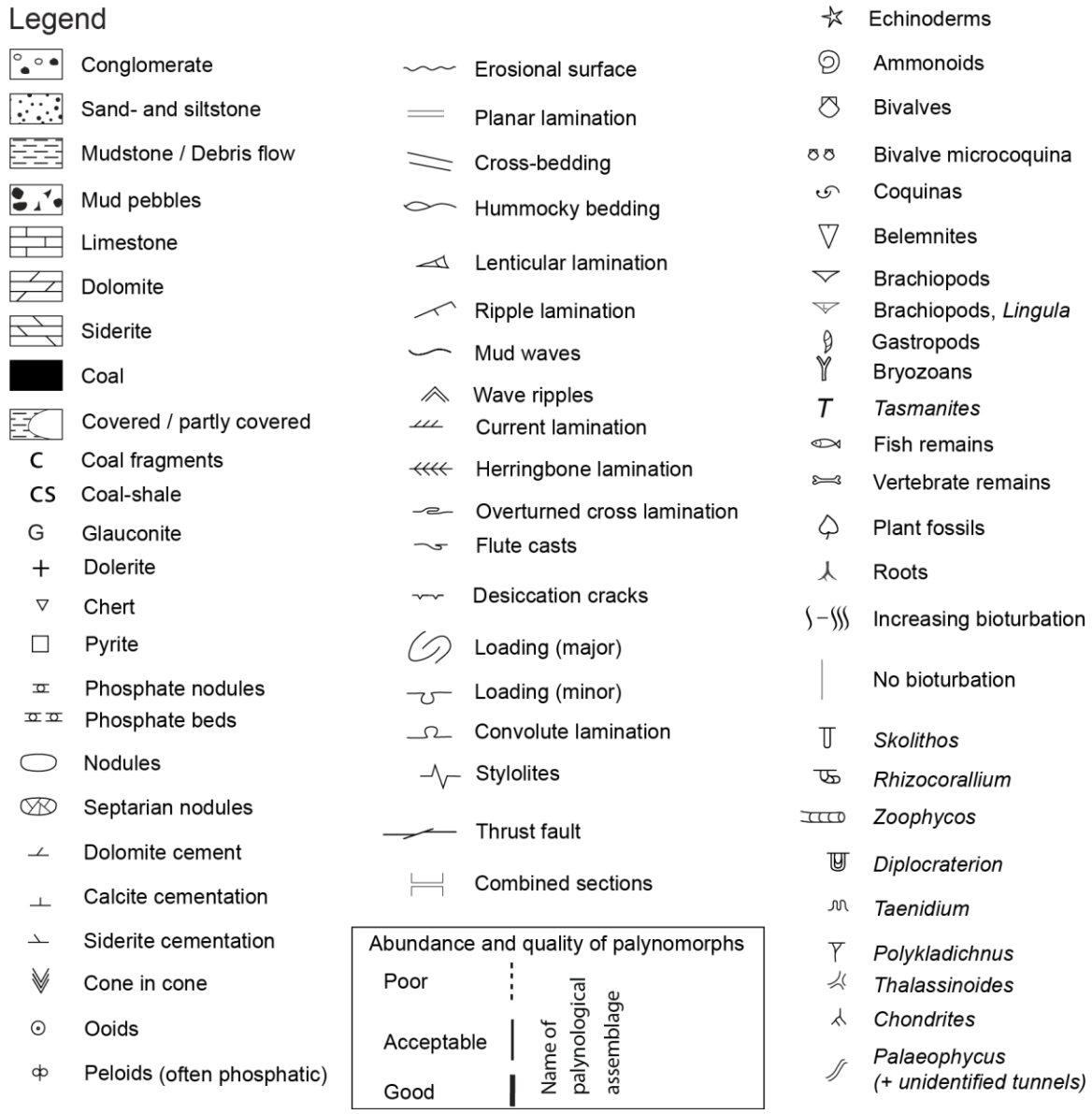

Legend to the stratigraphic columns in appendix 3 – 5, Legend after Vigran et al., 2014

Appendix 3

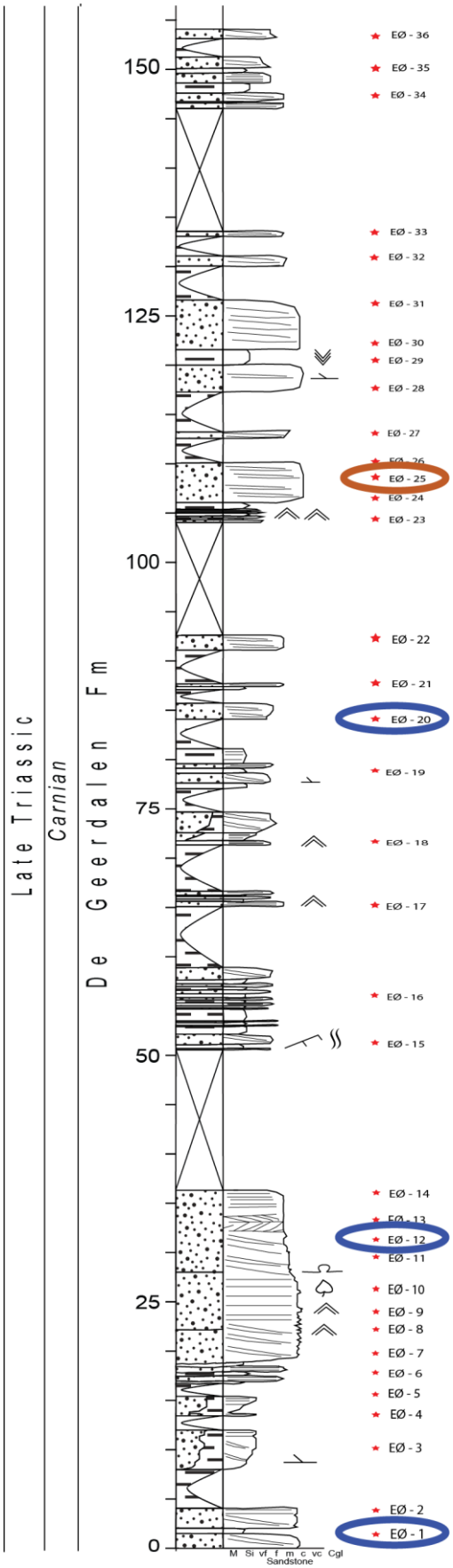

Negerfjellet simplified stratigraphic column with sample points. Coloured ellipses represent for blue: samples that have been turned into thin sections, for brown: samples that have been used for magnetic separation of chromium spinel.

Appendix 4

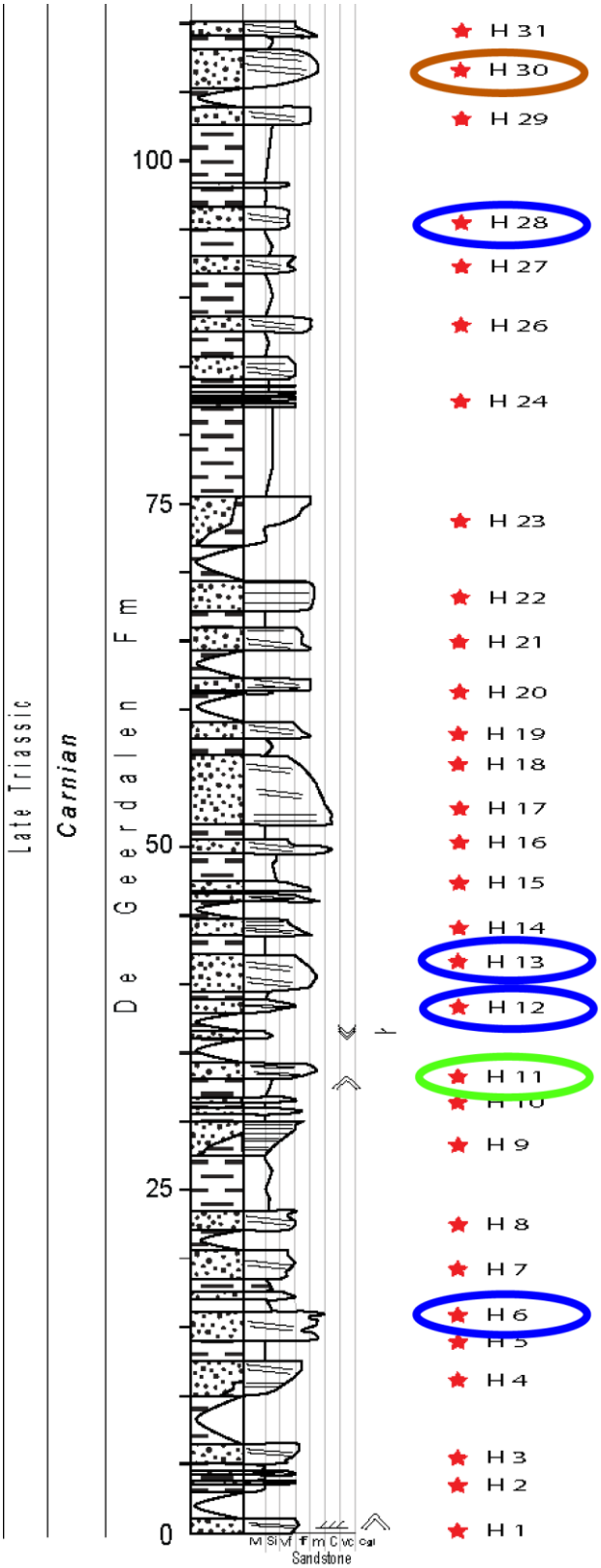

Simplified stratigraphic column with sample points from Iversenfjellet, Hopen. Coloured ellipses represent for blue: samples that have been turned into thin sections, for brown: samples that have been used for magnetic separation of chromium spinel, for green: samples that have been turned into thin sections and contributing chromium spinel compositions found by EPMA.

Appendix 5

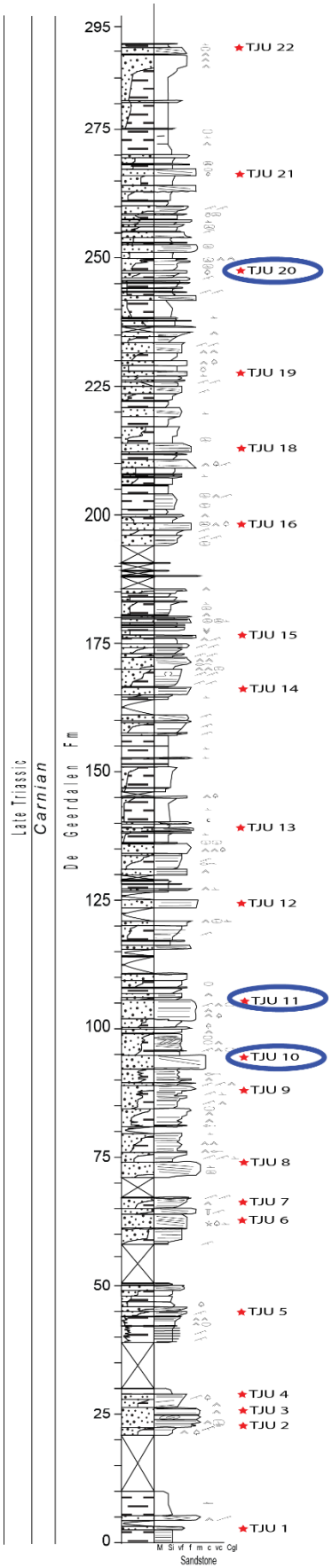

Simplified stratigraphic column with sample points from Tjuvfjordhorga, Edgeøya. Logging in collaboration with Gareth Lord (NTNU). Coloured ellipses represent for blue: samples that have been turned into thin sections, for brown: samples that have been used for magnetic separation of chromium spinel.